國立交通大學

土木工程學系碩士班

碩士論文

主動土壓力模型擋土牆之設計與建造

Design and Construction of

NCTU K_A Model Retaining Wall

研 究 生：侯鵬暉

指導教授：方永壽 博士

中華民國九十五年九月

主動土壓力模型擋土牆之設計與建造

Design and Construction of NCTU K_A Model Retaining Wall

研究生：侯鵬暉　　Student: Peng-Hui Hou

指導教授：方永壽 博士　　Advisor: Dr. Yung-Show Fang

國立交通大學
土木工程學系碩士班
碩士論文

A Thesis
Submitted to Department of Civil Engineering
College of Engineering
National Chiao Tung University
In Partial Fulfillment of the Requirements
for the Degree of
Master
in
Civil Engineering

September 2006
Hsinchu, Taiwan, Republic of China

中華民國九十五年九月

主動土壓力模型擋土牆之設計與建造

學生：侯鵬暉　　指導教授：方永壽 博士

國立交通大學土木工程學系碩士班

Abstract (in Chinese)

本研究探討夯實土壓力作用於垂直擋土牆上主動土壓力之影響。本研究使用重新設計建造之 NCTU K_A 模型檔土牆模型設備，探討平移模式牆位移所造成之土壓力變化，根據實驗結果，得到以下結論：

1. 由夯實造成之土壤壓力，隨著牆面外移而迅速消散。達到主動土壓力所需之牆移動量 S/H 為 0.0010。
2. 主動土壓力分布在從牆頂往下起算牆高三分之一內，側向土壓力略高於 Coulomb 理論解，於牆高中間三分之一的範圍，與 Coulomb 理論解相近，牆底往上起算三分之一牆高內，則略低於 Coulomb 理論解。
3. 水平土壓力係數 K_h 隨著牆位移增加而下降並達到穩定。主動狀態於牆位移約 S/H 為 0.001 時發生。
4. 實驗 $K_{a,h}$ 之數據，與 Coulomb 及 Rankine 的預測相符。
5. 主動合力位置為距牆底 0.55H 處。
6. 由夯實所得之主動係數 $K_{a,h}$ 值，與 Coulomb 和 Rankine 的預測相符。
7. 主動土壓力所造成的破壞面，於土壤表面出現的分裂位置，則與 Rankine 之預測位置相符。

關鍵字：夯實、土壤壓力、模型測試、擋土牆、砂

Design and Construction of NCTU K_A Model Retaining Wall

Student: Peng-Hui Hou Advisor: Dr. Yung-Show Fang

Department of Civil Engineering

National Chiao Tung University

Abstract

This paper presents experimental data of earth pressure acting against a vertical rigid wall, which moved outward a mass of dry sand with a stress-free horizontal surface under translation wall-movement. To investigate the variation of earth pressure induced by compaction and active wall movement, the instrumented K_A model retaining wall facility was designed and constructed at National Chiao Tung University. Based on experimental data, the following conclusions can be drawn.

1. The earth pressure induced by compaction vanished rapidly with the active wall movement. An active state of stress is reached at the wall movement of S/H = 0.0010.
2. The distribution of active earth pressure is slightly higher than Coulomb's solution at the upper one-third of wall height, approximately in agreement with Coulomb's solution in the middle one-third, and lower than Coulomb's solution at the lower one-third of wall surface. Stresses that was locked-in the soil element has been released with the lateral extension of the active soil wedge.

3. The horizontal earth presure coefficient K_h decreases with increasing wall movement and finally a constant total thrust is reached. The active condition occurred at the wall movement of approximately S/H= 0.001.
4. The experimental $K_{a,h}$ values are in good agreement with Coulomb and Rankine's prediction.
5. The active thrust is located at about 0.55H above the base of the wall.
6. The active coefficient $K_{a,h}$ values obtained with compacted dense sand from this study are in fairly good agreement with Coulomb and Rankine's prediction.
7. The Rankine theory is suitable to predict the location of surface crack for active failure.

Keywords: compaction, earth pressure, model test, retaining wall, sand.

Table of Contents

List of Tables

List of Figures

List of Symbols

C_u	:	Uniformity Coefficient
e_{max}	:	Maximum Void Ratio of Soil
e_{min}	:	Minimum Void Ratio of Soil
F	:	Force
G_s	:	Specific Gravity of Soil
h	:	Location of Total Thrust
H	:	Effective Wall Height
i	:	Slop of Ground Surface behind Wall
K_o	:	Coefficient of Earth Pressure At-Rest
K_a	:	Coefficient of Active Earth Pressure
K_h	:	Coefficient of Horizontal Earth Pressure
$K_{a,h}$	:	Coefficient of Horizontal Active Earth Pressure
P_a	:	Total Active Force
RT	:	Rotation about Wall Top
RTT	:	Rotation about a Point above Wall Top
RB	:	Rotation about Wall Base
RBT	:	Rotation about a Point below Wall Base
σ_h	:	Horizontal Earth Pressure
σ_N	:	Normal Stress
S	:	Wall Displacement
T	:	Translation
z	:	Depth from Surface
γ	:	Unit Weight of Soil
ϕ	:	Angle of Internal Friction of Soil
δ	:	Angle of Wall Friction
τ	:	Shear Stress

Chapter 1

Introduction

Retaining walls are frequently used to hold back the earth and maintain a difference in the elevation of the ground or water surface. In highway constructions, retaining structures are used along cuts or fills where space is inadequate side slopes. Bridge abutments and foundation walls that must support earth fills are also designed as retaining structures. Fig. 1.1 shows the common uses of retaining walls.

The lateral earth pressure induced by active wall movements has been studied with experimental methods by different researchers (Terzaghi, 1934; Macky and Kirk,1967; Bros, 1972; Sherif et al., 1984; Fang and Ishibashi, 1986, and Fang et al., 1997). Terzaghi (1934) noted that backfill compaction significantly affected lateral earth pressures and resulting structure deflections. From an engineering point of view, the active earth pressure distribution behind the wall has a great influence on the adequate design of the retaining structures. It affects not only the bending moment and shear stress distributions within the body, but also the safety of the structure. Therefore, the active earth pressure and the earth pressure induced by compaction become the subject of this study.

1.1 Objective of Study

Traditionally, civil engineers build the retaining structures to resist the active force. In most cases, civil engineers calculate the active earth pressure behind a retaining wall using either Coulomb's or Rankine's theory. They assume that earth pressure distribution is linear, and the location of resultant force is located at one third of the wall height above the wall base. Another method to estimate the active and passive earth pressure acting on a retaining structure is the general wedge theory (Terzaghi, 1941). However, this method is a little more complicated, and the estimated active earth pressure is close to the value determined with Coulomb theory (Morgenstern and Eisenstein, 1970).

For granular soils, achieving a relative density of 70~75% is generally recommended (NAVFAC DM-7.2, US Navy 1982). Therefore, the backfill encounterd in the field would be dense soil. Hand tampers and vibratory compaction equipments are commonly used to compact the fill. Terzaghi (1934) reported that compaction efforts would influence the magnitude and distribution of lateral earth pressure. Peck and Mesri (1987) presented a method to evaluate the compaction induced earth pressure.

In Fig. 1.2, the active earth pressure is considered to push the wall. How does the active wall movement affect the compaction-induced earth pressure? Is the design of retaining structures based on the Coulomb's active earth pressure theory totally appropriate? This becomes the main subject of investigation in this study.

1.2 Research Outline

The investigation has been conducted with a newly designed K_A model retaining wall facility in the Foundation Engineering Model Laboratory of National Chiao Tung University. The theories and experimental findings associated with active earth pressure are introduced in Chapter 2. The design of the NCTU K_A model retaining wall facility is discussed in Chapter 3.

Tests results regarding the characteristics of backfill and interface behavior are summarized in Chapter 4. Soil density control experiment were conducted to study soil density distribution in the backfill. Tests results are disscussed in Chapter 4.

In Chapter 5, test results regarding earth pressure due to vibratory compaction and active wall movement were discussed. The backfill with a relative desity of 75% was achieved by compaction method. The variations of lateral earh pressure, total soil thrust, and its point of application as a function of active wall movement are reported. Tests results are compared with the well-known Rankine and Coulomb theories. Based on the experimental results, an estimation of active earth pressure for a compacted cohesionless backfill is suggested.

1.3 Organization of Thesis

This thesis is divided into the following parts:

1. Review of theories regarding the active earth pressure and model retaining wall tests. (Chapter 2)
2. A detail description for the design of NCTU K_A model retaining wall. (Chapter 3)
3. Discussion of backfill characteristics and interface characteristics. (Chapter 4)
4. Experimental results regarding the reduction of compaction induced earth pressure with active wall movement. (Chapter 5)
5. Conclusions. (Chapter 6)

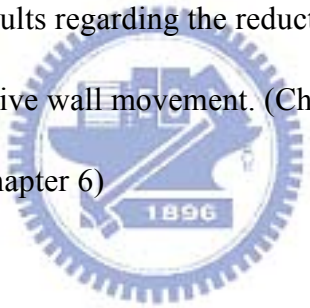

Chapter 2

Literature Review

The Coulomb and Rankine earth pressure theories are often applied methods to calculate the lateral force of earth pressure acting on a retaining wall. Experimental studies of active earth pressure have been reported by Terzaghi (1934), Mackey and Kirk (1967), Bros (1972), Sherif et al. (1982), Fang and Ishibashi (1986), and Fang et al.(1997). The major findings of these researches are summarized in this chapter.

2.1 Active Earth Pressure Theories

2.1.1 The Coulomb Theory

Coulomb (1776) proposed a method of analysis that determines the resultant horizontal force on a retaining system for any slope of wall, wall friction, and slope of backfill. The Coulomb theory is based on the assumption that soil shear resistance develops along the wall and failure plane. Detailed assumptions are made as the followings:

1. The backfill is isotropic and homogeneous.
2. The rupture surface is plane, as plane BC in Fig. 2.1(a). The backfill surface is a plane surface as well.
3. The frictional resistance is distributed uniformly along the rupture surface.
4. Failure wedge is a rigid body.

5. There is a friction force between soil and wall when the failure wedge moves toward the wall.

6. Failure is a plane strain condition.

To create an active state, the wall is designed moved away from the soil mass. If the wedge ABC in Fig. 2.1(a) moves down relatively to the wall, and the wall friction angle δ will develop at the interface between the soil and wall. Let the weight of wedge ABC be W and the force on BC be F. With the given value θ, and the summation of verticle forces and horizontal forces, the resultant soil thrust P can be calculated as shown in Fig. 2.1(b).

To test different wedge scenarios, the corresponding values of P can be acquired. The upper part of Fig. 2.2 illustrates the curve of P according to different wedge scenarios. And the maximum P is the Coulomb's active force P_a as Eq. (2.1).

$$P_a = \frac{1}{2}\gamma H^2 K_a \tag{2.1}$$

where

Pa = total active force per unit length of wall

Ka = coefficient of active earth pressure

γ = unit weight of soil

H = height of wall

and

$$K_a = \frac{\sin^2(\phi+\beta)}{\sin^2\beta\sin(\beta-\delta)\left\{1+\sqrt{\frac{\sin(\phi+\delta)\sin(\phi-i)}{\sin(\beta-\delta)\sin(\beta+i)}}\right\}^2} \tag{2.2}$$

where

ϕ = internal friction angle of soil

δ = wall friction angle

β = slope of back of the wall to horizontal

i = slope of ground surface behind wall

2.1.2 The Rankine Theory

Rankine (1875) considered the soil in a state of plastic equilibrium and used essentially the same assumptions as Coulomb. The Rankine theory assumes that there is no wall friction and failure surfaces are straight planes, and that the resultant force acts parallel to the backfill slope. Detailed assumptions are made as the followings:

1. The backfill is isotropic and homogeneous.
2. Retaining wall is a rigid body. The wall surface is vertical to the ground and the friction force between the wall and the soil is neglected.
3. Elastic equilbrium is not applicable to the stress condition in the failure wedge.

Rankine assumed there is no friction between wall surface and backfill, and the backfill is cohesionless. The earth pressure on plane AB of Fig. 2.3(a) is the same as that on plane AB inside a semi-infinite soil mass in Fig. 2.3(b). For active condition, the active earth pressure σ_a at a given depth z can be expressed as:

$$\sigma_a = \gamma z K_a \tag{2.3}$$

The total active force P_a per unit length of the wall is equal to

$$P_a = \frac{1}{2}\gamma H^2 K_a \tag{2.4}$$

The direction of resultant force P_a is parallel to the ground surface as Fig. 2.3(b), where

$$K_a = \cos i \frac{\cos i - \sqrt{(\cos^2 i - \cos^2 \phi)}}{\cos i + \sqrt{(\cos^2 i - \cos^2 \phi)}} \tag{2.5}$$

2.1.3 The Terzaghi Theory

The assumption of plane failure surface made by Coulomb and Rankine, however, does not apply in practice. Terzaghi (1941) suggested that the failure surface in the backfill under an active condition was a log spiral curve, like the curve bd in Fig. 2.4, but the failure surface dc is still assumed plane.

The illustration in Fig. 2.5 shows how Terzaghi and Peck (1967) calculated the active resistance with trial wedge method. The line d_1c_1 makes an angle of $45^\circ + \phi/2$ with the surface of the backfill. The arc bd_1 of trial wedge abd_1c_1 is a logarithmic spiral formulated as the following equation

$$r_1 = r_0 e^{\theta \tan \phi} \tag{2.6}$$

O_1 is the center of the log spiral curve in Fig. 2.5, where $O_1b = r_1$, $O_1d_1 = r_0$, and $\angle bO_1d_1 = \theta$. For the equilibrium and the stability of the soil mass abd_1f_1 in Fig. 2.6, the following forces per unit width of the wall are considered.

1. Soil weight per unit width in abd1f1: W1 = γ × (area of abd1f1)

2. The resultant force Pd1 in the zone of Rankine's active state, acting horizontally on the vertical face d1f1 at a distance of Hd1/3 upward from d1:

$$P_{d1} = \frac{1}{2}\gamma(H_{d1})^2 \tan^2(45° - \frac{\phi}{2}) \tag{2.7}$$

where

Hd1 = d1f1

Pd1 acts horizontally at a distance of Hd1/3 measured vertically upward form d1.

3. The resultant force of the shear and normal forces dF, acting along the surface of sliding bd1. At any point of the curve, according to the property of the logarithmic spiral, a radial line makes an angle ϕ with the normal. Since the resultant dF makes an angle ϕ with the normal to the spiral at its point of application, its line of application will coincide with a radial line and will pass through the point O1.

4. The active force per unit width of the wall P1. P1 acts at a distance of H/3 measured vertically form the bottom of the wall. The direction of the force P1 is inclined at an angle δ with the normal drawn to the back face of the wall.

5. Moment equilibrium of W1, Pd1, dF and P1 about the point O1:

$$W_1[l_2] + P_{d1}[l_3] + dF\ (0) = P_1[l_1] \tag{2.8}$$

or

$$P_1 = \frac{1}{l_1}\left[W_1 l_2 + P_{d1} l_3\right] \tag{2.9}$$

where l_2, l_3, and l_1 are the moment arms for forces W1, Pd1, and P1, respectively.

The trial active forces per unit width in various trial wedges are shown in Fig. 2.7. Let P_1, P_2, P_3, …, and P_n be the forces that respectively correspond to the trial wedges 1, 2, 3, …, and n. The forces are plotted to the same scale as shown in the upper part of the figure. A smooth curve is plotted through the points 1, 2, 3, …, n. The maximum P_1 of the smooth curve defines the active force P_a per unit width of the wall.

2.1.4 Comparison of Active Earth Pressure Coefficient K_a

In many theories, the soil mass can be described in a state of limiting equilibrium, and shear strength of soil is expressed with Mohr-Coulomb failure criterion. However, the assumptions differ in the shape of the failure surface. Coulomb (1776) assumed that sliding would occur along a planar sliding surface. Brinch Hansen (1953) assumed the soil wedge slip along a circular surface. Janbu (1957) restricted to a particular shape of slip surface, used the method of slices and satisfied equilibrium in approximate manner. Terzaghi (1941) proposed the logarithmic spiral slip surface.

The coefficient of active earth pressure K_a in different theories were compared by Morgenstern and Eisenstein (1970). The variation of K_a is the function of internal friction angle of backfill in Fig. 2.8, where the wall friction angle δ is

equal to ϕ and $\phi/2$. For the case $\delta = \phi/2$, the total range of variation of K_a is generally less than 15% in Rankine's solution. In this study, K_a values calculated with the Coulomb theory and Rankine theory are compared with experiment results.

2.2 Laboratory Model Retaining Wall Tests for Active State

2.2.1 Model by Terzaghi

Terzaghi (1934) studied the lateral pressure of compacted sand against a large scale model wall at MIT. The face of the wall is 14 ft. in width and 7 ft. in height. The dimension of the soil bin is 14 ft. × 14 ft. × 7 ft. as illustrated in Fig. 2.9. Twenty Goldbeck pressure cells were used to measure the variation of earth pressure, ten built into the wall and ten rested into the floor of the bin. For the wall under translation and rotation about base modes (RB), the earth pressure coefficient K (defined as $\sigma_h/\gamma z$) was measured at an elevation equal to one-half of the height of backfill as shown in Fig. 2.10. With a small displacement of the wall, the earth pressure reduced to the fully active state. For a compacted backfill 4.5 ft. in height, an outward displacement of about 1.5 mm (1/1000 of the depth of the backfill) had lead the pressure to an active state. The difference of the K curve for the wall which yields by tilting (Test 1) is not obvious from that of the wall which yields parallel to its original position (Test 2).

Fig. 2.11 shows the relation between the height of the center of pressure (defined as h_c/h) and the yield of the wall. According to Coulomb's theory, the

resultant force for level backfill should be located at one-third of the backfill depth above the base (h_c/h= 0.33). For rotation about base modes (Tilting wall, RB) mode, the height of center of pressure is decreased when the wall starts to move. However, after the wall movement equals to 0.00036h, the height of center of pressure gradually rises with the increasing wall movement.

2.2.2 Model by Mackey and Kirk

Mackey and Kirk (1967) experimented on lateral earth pressure by using a steel model wall. This soil tank was made of steel with internal dimension of 36 in. × 16 in. × 15 in. as shown in Fig. 2.12. In their observation, when the wall moved away from the soil, the earth pressure decreased (see Fig. 2.13) and then increased slightly to reach a constant value. Mackey and Kirk concluded that if the backfill is loose, the obtained active earth pressure would be within 14 percent off those theoretical values by the methods listed in Table 2.1.

Mackey and Kirk utilized a powerful beam of light to observe the failure surface in the backfill. It could trace the position of the shadow, formed by changes of the sand surface in different level. It was found that the failure surface due to the translational wall movement was a curve in the backfill (Fig. 2.14), rather than a plane assumed by Coulomb.

2.2.3 Model by Bros

Bros (1972) experimented on various movements of model retaining wall to find the influence by the values and distribution of active and passive earth

pressures. The model arrangement is illustrated in Fig. 2.15. The main structure consists of three vertical steel-frames supporting the soil bin, which is 0.7 m in width, 0.85 m in height, and 1.6 m in length. The pressure cells are diaphragm type. The earth pressures were measured with the deforming diaphragm with electric-resistivity strain gauges. In the study, clean, dry, quartz sand from Odra-river was used. The dense state was obtained by vibrating sand of each 12-15 cm layer with electric vibrator.

The outward translation of the wall caused the mobilization of friction between the backfill and side-wall, which tends to decrease the measured lateral pressures. The coefficient of horizontal earth pressure K as a function of wall displacement S is shown in Fig.2.16. It was concluded that the active condition was reached at the wall displacement of 0.0006h (h = height of backfill) under a translational mode. Fig. 2.17 shows that the active conditions are reached at the wall displacement of 0.0035h and 0.0012h~0.0018h, under RB and RT mode respectively.

2.2.4 Model by Sherif, Ishibashi, and Lee

Sherif et al. (1982) compared their experiment results of active static and dynamic earth pressure with Coulomb and Mononobe-Okabe equations. Their experiments were conducted at the University of Washington. The model system consists of four components: (1) shaking table and soil box; (2) loading and control units; (3) retaining wall; and (4) data acquisition system.

The shaking table was 3 m in length and 2.4 m in width, as shown in Fig.

2.18(a). It was made of steel. The rigid soil box of 2.4 m in length, 1.8 m in width, and 1.2 m in height was built on the shaking table. The movable model retaining wall and its driving system are shown in Fig. 2.19. The model wall consists of the main frame and the center wall. The center wall was 1 m in width, 1 m in height, and 0.127 m in thickness. Six soil pressure transducers were mounted on the center line of the wall surface at different depths to measure the soil pressure distribution against the main body of the center wall (Fig. 2.18b).

Fig. 2.20 illustrates different values of K_{sh}, h/H and $\tan\delta$ relative to wall displacements, where δ is wall friction angle, (h/H) represents the point of application of the soil thrust, and K_{sh} is the static horizontal coefficient of earth pressure. The density of the loose Ottawa sand is ρ =1.54 g/cm^3, and the corresponding angle ϕ is 31.5°. The speed of wall movement stayed constant as 1.5 x10^{-3} in/sec. The pattern of wall movement was translational. In Fig. 2.20, the K_h value of loose soil gradually decreases until the displacement of the wall movement is significant. The value of K_h remains stable regardless of the soil density after the displacement reaches H/1000. Sherif et al. concluded that the experiment $K_{a,h}$ showed obvious correlation with the Coulomb theory, shown as Fig. 2.21.

2.2.5 Model by Fang and Ishibashi

Fang and Ishibashi (1986) conducted their experiments with respect to the distribution of the active stresses applying three different wall movement modes: (1) rotation about top, (2) rotation about heel, and (3) translation. Their

experiments were also conducted at the University of Washington.

In Fig. 2.22, there is a sharp fall in the pressure behind the lower pressure transducer SPT3, SPT4, SPT5 and SPT6 with wall rotation. And then it stays constant. On the other hand, there is an initial increase in the upper transducer SPT1 and SPT2 with increasing wall rotation. The possible reason may be the arching formed in the upper portion of the backfill soil. Figure 2.23 shows the typical change of lateral stress distribution in different stages of wall rotation. It shows that the arching phenomenon dominates the backfill performance behind the upper portion of the wall when wall rotated about the top.

Figure 2.24 shows the typical horizontal pressure distribution behind a wall rotated about the base. It shows that the lateral pressure of the upper elevation decreases very quickly. However, there is only a very gentle decline in the lateral pressure near the base of the wall with wall rotation. The fully active state is difficult to be reached near the base. In brief, the value of horizontal earth pressure coefficient K_h drops dramatically at the beginning and then keeps constant. Accordingly the total thrust in Fig. 2.25 is not be able to return to the position of H/3 above the bottom of the wall, which means the existence of the remaining part of the extra stress near the base of the wall.

Figure 2.26 shows the lateral earth pressure measured at various depths. The lateral pressure falls rapidly due to the translational wall displacement. Most of the measurements reach the minimum value at approximately 10×10^{-3} in. (0.25 mm) wall displacement and then stay stable thereafter.

Figure 2.27 shows the horizontal earth pressure distributions at different translational wall movements. The measured active stress is slightly higher than Coulomb's solution at the upper one-third of wall height, approximately in agreement with Coulomb's prediction in the middle one-third, and lower than Coulomb' at the lower one-third of wall surface. However, the magnitude of the active total thrust Pa at S = 20×10^{-3} in. (0.5 mm) is almost the same as the value calculated apply to the Coulomb theory.

Figure 2.28 shows the K_a is the function of soil density and internal friction angle. The value of K_a decreases while the angle of ϕ increases. There might be a underestimation of the coefficient K_a in Coulomb's solution for rotational wall movement.

2.2.6 Model Study by Fang et al.

Fang et al. (1997) presented experimental data of earth pressure acting against a vertical rigid wall, which moved away from or toward a mass of dry sand with an inclined surface. The instrumented NCTU retaining-wall facility was used to investigate the variation of earth pressure induced by the translational wall movement.

Based on their experimental data, it has been found that the earth-pressure distribution is essentially linear at each stage of wall movement. As shown in Fig. 2.29, the wall movement required for the loose backfill to reach an active stage increase with an increasing backfill inclination. Fig. 2.30 shows the experimental active earth-pressure coefficients for various backfill sloping angles are in good

agreement with the values calculated by Coulomb's theory. It may be observed in the figure that it is not appropriate to adopt the Rankine theory to determine active earth pressure against a rigid wall with sloping backfill.

2.3 Effects of Soil Compaction in Earth Pressure

Compaction a soil can produce a stiff, settlement-free and less permeable mass. It is usually accomplished by mechanical means that cause the density of soil to increase. At the same time the air voids are reduced and the coordination number of the grains is increased. It has been realized that the compaction of the backfill material has an important effect on the earth pressure on the wall.

Several theories and analytical methods have been proposed to analyze the residual lateral earth pressures induced by soil compaction. Most of these theories introduce the idea that compaction represents a form of overconsolidation, where stresses resulting from a temporary or transient loading condition are retained following removal of this load.

2.3.1 Study of Peck and Mesri

Based on the elastic analysis, Peck and Mesri (1987) presented a calculation method to evaluate the compaction-induced earth pressure. The lateral pressure profile can be determined by four conditions on σ_h, as illustrated in Fig. 2.31 and summarized in the following.

1. Lateral pressure resulting from the overburden of the compacted backfill,

$$\sigma_h = (1-\sin\phi)\gamma z \tag{2.10}$$

2. Lateral pressure limited by passive failure condition,

$$\sigma_h = \tan^2(45+\phi/2)\gamma z \tag{2.11}$$

3. Lateral pressure resulting from backfill overburden plus the residual horizontal stresses,

$$\sigma_h = (1-\sin\phi)\gamma z + \frac{1}{4}(5^{1.2\sin\phi}-1)\Delta\sigma_h \tag{2.12}$$

where $\Delta\sigma_h$ is the lateral earth pressure increase resulted from the surface compaction loading of the last backfill lift and can be determined based on the elastic solution.

4. Lateral pressure profile defined by a line which envelops the residual lateral pressures resulting from the compaction of individual backfill lifts. This line can be computed by Eq. 2.13

$$\frac{\Delta\sigma_h}{\Delta z} = \frac{1-\sin\phi}{4}(5-5^{1.2\sin\phi})\gamma \tag{2.13}$$

Fig. 2.31 indicates that near the surface of backfill, from point a to b, the lateral pressure on the wall is subject to the passive failure condition. From b to c, the overburden and compaction-induced lateral pressure profile is determined by Eq. 2.12. From c the lateral pressure increases with depth according to Eq. 2.13 until point d is reached. Below d, the overburden pressure exceeds the peak stress in effective in compaction. In the lower part of the backfill, the lateral pressure is directly related to the effective overburden pressure.

2.3.2 Study of Chen

Chen (2003) reported some experiments in non-yielding retaining wall at National Chiao Tung University (Fig. 2.32) to investigate influence of earth pressure due to vibratory compaction. Air-dry Ottawa sand was used as backfill material. Vertical and horizontal stresses in the soil mass were measured in loose and compacted sand. Based on his test results, Chen (2003) proposed four points of view: (1) the compaction process does not result in any residual stress in the vertical direction. The effects of vibratory compaction on the vertical overburden pressure are insignificant, as indicated in Fig. 2.33 and Fig. 2.34; (2) after compaction, the lateral stress measured near the top of backfill is almost identical to the passive earth pressure estimated with Rankine theory (Fig. 2.35). The compaction-influenced zone rises with rising compaction surface. Below the compaction-influenced zone, the horizontal stresses converge to the earth pressure at-rest, as indicated in Fig. 2.35(e); (3) when total (static + dynamic) loading due to the vibratory compacting equipment exceeds the bearing capacity of foundation soils, the mechanism of vibratory compaction on soil can be described with the bearing capacity failure of foundation soils (Fig. 2.36); (4) the vibratory compaction on top of the backfill transmits elastic waves through soil elements continuously. For soils below the compaction-influenced zone, soil particles are vibrated. The passive state of stress among particles is disturbed. The horizontal stresses among soil particles readjust under the application of a uniform

overburden pressure and constrained lateral deformation, and eventually converge to the at-rest state of stress.

Chapter 3

Design of NCTU K_A Model Retaining Wall Facility

The design of NCTU K_A model retaining wall facility are discussed in this chapter. The model wall in this study is assumed a rigid body, such as a gravity retaining wall. At the beginning of design, two important testing parameters have been considered: (1) the wall height, and (2) the maximum wall displacement.

The K_A model wall facility is designed to investigate active earth pressure. At the same depth Z, the active earth pressure ($\sigma_a = K_a \gamma Z$) would be smaller than the earth pressure at rest ($\sigma_o = K_o \gamma Z$). Consequently, it is necessary to increase the wall height (increase the overburden pressure) in order to obtain more obvious experimental σ_a data. According to the space available in the NCTU foundation model lab, the effective wall height H (actually the height of backfill) was evaluated and selected to be 1.0 m.

It is important for the designer to consider how much wall displacement is required to achieve an active state in the backfill. Table 3.1 shows the range of wall displacement reported by previous researchers for different wall movement modes to achieve an active state of stress. Based on their studies, the wall displacements from 0.0005H to 0.0040H could lead to active states. The NCTU K_A Model Retaining Wall is designed to observe the active failure surface in the backfill. Fang (1983) reported that the surface failure cracks appeared when the wall

displacement reached H/150. With a factor of safety of 3.0, H/50 (20 mm) was selected as the largest active displacement for the model wall.

3.1 Design Motivation

In order to study the variation of earth pressure more extensively, the K_A model wall facility was proposed. This newly designed and constructed retaining wall to investigate active earth pressure has the following features:

3.1.1 Large-scale model wall

The previous NCTU model wall was designed for both active and passive earth pressure experiments. Subjected to tremendous passive earth pressure acting on the model wall, the height of the wall was limited to 0.5 m. However in the new design, the wall is designed mainly for active earth pressure experiments. The earth pressure would decrease from at-rest to active state of stress. The increased height of 1.0 m to enhance the investigation range of lateral earth pressure distribution. With the new facility, the effects of compaction on earth pressure can now be observed in both shallow and deeper location.

3.1.2 Wall driven by servo motors

The servo motor can accurately control both of the velocity and position of the model wall. In the previous retaining wall experiments, the start and stop of model wall were controlled manually. For the new K_A model wall experiments, the wall movements can be controlled more accurately.

3.1.3 Large wall displacement

The cracks on the soil surface can be observed only at a large active wall movement. With the large wall displacement (S = 20 mm) design for the new model wall, the earth pressure due to the backfill in a critical state can also be investigated.

3.2 Types of Experiments

The K_A model wall facility is designed for various types of earth pressure experiment. Possible research subjects with the new model wall are summerized as the follows:

1. Relative density of backfill

The intensity and distribution of active earth pressure acting on the wall would be affected by the relative density of soil. Experimental methods such as air-pluviation and soil compaction can be used to create different backfill densities.

2. Wall movement mode

With the new model wall, five types of active wall movement modes are possible: (1) rotation about the wall top (RT mode, Fig. 3.1(a)); (2) rotation about the wall base (RB mode, Fig. 3.1(b)); (3) translation mode (T mode, Fig 3.1(c)); (4) rotation about a point above wall top (RTT mode, Fig. 3.2(a)),and (5) rotation about a point below wall base (RBT mode, Fig. 3.2(b)).

It should be mentioned that (1), (2) and (3) modes are actuall special cases of

(4) and (5) modes.

3. Adjacent stiff rock face

Wang (2005) and Chen (2005) designed and consa supporting system of the steel interface plate (Fig. 3.3) and the supporting frames (Fig. 3.4) to simulate the effect of adjacent rock face behind the retaining wall, as shown in Fig. 3.5. Various scenarios of interface installations were simulated. This interface plate was integrated in the NCTU K_A model retaining wall. Hence, the effect of the rock face can also be simulated. And the distribution of earth pressure can be observed in active state.

4. Step movements of wall

When a retaining wall is built in the field, it is necessary to fill up and then compact the backfill behind the wall in layers. The wall displacement would occur progressively during the filling and compaction of backfill. Therefore, in order to simulate the field condition, it would be interesting to investigate the variation of earth pressure due to the step movements of retaining wall.

3.3 NCTU K_A Model Retaining Wall Facility

The entire NCTU K_A model retaining wall facility consists of four components, namely: (1) soil bin; (2) model wall; (3) driving system; and (4) data acquisition system. The design of these components are introduced in the following sections.

3.3.1 Soil Bin

1. Length of Soil Bin

Fig. 3.6 shows, for H=1.0m, the length of active failure wedge approximates to 577 mm based on the Rankine theory. Loose backfill condition is considered with an inertial friction angle of 30 degrees. The soil bin is designed to simulate the intrusion adjacent rock face behind the wall as shown in Fig. 3.6. In Fig. 3.6, with the steel interface plate inclined at $\alpha = 45°$, the length of soil bin at the top of the model wall should be at least 1.2 m. The design length of the soil bin is 1.5m, to tolerate possible uncertainties.

2. Width of Soil Bin

The selection of the width of the soil bin used to hold the backfill is governed by the friction effect along the side walls. Terzaghi (1932) experimented on small-scale tests in several model retaining walls and suggested the adequate length of the wall twice as long as the depth of the fill.

The width (W) of the soil bin for this study is set to be 1.5 m, which is 1.5 times of the the backfill height. To efficiently reduce the side-wall frictional effect, a lubrication layer fabricated with plastic sheets is placed between the backfill and the side wall. The measured friction angle at the soil-sidewall interface with this method is about $\delta = 7.5°$. With the design considerations mentioned, the side wall friction effect on K_a will be effectively reduced.

3. Structure of Soil Bin

The soil bin made of steel has internal dimension of 1500 mm × 1500 mm ×

1100 mm as shown in Fig. 3.7 and 3.8. The major concern to choose the material is rigidity. Both sides of the soil bin are made with 30 mm-thick transparent acrylic plates. Therefore, the behavior of the backfill during shear can be observed. Fig. 3.9 shows outside the acrylic plates, U-shaped steel beams with steel columns of 20 mm in thickness were welded. In this way the lateral displacement of the acrylic side wall will be constrained during the loading process. The side walls are confined laterally to ensure the plane strain condition in the backfill. For observing the active failure wedge in the soil mass, a spacious clearence (600mm-wide) is reserved without steel reinforcements. The reinforcement of end wall with steel beams and columns is illustrated in Fig. 3.10.

The bottom of the soil bin is covered with a layer of SAFETY WALK (3M), which is a anti-slip frictional material. It generates adequate friction between the soil and the base of the bin.The end wall parallel to the model retaining wall is made of a 20 mm thick steel plate. All corners, edges and screw-holes of the soil bin were sealed to avoid leakage.To create a plane strain condition for the model test, the following rules should be followed:

1. Rigidity: The soil bin is nearly rigid that lateral deformation of side wall becomes negligible.
2. Frictionlessness: The friction between the backfill and the side walls should be minimized. The lubrication layer is made of one thick and two thin plastic sheets between the side walls and the soil.

3. Uniformity: The properties of backfill should be uniform along the width of the retaining wall. The method to control the uniformity of backfill will be discussed in Chapter 4.

3.3.2 Model Wall

1. Positions of Driving Rods

The positions of the upper and lower wall driving rods are determined based on the distribution of lateral earth pressure, which is assumed linear with depth as shown in Fig. 3.11. The mechanics of materials theories is used to analyze the deflection of wall face. The wall is considered as a beam and a 2-dimensional analysis is made. The discontinuity functions are used to determine beam deflections.The reactions R_B and R_C in Fig. 3.11 are formulated as

$$R_B = \frac{qH}{2b}\left(a+b-\frac{2}{3}H\right), \quad R_C = \frac{qH}{2b}\left(\frac{2}{3}H-a\right) \tag{3.1}$$

where

R_B = reaction at upper driving rod

R_C = reaction at lower driving rod

H = height of backfill

q = intensity of lateral pressure at depth H

a = distance from soil surface to upper driving rods

b = distance from soil surface to lower driving rods

Gere and Timoshenko (1984) developed the load intensity $q(Z)$ of the equivalent distributed load:

$$q(Z) = -R_B u(Z-a)(Z-a)^{-1} - R_C u(Z-a-b)(Z-a-b)^{-1} + \frac{q}{H} Z \tag{3.2}$$

where

$-R_B u(Z-a)(Z-a)^{-1}$ and $-R_C u(Z-a-b)(Z-a-b)^{-1}$ are discontinuous functions, and Z denotes the depth from the soil surface. Substituting R_B and R_C of Eq. (3.1) in Eq. (3.2), and applying the differential relationship of the external load and beam deflection, the following equation is obtained:

$$EIy'''' = q(Z) = -\frac{qH}{2b}\left(a+b-\frac{2}{3}H\right)u(Z-a)(Z-a)^{-1}$$

$$-\frac{qH}{2b}\left(\frac{2}{3}H-a\right)u(Z-a-b)(Z-a-b)^{-1} + \frac{q}{H}Z \tag{3.3}$$

where

E = Young's modulus

I = moment of inertia

y = wall deflection

Integrating equation (3.3), with the boundary conditions for beam deflection, for translation case.

$$y(a) = 0, \quad y(a+b) = 0$$

Thus, the final expressions for $y(Z)$ becomes

$$EIy = -\frac{qH}{12b}\left(a+b-\frac{2}{3}H\right)u(Z-a)(Z-a)^3$$

$$-\frac{qH}{12b}\left(\frac{2}{3}H-a\right)u(Z-a-b)(Z-a-b)^3$$

$$+\frac{1}{120}\left(\frac{q}{H}\right)Z^5+\frac{Z}{120b}\left(\frac{q}{H}\right)a^5+\frac{qHZ}{12}\left(a+b-\frac{2}{3}H\right)b$$

$$-\frac{Z}{120b}\left(\frac{q}{H}\right)(a+b)^5+\frac{a}{120b}(a+b)^5-\frac{aqH}{12}\left(a+b-\frac{2}{3}H\right)b$$

$$-\frac{a}{120b}\left(\frac{q}{H}\right)a^5-\frac{1}{120}\left(\frac{q}{H}\right)a^5 \qquad (3.4)$$

To reduce the maximum wall deflection and generate a relatively uniform distribution of wall deformation, the vertical positions of the wall driving rods are subjected to $\delta_A=\delta_D=\delta_E$.

where

$\delta_A=$ deflection at point A

$\delta_D=$ deflection at point D

$\delta_E=$ max. deflection between point B and point C (deflection at point E)

The result of Eq. (3.4) with the constrant mentioned is obtained:

$a=$ 360 mm, $b=$ 472.64 mm, $Z_1=$ 590 mm, where $Z_1=$ distance from soil surface to point E. Based on the result above, the upper driving rods are positioned at 360 mm below soil surface, which is 430 mm below the top of the wall. The lower driving rods are positioned at 472 mm below the upper rods.

2. Thickness of Model Wall

The model wall is designed for active earth pressure tests only. The model wall is designed to resist earth pressure at rest following Jaky's formula. The lateral earth pressure is computed for dry Ottawa sand which has the unit weight γ=15.14 kN/m^3, with an internal friction angle of ϕ=30°.

The loading condition of the beam is shown in Fig. 3.11. The intensity of Jaky earth pressure at the base of the wall is calculated as the following:

$$q = K_0 \gamma HW = (1-\sin\theta)\gamma HW$$

$$= (1-\sin 30°)\left(15.14 kN/m^3\right)(1m)(1.5m)$$

$$= 11.35 kN/m$$

The maximum deflection of the model wall is calculated from Eq. (3.4):

$$EI\delta_{\max} = -\frac{qH}{12b}\left(a+b-\frac{2}{3}H\right)u(Z-a)(Z-a)^3$$

$$-\frac{qH}{12b}\left(\frac{2}{3}H-a\right)u(Z-a-b)(Z-a-b)^3$$

$$+\frac{1}{120}\left(\frac{q}{H}\right)Z^5+\frac{Z}{120b}\left(\frac{q}{H}\right)a^5+\frac{qHZ}{12}\left(a+b-\frac{2}{3}H\right)b$$

$$-\frac{Z}{120b}\left(\frac{q}{H}\right)(a+b)^5+\frac{a}{120b}(a+b)^5-\frac{aqH}{12}\left(a+b-\frac{2}{3}H\right)b$$

$$-\frac{a}{120b}\left(\frac{q}{H}\right)a^5-\frac{1}{120}\left(\frac{q}{H}\right)a^5$$

where

E = Young's modulus of the wall $= 190 GPa$

$q =$ intensity of earth pressure at wall base $= 11.35 kN/m$

$H =$ wall height $= 0.5m$

$a = 0.36m$, $b = 0.472m$, and $Z_1 = 0.59m$

the maximum deflection in Eq. (3.4) can be transformed to Eq. (3.5).

$$EI\delta_{\max} = 9.16 \times 10^{-5} q \tag{3.5}$$

Ichihara and Matsuzawa (1973) plotted the coefficient of earth pressure K relative to wall displacement S for a 550 mm high wall backfilled with dry uniform sand (Fig.3.12). The wall movement from zero to 0.001 mm in their study (S/H = 0.0000018) corresponds to the value from 0.88 to 0.8772 of K. The ΔK holds 0.41% of the range between 0.88 and 0.8772. This deformation amount (S/H = 0.0000018) is satisfying since the wall is not a perfectly rigid body. Consequently for the 1000 mm-high NCTU model wall, it can be considered as a rigid wall if the maximum wall deflection is less than 0.0018 mm.

From equation (3.5):

$$EI\delta_{\max} = 9.16 \times 10^{-5} q$$

$$I = \frac{\left(9.16 \times 10^{-5} m^4\right) \times \left(11.35 kN/m\right)}{\left(190 \times 10^9 N/m\right) \times \left(0.0018 \times 10^{-3} m\right)} = 3.03 \times 10^{-6} m^4$$

The typical cross section of the loaded beam is shown in Fig. 3.13. For the moment of inertia of the section under consideration:

$$I = \frac{bH^3}{12} = \frac{(1.5m)H^3}{12} = 3.03 \times 10^{-6} m^4$$

$$H = 0.029m = 29mm$$

The NCTU wall thickness should be calculated at least 29 mm to minimize the effect of wall deflection. The final wall thickness of 50 mm is adopted. The thickness of the central part of the model wall is 45 mm for installation of the soil pressure transducers.

3. Structure of Model Wall

Fig. 3.14 and 3.15 shows the dimensions of the model wall. The steel model wall is 1,500 mm wide, 1,070 mm high, and 50 mm thick. The model wall is vertically supported by two rollers. Two driving systems seperately control the upper and the lower driving rods to simulate various kinds of wall movement in the field.

Fig.3.16 and Fig. 3.17 shows two 45-degree notches has been grooved at the bottom of the model wall. Other two notches are grooved on the top of the fixed bed, which is below the wall. The top grooves are located exactly above the bottom ones. Two 30 mm-diameter steel balls allow the model wall to move parallel to the longitude of the soil bin. The gap clearance between the model wall and the fixed bed shown in Fig. 3.18 is influenced by the thickness of the wall and the desired wall rotation angle. A smaller gap can reduce leakage of the backfill during wall movement. The gap width is designed to be 1 mm, corresponding to the wall thickness of 50 mm and the wall rotation of $\pm 2°$.

The soil pressure transducers are installed on the model wall to observe the distribution of lateral earth pressure. The arrangement of the transducers should be close enough to closely monitor the distribution of pressure changes with depth.

Ten soil pressure transducers (Kyowa PGM-02KG) shown in Fig. 3.19 were arranged along the center line of the model wall as shown in Fig. 3.20. In addition, other three transducers were placed between the center line and the side wall to investigate the side wall effects. The soil pressure transducers were built very stiff to eliminate the effects of soil arching. They were flush-mounted to the surface of the model wall.

The NCTU K_A model retaining wall can simulate different types of wall movements. The geometry of the model wall rotation about the top (RT mode) in active state is shown in Fig. 3.21. The lateral movement ratio of the lower driving rods over the upper rods is (360+472)/360 = 2.31. If the maximum horizontal wall movement at the base of the wall is 0.005H (5mm) with the backfill height (H=1000 mm). In this situation, the lower driving rods should move 4.17mm, and the movement is 1.80 mm at the upper rods.

The geometry of the model wall rotation about the base (RB mode) in active state is shown in Fig. 3.22. The lateral movement ratio of the upper driving rods over the lower rods is (472+168)/168=3.81, regardless of the level of soil surface. With the maximum wall movement at the top of backfill 0.005H (5mm), the upper driving rods moves 3.2 mm and the lower rods moves 0.84 mm.

In the experiments, Ottawa sand would be deposited by air-pluviation into the soil bin. An acrylic cover shown in Fig. 3.23 was designed and constructed allocated to protect the servo motor and driving system from dust. An opening was made at the back side of the acrylic cover, so that operators can enter the space to

replace soil pressure transducers and set up displacement dial gauges behind the model wall.

3.3.3 Driving System

The driving system is used to push and pull the model retaining wall. It consists of four componets: (1) driving rods; (2) servo motor; (3) control panel; and (4) inductive proximity switch. Fig. 3.24 illustrates the operation of wall driving system, and the details are described in the following sections.

1. Driving Rods

Four driving rods are attached on the model wall to push and pull the model wall. Fig. 3.25 shows the hinge-and-slider connection connecting between the driving rod and the model wall. The connection could keep the driving rod at the same elevation when the model wall rotates.

2. Servo Motor

The servo motor uses feedback signals to control the speed of driving rods accurately. Two servo motors (Sinano Electric 8CB75-2DE7FAS) shown in Fig.3.26 have been installed to propel the upper and lower driving rods independently. The maximum rotation speed of motor is 3000 rpm. In Fig.3.27, two speed reducers (gear ratio 60:1) are installed in front of the motors to control the speed of shaft. The horizontal shaft propel the two worm gear linear actuators (worm gear ratio 16:1). After conversions, it needs 960 revolutions of motor to pull each pitch distance of 8mm. The rotation speed of motor is subject to the capacity of 1PG (AX_{2n}-1PG), which can generate 100,000 pulses per seconds. The motor

needs to receive 8000 pulses for each revolution (8000 ppr). Thus the maximum wall speed can be programmed to 0.001 mm/s to 0.1 mm/s through the Programmable Logic Controller (PLC) in the control panel. The speed of driving rod can be easily operated from the touch-control LCD display.

3. Control Panel

The control panel has attached a touch-control LCD display (Fig. 3.28) to input the controlled paramters. There are three operation modes on the control panel to control wall movements. The first mode is to input the speed and running time for upper and lower rods respectively. The second one is to input the positon coodinates of upper and lower driving rods. And the third is to input an additional displacement from present position coodinates. Threrfore, various experimental demands for wall movements can be achieved. In Fig. 3.29, the wall speed and running time can be set on the LCD screen of the control panel.

4. Inductive Proximity Switch

In Fig. 3.30, the inductive proximity switch (IFRM 08N1701/L) and the limit switches are set on the driving rod. The inductive proximity switch detects the position of an object and transforms a electronic signal. The initial position of the metal ring is right below the sensor. After the motor begins to operate, the metal ring starts to move with the same speed as the wall. When the wall returns to the initial position, the inductive switches can sense the matal ring and send a “stop” signal to the servo drive. This mechanism ensures that the model wall will return to its original position after each test.

The purpose of limit switches is to prevent unusual operation of motors. If the servo motors do not follow the commands from contorl panel, it will stop the operation of servo motors when metal rings pass through the limit switches.

3.3.4 Data Acquisition System

Due to the considerable amount of data collected by the soil pressure transducers and displacement transducers, a data acquisition system shown in Fig. 3.31 was used for this study. It is composed of the following four parts: (1) dynamic strain amplifiers (Kyowa: DPM601A and DPM711B); (2) NI adaptor card; (3) AD/DA card; and (4) personal computer. The analog obtained signals from the sensors are filtered and amplified by dynamic strain amplifiers. Analog experimental data are converted to digital data by the A/D – D/A card. The LabVIEW program is used to acquire test data. Experimental data are stored and analyzed with a Pentium 4 personal computer.

Chapter 4

Backfill and Interface Characteristics

The properties of the backfill (Ottawa sand) the friction between the backfill and the acrylic sidewalls, and the friction between the backfill and the steel model wall are discussed in this chapter. The following sections include: (1) backfill properties; (2) the method to prepare the backfill; (3) the method to control soil density; (4) sidewall friction; and (5) model wall friction.

4.1 Backfill Properties

4.1.1 Characteristics of Backfill

Air-dry Ottawa silica sand (ASTM C-778) is used in the experiments. Table 4.1 lists out the physical properties of Ottawa sand. Grain-size distribution of the backfill is shown in Fig. 4.1. The major reasons to select Ottawa sand as the backfill material are listed below.

1. the round particle shape can avoid problems of angularity,
2. the uniform distribution of grain size (coefficient of uniformity Cu = 1.78) can avoid problems of soil gradation,
3. the high particle rigidity can reduce disintegration of soil particles under loading
4. the high permeability can drain very fast and avoid water pressure against the wall.

Direct shear tests were conducted to establish the relationship between unit weight γ of backfill and its internal friction angle ϕ. The shear box has a square cross section (60 mm × 60 mm) as shown in Fig. 4.2. Figure 4.3 illustrates the relationship established by Chang (2000). It shows that the soil strength rises with increasing soil density. The empirical relationship for the air-pluviated backfill is

$$\phi = 6.43\gamma - 68.99 \tag{4.1}$$

where

ϕ = angle of internal friction of soil (degree)

γ = unit weight of soil (kN/m3)

Eq. (4.1) is applicable for the range of γ = 15.45 ~ 17.4 kN/m^3.

For compacted backfill, the following relationship can be formulated.

$$\phi = 7.25 - 79.51 \tag{4.2}$$

Eq.(4.2) is applicable for the range of γ = 15.8 ~ 17.05 kN/m^3.

4.1.2 Air Pluviation of Backfill

To control the soil density in the backfill, Ottawa sand was deposited by air-pluviation method into the soil bin. The air-pluviation is a popular method to reconstitute laboratory sand specimens. Rad and Tumay (1987) concluded that pluviation is an efficient method to provide reasonable homogeneous specimens with desired density. Lo Presti et al. (1992) also mentioned that the pluviation method could shorten the time to acquire good specimens. Fig. 4.4 shows the Air-pluviation process of Ottawa sand. Soil particles flow through a calibrated slot of the soil hopper into the soil bin.

Das (1994) defined the loose sand has the relative density D_r of 15~50%, and the dense sand has D_r= 70~85%. Ho (1999) established the relationship among slot opening, drop height, and soil density as shown in Fig. 4.5.

4.1.3 Compaction of Backfill

To create a dense condition to simulate field conditions, the air-pluviated loose backfill was densified with a vibratory compactor. Air-dry Ottawa sand was shoveled from the soil storage into the soil hopper, air-pluviated into the soil bin, then compacted with a soil compactor.

The vibratory soil compactor with the base area of 225 mm × 225 mm is illustrated in Fig. 4.6 and Fig. 4.7. The acentric motor is fixed on the steel compaction plate of the compactor. The height of the handle is 1.0 m, and of the mass of the compactor is 12.1 kg (0.119kN). Chen (2003) reported the peak cyclic vertical force (static + dynamic) measured with a load cell placed under the base plate of the vibratory compactor was 1.767kN, and the frequency of vibration is 44 Hz. With the 225 mm × 225 mm compaction plate, the peck cyclic normal stress σ_{cyc} applied on the surface of soil was 34.9 kN/m^2.

With the square compactor, each lift of backfill was contolled compacted to be 0.2 m-thick after compaction. The top surface of the lifts were carefully maintained to make a horizontal soil surface.The surface of the backfill was divided into 6 lanes shown in Fig. 4.8. Each lift was densified with a square vibratory compactor. Each lane was densified with the compactor for a pass of 70 seconds. The compaction procedures were repeated until the height of the compacted backfill

reached 1 m. Fig. 4.9 shows the compaction of the backfill with the square compactor.

Chang (2002) reported that the soil density achieved by the compaction was affected by the number of acentric plates attached to the motor on the soil compactor. The number of the acentric plate varies from 1 + 1 to 10 + 10. And the relative densities ranges from 38 % to about 95 %. In this study, the number of acentric plates attached to the motor was 8 + 8, which means 8 pieces of acentric plates were attached to the front-end of the motor axis, and another 8 pieces were attached to the rear-end.

4.1.4 Distribution of Soil Density

To study the distribution of the soil density in the soil bin, soil density control cups were used. The soil density control cups are made of acrylic as shown in Fig. 4.10 and Fig. 4.11. Density cups were buried in the soil mass in different elevations and at different locations in the backfill as shown in Fig. 4.12 and Fig. 4.13.

After compaction, the buried soil density cups were carefully dug out of the soil. The density of the soil sample was calculated as the weight of the soil in the cup devided by the cup volume. The distribution of the soil density at different elevations is shown in Fig. 4.14. Excluding the 2 data points in the top 0.15 m, the mean relative density is D_r = 77.8 % with a standard deviation of 3.4 %. Das(1994) defined the relative density of the dense granular soil to be D_r = 70~85 %. It is obvious that the Ottawa sand has been compacted to a dense state. It also may be seen in Fig. 4.14 that the soil density near the surface of fill was not as dense as

expected. D'Appolonia et al. (1969) reported that, with a low confining pressure, the soil near the surface may not be dense after compaction (Fig. 4.15).

4.2 Interface Friction

4.2.1 Side Wall Friction

To constitute the plane strain condition for the model wall experiments, the shear stress between the backfill and sidewall should be eliminated. A lubrication fabricated layer with plastic sheets was equipped for all experiments to reduce the interface friction between the sidewall and the backfill. The lubrication layer consists of one thick and two thin plastic sheets as suggested by Fang et al.(2004). All plastic sheets had been vertically placed next to both side-walls before the backfill was deposited (Fig. 4.16).

The friction angle between the plastic sheets and the sidewall was determined by the sliding block tests. The schematic diagram and the photograph of the sliding block test by Fang et al. (2004) are illustrated in Fig. 4.17 and Fig. 4.18. The sidewall friction angle δ_{sw} is determined based on physics principles. Fig. 4.19 shows the variation of friction angle δ_{sw} with normal stress σ based on the plastic sheet lubrication method. The friction angle measured was 7.5°. With the plastic – sheet lubrication method, the interface friction angle is almost independent of the applied normal stress. The shear stress between the acrylic side-wall and backfill could be effectively reduced with the plastic-sheet lubrication layer.

4.2.2 Model Wall Friction

Direct shear tests were conducted to obtain the friction angle δ_w between the backfill and the steel model wall. A smooth steel plate (63 mm in diameter and 25 mm in height, made of the same material as the model wall) was replaced in the lower shear box. Ottawa sand was poured and compacted in the up shear box. Fig. 4.20 shows the arrangement of this test.

Fig. 4.21 illustrates the relationship between the unit weight of the backfill γ and the wall friction angle δ_w. An empirical relationship can be formulated as below

$$\delta_w = 3.02\gamma - 29.49 \tag{4.3}$$

where

δ_w = wall friction angle (degree)

γ = unit weight of backfill (kN/m3)

Equation (4.3) is applicable for the range of γ = 15.5 ~16.9 kN/m^3.

A comparison among the internal friction angle of sand ϕ, wall friction angle δ_w, and sidewall friction angle δ_{sw} is shown in Fig. 4.22. With the same unit weight, the sequence of the friction angle is $\phi > \delta_w > \delta_{sw}$.

Chapter 5

Experimental Results

This chapter reports experimental results regarding the horizontal earth pressures associated with soil compaction and active wall movement. For all experments, the surface of backfill was horizontal and the backfill was filled up to 1.0 m above the base of the model wall. The experimental study was conducted in the new NCTU K_A model retaining wall facility discussed in Chapter 3.

5.1 Earth pressure due to compaction

Chen (2003) reported experimental results regarding the compaction-induced earth pressure as shown in Fig. 2.35. All of his experiments were conducted in NCTU non-yielding retaining wall facility. Chen (2003) reported that after compaction, extra horizontal earth pressure was induced by vibratory compaction (Fig. 2.35(e)). Chen (2003) indicated that below the compaction-influenced zone, the horizontal stresses converge to the earth pressure at-rest, as indicated in Fig. 2.35(e). For the tests with the new K_A model retaining wall, it is very difficult to achieve an at-rest state in the backfill. As listed in Table.5.1, after filling and compaction of backfill, the K_A model wall has already moved in the active direction. Fig. 5.1 illustrates the variation of wall movements during compcation of backfill. Therefore, experimental results regarding the earth pressure at-rest after compaction has been borrowed from Chen's study.

5.2 Wall movement required to achieve active state

Chang (2000) establish the wall movement required for the backfill to achieve an active state of $(S/H)_a$ for different soil internal friction angles (Fig. 5.2). For dense sand, the required $(S/H)_a$ is about 0.0005~0.001. For loose sand, the $(S/H)_a$ required is about 0.0016~0.0030. In this study, the maximum $(S/H)_a$ required for compacted dense sand is about 0.0010. However for most experiments in this study, the wall movement varies from 0 up to 0.003H.

5.3 Experimental results

5.3.1 Distribution of horizontal earth pressure

All tests are considered as T mode wall movement, and actual wall positions during wall movement is shown in Fig. 5.3. Fig. 5.4~5.6 shows the distribution of lateral earth pressure for the dense backfill with a relative density of approximately 75%. It could be observed in Fig. 5.4 that earth pressure induced by compaction vanished rapidly with the active wall movement. An active state of stress is reached at the wall movement of S/H=0.0010. The distribution of active earth pressure is slightly higher than Coulomb's solution at the upper one-third of wall height, approximately in agreement with Coulomb's solution in the middle one-third, and lower than Coulomb's solution at the lower one-third of wall surface. This experimental result is quite similar to the result from Fang and Ishibashi (1986)

shown in Fig. 2.24.

Fig. 5.7~5.9 shows the distribution of earth pressure from different tests at the wall movements of S/H= 0.001, 0.002, and 0.003. It may be seen in Fig. 5.7 that, at the active wall movement of S= 0.001H, the extra earth pressure induced by compaction was relaxed by the active wall movement. It is possible that the stresses that were locked-in the soil element has been released with the lateral extension of the active soil wedge.

5.3.2 Variation of horizontal earth pressure coefficient

In Fig. 5.10, the horizontal earth pressure coefficient K_h decreases with increasing wall movement and finally a constant total thrust is reached. The coefficient K_h is defined as the ratio of the horizontal component of total thrust to $\gamma H^2/2$. The ultimate value of K_h is defined as the active earth pressure coefficient $K_{a,h}$. For the three set of data shown in Fig. 5.10, the active condition occurred at the wall movement of approximately S/H= 0.001. The active thrust P_h is calculated by summing the earth pressure acting on the wall. For comparison purposes, the active earth coefficients determined from Coulomb and Rankine theories are also plotted in Fig. 5.10. It is found that the experimental $K_{a,h}$ values are in good agreement with Coulomb and Rankine's prediction.

5.3.3 Location of soil-thrust

Fig. 5.11 shows the point of application h/H of the soil thrust with the wall movement. The distance between the point of application of total resultant force and

wall base is defined as h. Fig. 5.4 shows that the distribution of lateral earth pressure is not linear with depth with the active wall movement. In Fig. 5.7, at the wall movement of S/H=0.001, the distribution of active pressure is slightly higher than Coulomb's solution at the upper H/3 of wall, and lower than Coulomb's solution at the lower H/3 of wall. This is the reason why the active thrust is located at about 0.55H above the base of the wall.

5.3.4 Active earth pressure coefficient

Fig. 5.12 displays the experimental and theoretical relationships between the active earth pressure coefficient $K_{a,h}$ and the internal friction angle ϕ of the backfill. Experimental data reported by Terzaghi (1934), Mackey and Kirk (1967), Bros (1972), Sherif et al. (1982), Fang et al. (1997) and Chang (2000) are also included in Fig. 5.12. The active coefficient $K_{a,h}$ values obtained with compacted dense sand from this study are in fairly good agreement with Coulomb and Rankine's prediction. Based on the experimental data, it is found that the Coulomb and Rankine theories may slightly overestimate the $K_{a,h}$ value for medium dense and dense backfill.

5.4 Surface crack

To study the sliding of active wedge and observe the extent of failure zone, special experiments were conducted. For these tests, the maximum wall movement reached was 16 mm (S/H=0.016). For the compacted sand, the surface crack of the top of backfill occurs at the wall movement of S/H=0.008. Fig. 5.13 and Fig. 5.14

shows the surface cracks on the backfill at the translational wall movement of 16 mm (S/H = 0.016). In Fig. 5.13, the distance between the surface of model wall and the crack is about 470 mm to 490 mm. It is quite close to the prediction of d = 477 mm based on Rankine's theory. In Fig. 5.14, the distance between the surface of wall and the crack is about 460 mm. It is in good agreement with the prediction of d = 458 mm based on Rankine's theory. It can be concluded that the Rankine theory is suitable to predict the location of surface crack for active failure.

5.5 Mechanism of stress reduction of compaction-induced pressure

Chen (2003) proposed the mechanism of lateral stess increase due to backfill compaction. The bearing capacity failure of a surface footing is used to interpret the mechanism of soil behavior due to vibratory compaction. Fig. 2.36 shows if the cyclic compacity stress σ_{cyc} applied on the surface of fill exceeded the ultimate bearing capacity q_{ult} of foundation soil, the loaded surface ab would settle and shear failure zone would develop in the uppermost layer of fill. In Fig. 2.36 (a), the soil element A in zone III would be in the passive Rankine zone. The soil element is compressed laterally. The moving and capacity of the tamper all over the soil surface would result in a passive soil layer near the top of the compacted fill.

In this study, with the active wall movement, the soil elements near the model wall is subjected to lateral extension. With the increasing wall movement, the soil elements in the compaction influenced zone are allowed to expand laterally, and the

passive state of stress no longer exists. Eventually, an active state is reached and the extra horizontal pressure induced by compaction would gradually vanish.

Chapter 6

Conclusions

This paper studies the reduction of compaction-induced earth pressure with active wall movement. A new K_A model retaining wall facilty of National Chiao Tung University has been designed and constructed. Based on the experimental data obtained during this investigation, the following conclusions can be drawn about earth pressure acting on a rigid wall that moves toward a backfill of dry sand under translational movement.

1. The earth pressure induced by compaction vanished rapidly with the active wall movement. An active state of stress is reached at the wall movement of S/H = 0.0010.
2. The distribution of active earth pressure is slightly higher than Coulomb's solution at the upper one-third of wall height, approximately in agreement with Coulomb's solution in the middle one-third, and lower than Coulomb's solution at the lower one-third of wall surface. Stresses that was locked-in the soil element has been released with the lateral extension of the active soil wedge.
3. The horizontal earth presure coefficient K_h decreases with increasing wall movement and finally a constant total thrust is reached. The active condition occurred at the wall movement of approximately S/H= 0.001.

4. The experimental $K_{a,h}$ values are in good agreement with Coulomb and Rankine's prediction.
5. The active thrust is located at about 0.55H above the base of the wall.
6. The active coefficient $K_{a,h}$ values obtained with compacted dense sand from this study are in fairly good agreement with Coulomb and Rankine's prediction.
7. The Rankine theory is suitable to predict the location of surface crack for active failure.

References

1. Bowles, J. E. (1988). *Foundation analysis and design,* 4th Edition, McGraw-Hill Book Co., 474.
2. Brinch Hansen, J. (1953). "Earth pressure calculation." Danish Technical Press, Copenhagen.
3. Bransby, P.L., and Smith, A.A. (1975). "Side friction in model retaining wall experiments." *Journal of the Geotechnical Engineering Division*, ASCE, 101(GT7), July, 615-632.
4. Bros, B. (1972). "The influence of model retaining wall displacements on active and passive earth pressures in sand." *Proc., 5th European Conf. on Soil Mechanics*, Madrid, 1, 241-249.
5. Chang, S.Y. (2000). "Effect of backfill density on active earth pressure." Master of Engineering Thesis, Dept. of Civil Engineering, National Chiao Tung University, Hsinchu, Taiwan.
6. Chen, N. C. (2005). "Earth pressure at-rest near a vertical rock face." Master of Engineering Thesis, Dept. of Civil Engineering, National Chiao Tung University, Hsinchu, Taiwan.
7. Chen, T. J. (2002). "Earth pressure due to vibratory compaction." Ph.D. dissertation, Department of Civil Engineering, National Chiao Tung University, Hsinchu, Taiwan.

8. D'Appolonia, D. J., Whitman, R. V., and D'Appolonia, E. (1969). "Sand compaction with vibratory rollers."*Journal of the Soil Mechanics and Foundations Division*, ASCE, 95(SM1), 263-284.

9. Das, B. M. (1994). "Principal of geotechnical engineering." PWS Publishing Company, Boston.

10. Fang, Y. S. (1983). "Dynamic earth pressures against rotating walls." Ph.D. dissertation, Department of Civil Engineering, University of Washington, Seattle, Washington.

11. Fang, Y. S., and Ishibashi, I. (1986). "Static earth pressures with various wall movements." *Journal of Geotechnical Engineering*, ASCE, 112(3), Mar., 317-333.

12. Fang, Y. S., Chen, J. M., and Chen, C. Y. (1997). "Earth pressures with sloping backfill." *Journal of Geotechnical and Geoenvironmental Engineering*, ASCE, 123(3), March, 250-259.

13. Fang, Y. S., Chen, T. J., Holtz, R. D., and Lee, W. F. (2004). "Reduction of boundary friction in model tests." *ASTM Geotechnical Testing Journal*, 27(1), 1-10

14. Gere, J.M., and Timoshenko, S.P. (1984). "Mechanics of materials." Brooks/Cole.

15. Holl, D. L. (1941). "Plane strain distribution of stress in elastic media." *Iowa Engineering Experimental Station Bulletin*, 148-163.

16. Ichihara, M., and Matsuzawa, H. (1973). “Earth pressure during earthquake.” *Soils and Foundations*, Japanese Society of Soil Mechanics and Foundation Engineering, 13(4), 75-85.

17. Ingold, T. S. (1979). “Retaining wall performance during backfilling.” *Journal of the Geotechnical Engineering Division*, ASCE, 105(GT5), 613-626.

18. Ingold, T. S. (1979). “The effects of compaction on retaining walls.” *Geotechnique*, 29(3), 265-283.

19. Janbu, N. (1957). “Earth pressure and bearing capacity calculation by gerneral procedure of slices.” Proceedings, 4th Int. Conf. Soil Mechs. Found. Eng., London, 2, 207-212.

20. Lo Presti, D. C. F., Pedroni, S., and Crippa, V. (1992). “Maximum dry density of cohesionless soils by pluviation and by ASTM D 4253-83: A comparative study.” *ASTM Geotechnical Testing Journal*, 15(2), 180-189.

21. Mackey, R. D., and Kirk, D. P. (1967). “At rest, active and passive earth pressures.” *Proc., South East Asian Conference on Soil Mechanics and Foundation Engineering*, Bangkok, 187-199.

22. Matteotti, G. (1970). “Some results of quay-wall model tests on earth pressure.” *Proceeding, Institution of Civil Engineers,* 47, 185-204.

23. Morgenstern, N. R., and Eisenstein, Z. (1970). “Methods of estimating lateral loads and deformations.” Proceedings, ASCE Specialty Conference on Lateral Stresses in the Ground and the Design of Earth Retaining Structures, Cornell University, 51-102.

24. NAVFAC. (1982). Foundations and earth retaining structures design manual, Dept. of Navy, DM 7.2, Alexandria, Va.

25. Peck, R. B., and Mesri, G. (1987). Discussion of "Compacted-induced earth pressures under K_o-conditions." *Journal of Geotechnical Engineering*, ASCE, 113(11), 1406-1408.

26. Rad, N. S., and Tumay, M. T. (1987). "Factors affecting sand specimen preparation by raining." *ASTM Geotechnical Testing Journal*, 10(1), 31-37.

27. Sherif, M. A., Ishibashi, I., and Lee, C. D. (1982). "Earth pressure against rigid retaining walls." Journal of Geotechnical Engineering, ASCE, 108(5), May, 679-695.

28. Sowers, G. B., and Sowers, G. F. (1961). *Introductory soil mechanics and foundations*, New York: Macmillan, 386.

29. Terzaghi, K. (1932). "Record earth pressure testing machine." *Engineering News-Record*, 109, Sep., 29, 365-369.

30. Terzaghi, K. (1934). "Large retaining-wall tests." *Engineering News-Record*, 111, 136-140.

31. Terzaghi, K. (1941). "General wedge theory of earth pressure." ASCE Transaction, 106, 68-80.

32. Wang, F. J. (2005). "Effects of adjacent rock face inclination on earth pressure at-rest." Master of Engineering Thesis, Dept. of Civil Engineering, National Chiao Tung University, Hsinchu, Taiwan.

33. Wu, B. F. (1992). “Design and construction of National Chiao Tung University model retaining wall.” Master of Engineering Thesis, Dept. of Civil Engineering, National Chiao Tung University, Hsinchu, Taiwan.

Table 3.1. Wall displacements required to reach active state

Investigator	Soil Type	Type of Wall Movement	Max. Wall Displacement Required
Sowers and Sowers (1961)	Loose Sand	RB mode	0.0020 H
	Dense Sand		0.0005 H
Mackey and Kirk (1967)	Loose Sand	T mode	0.0040 H
	Dense Sand		0.0030 H
Matteotti (1970)	Sand	RB mode	0.0008 H
Bros (1972)	Sand	T mode	0.0006 H
		RT mode	0.0012~0.0018 H
		RB mode	0.0035 H
NAVFAC DM-7.2 (1982)	Loose Sand	—	0.0020 H
	Dense Sand		0.0005 H
Bowles (1988)	Loose Sand	—	0.0020~0.0040 H
	Dense Sand		0.0010~0.0020 H
Fang et al. (1997)	Loose Sand	T mode	0.0015 H

Note: RB = Rotation about base; RT = Rotation about top; T = Translation; and H = Wall height

Table 4.1. Properties of Ottawa sand

Shape	Rounded
e_{max}	0.76
e_{min}	0.50
G_s	2.65
D_{60}, mm	0.32
D_{10}, mm	0.21
C_u	1.78

Table.5.1 Active wall movement at the end of compaction

Test No.	$(S/H)_{up}$	$(S/H)_{down}$	$(S/H)_{avg}$
0826	0.00053	0.00050	0.00052
0827	0.00047	0.00051	0.00049
0829	0.00040	0.00053	0.00046

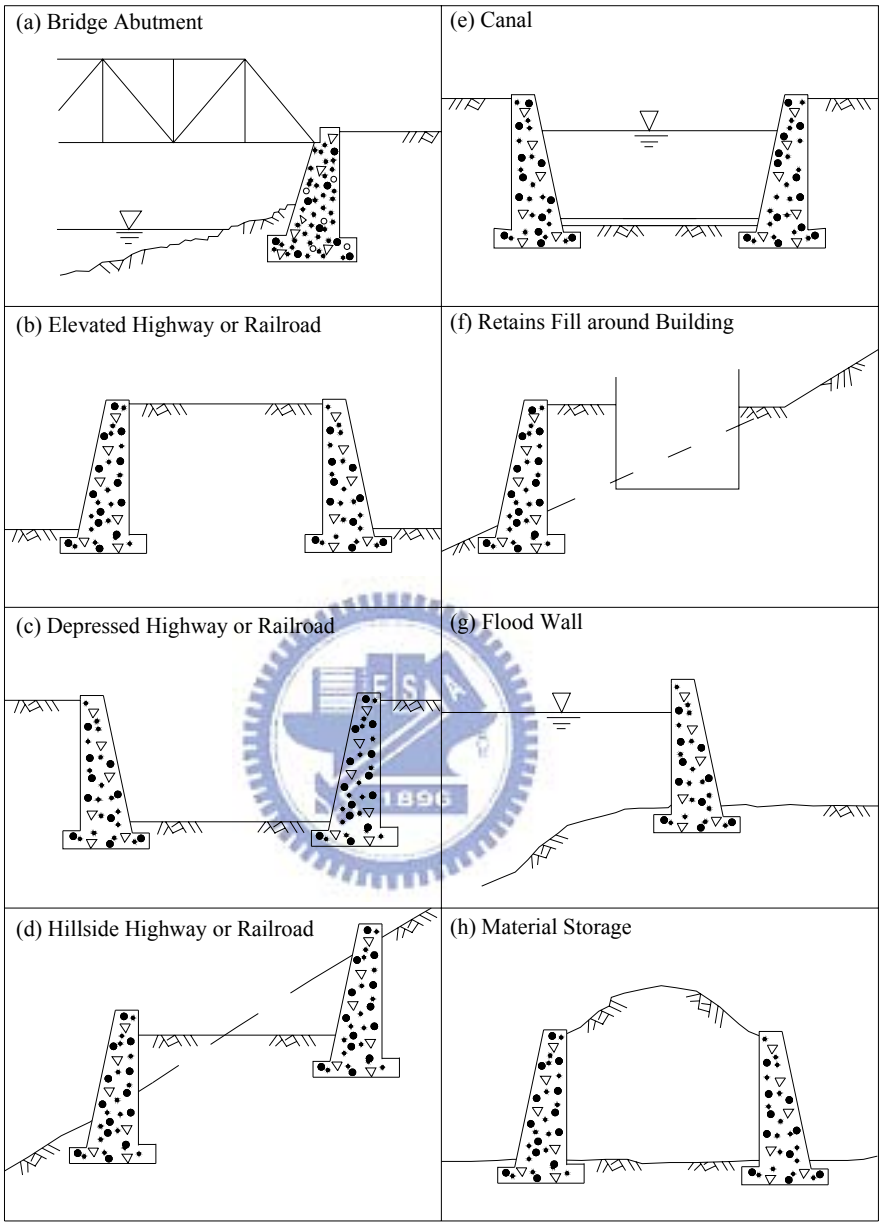

Fig. 1.1 Common uses of retaining walls (after Fang, 1983)

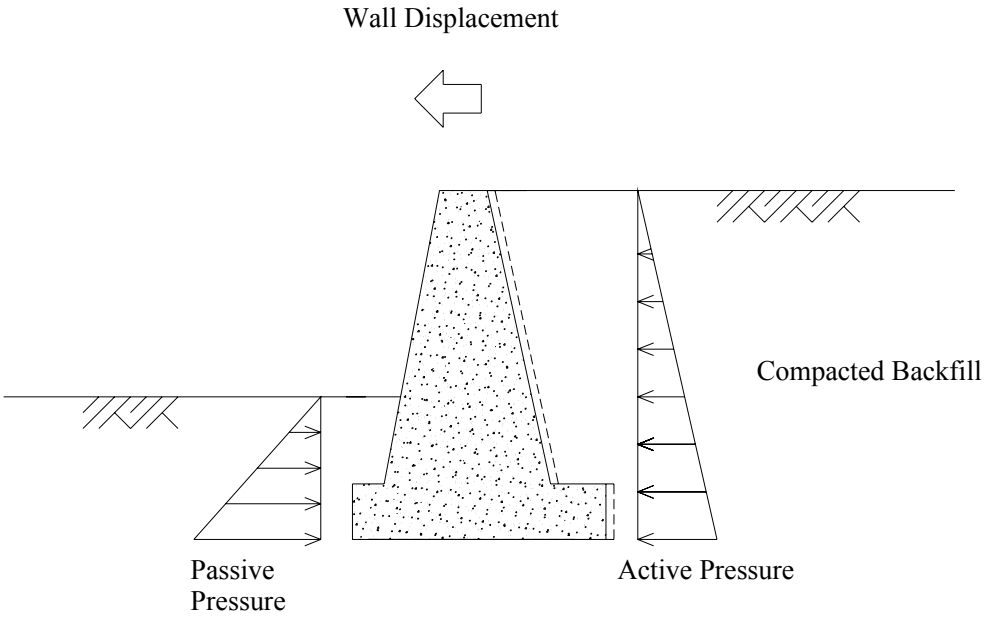

Fig. 1.2 Earth pressure under active wall movement

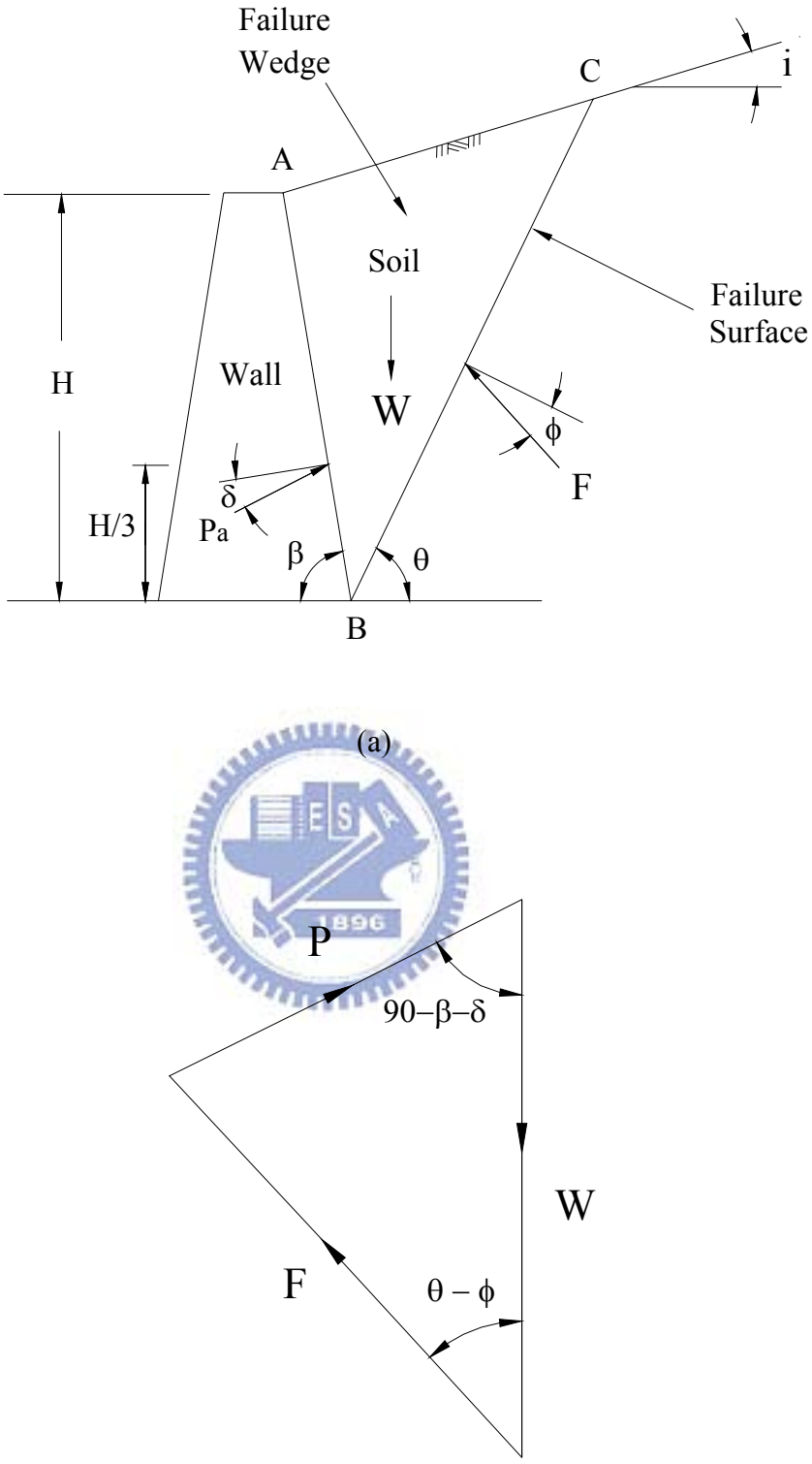

Fig. 2.1 Coulomb's theory of active earth pressure

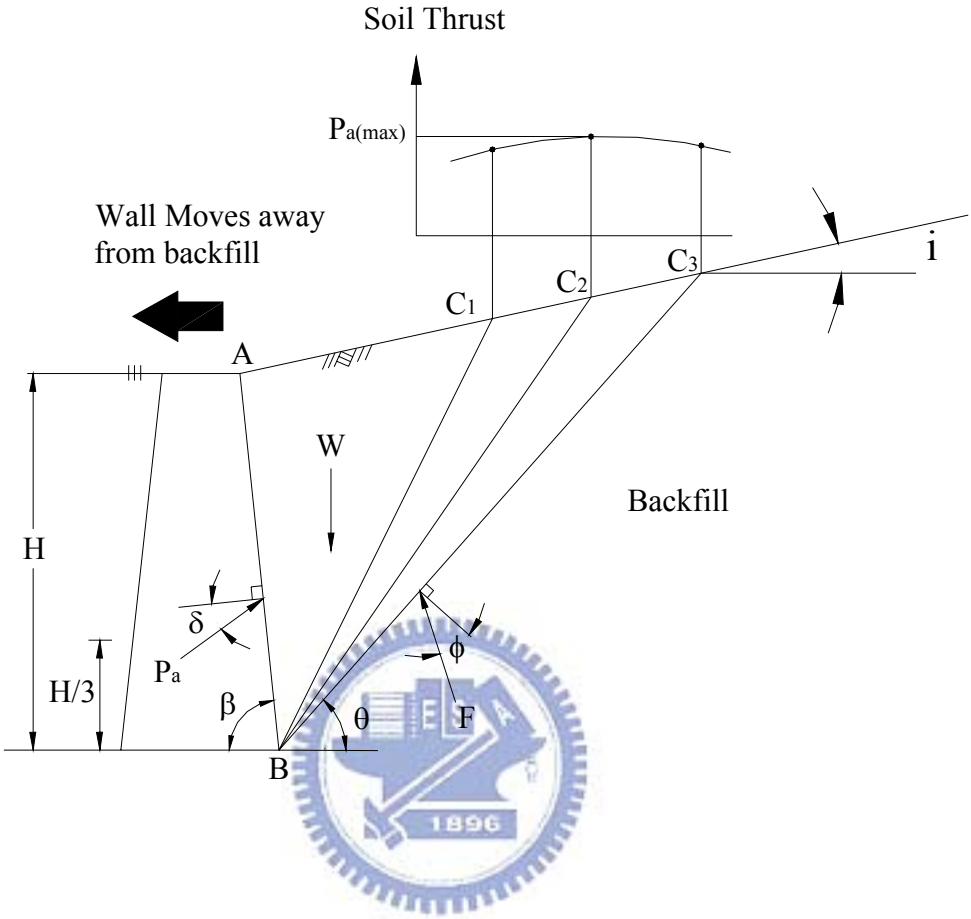

Fig. 2.2 Determination of Coulomb's active earth pressure

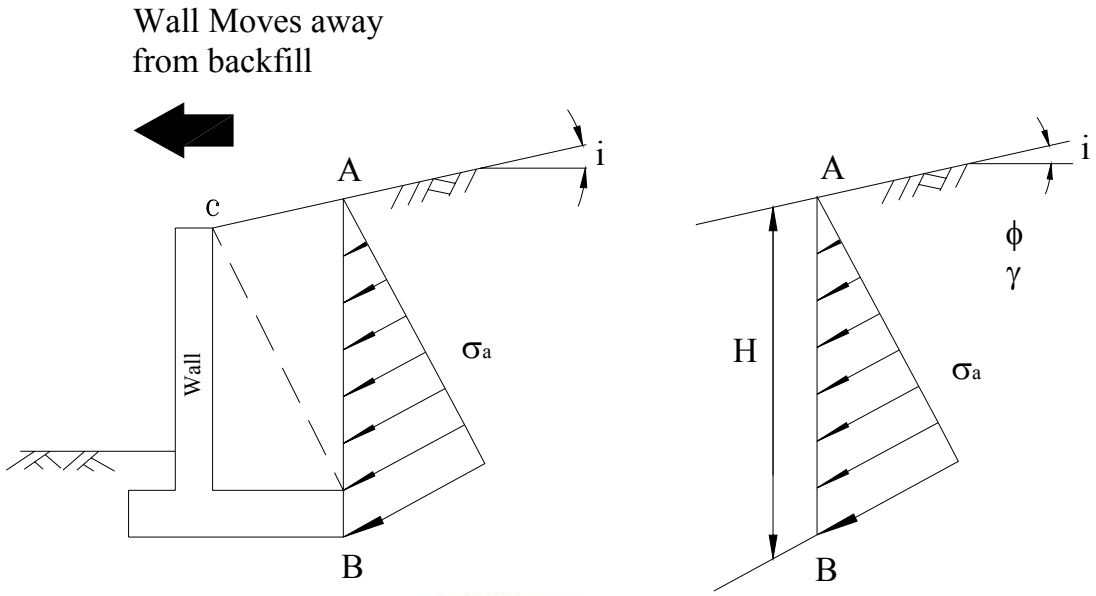

Fig. 2.3 Rankine's theory of active earth pressure

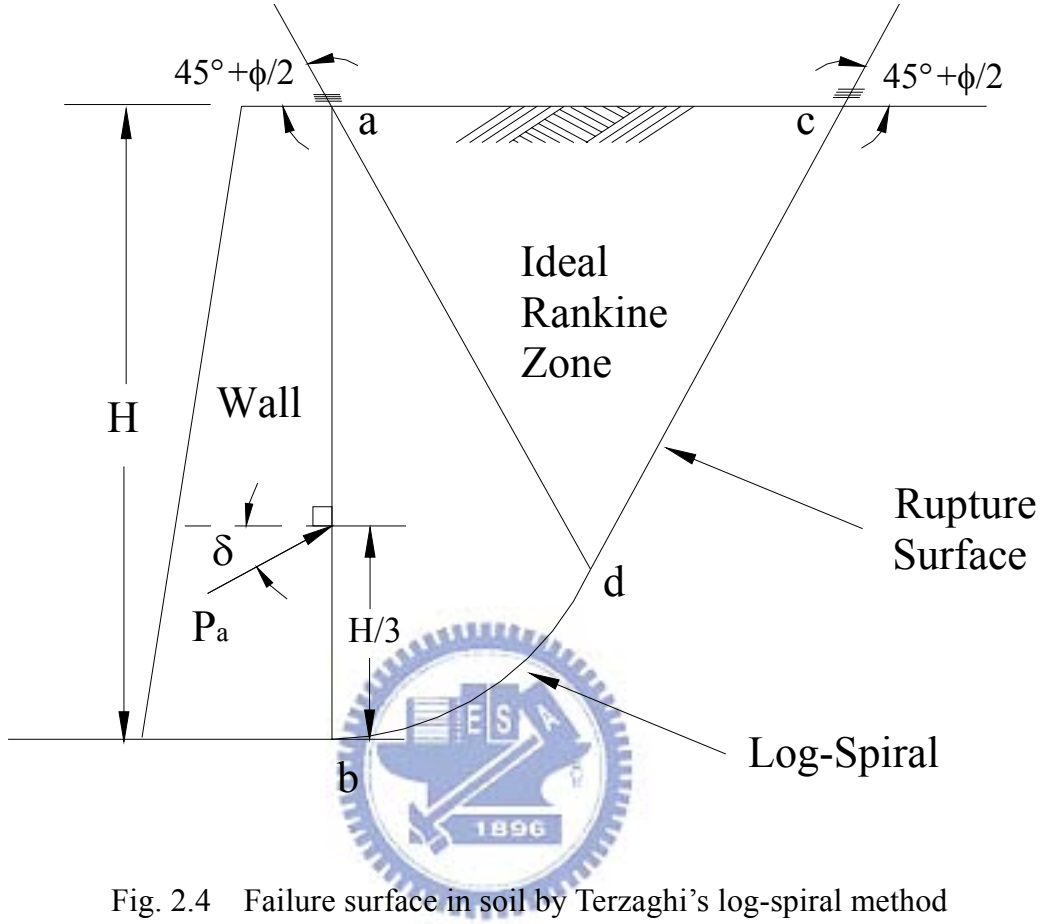

Fig. 2.4 Failure surface in soil by Terzaghi's log-spiral method

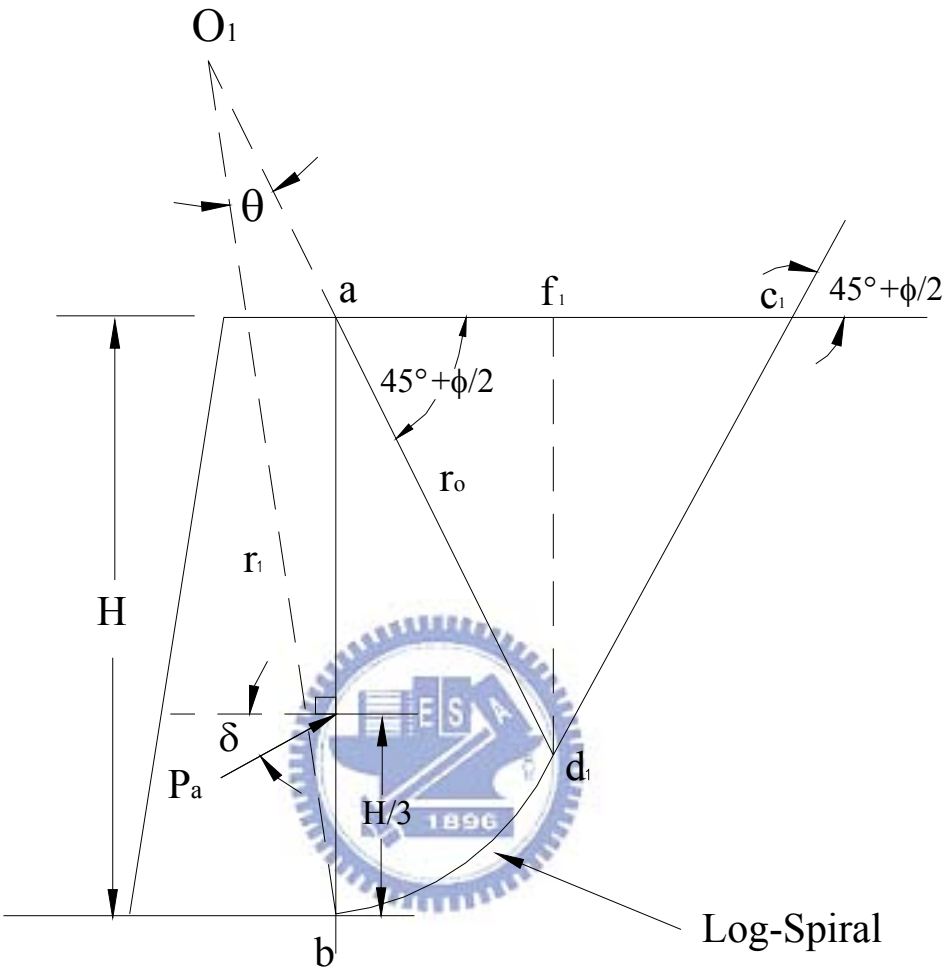

Fig. 2.5 Evaluation of active earth pressure by trial wedge method

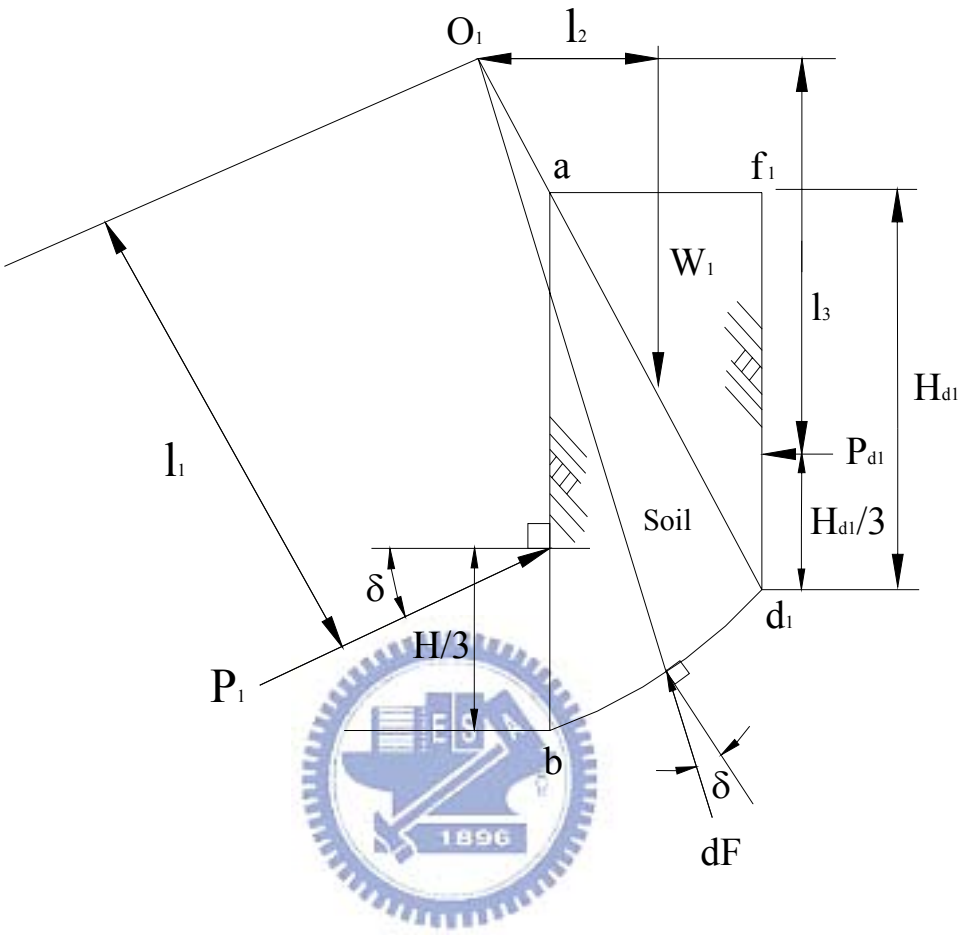

Fig. 2.6 Stability of soil mass abd_1f_1

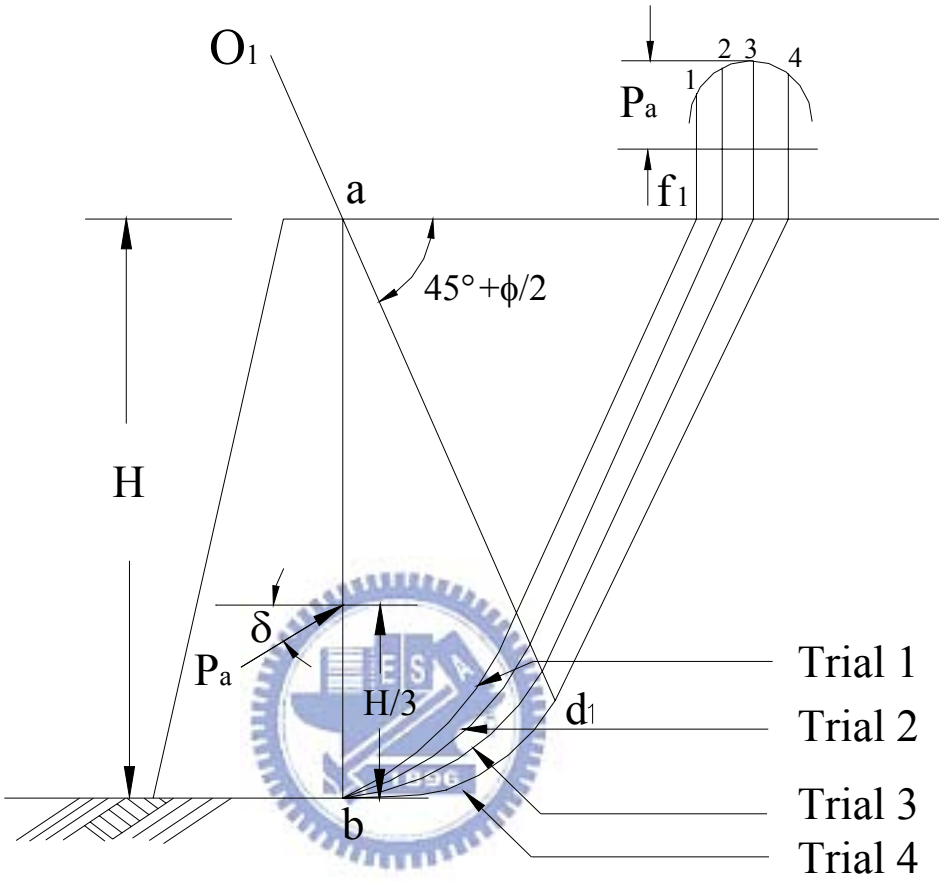

Fig. 2.7 Active earth pressure determination with Terzaghi's log-spiral failure surfaces

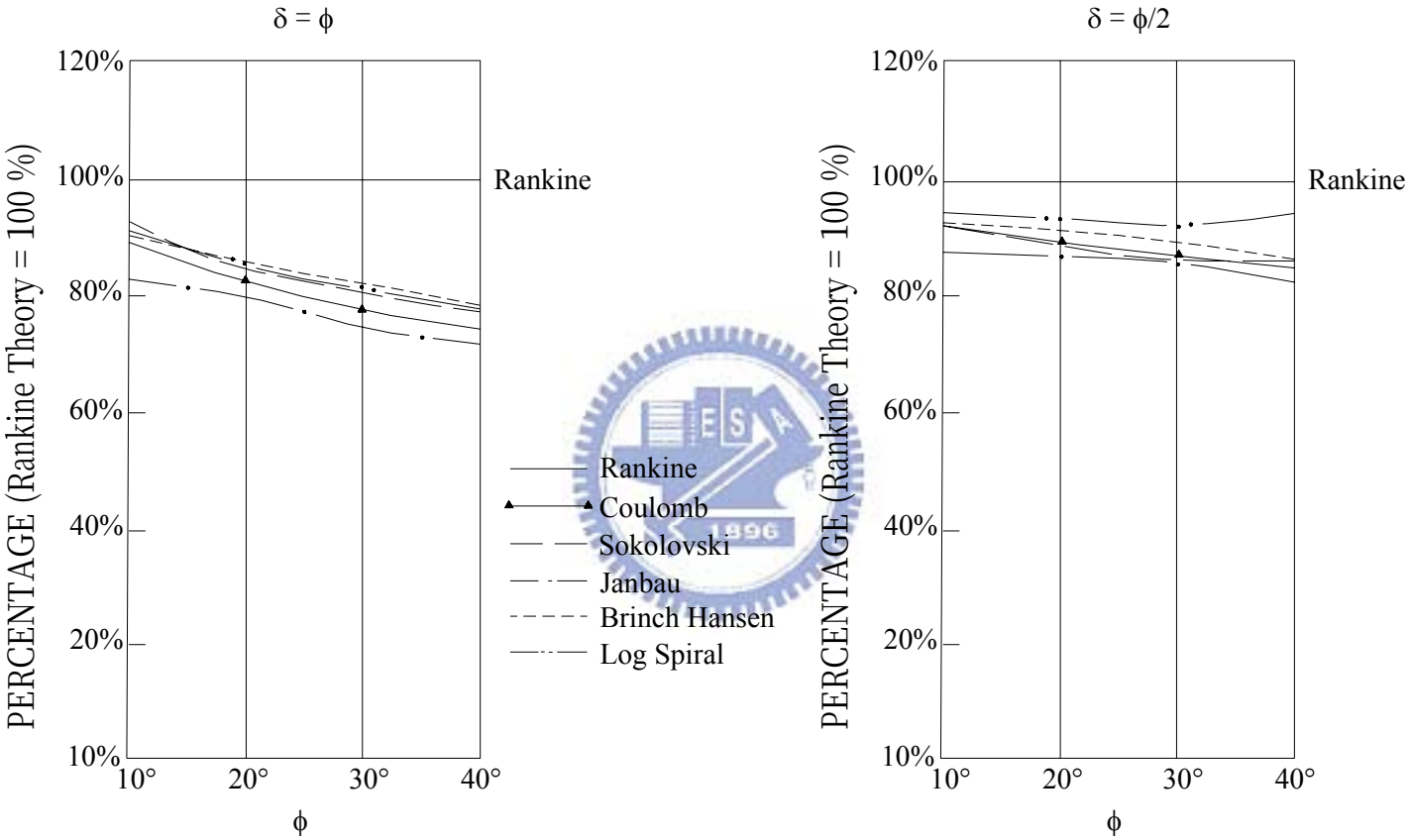

Fig. 2.8 Comparison of coefficient of horizontal component of active pressure for various theories (after Morgenstern and Eisenstein, 1970)

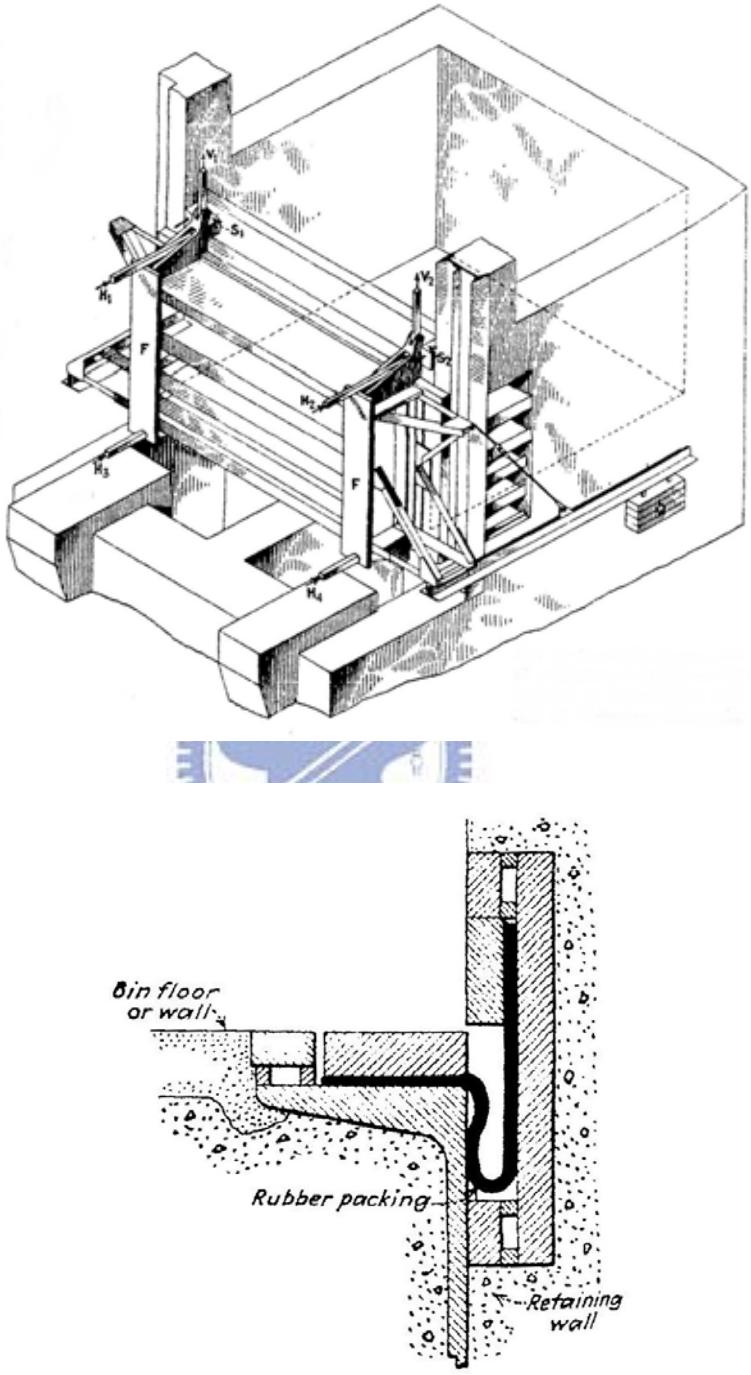

Fig. 2.9 MIT model retaining wall (after Terzaghi, 1932)

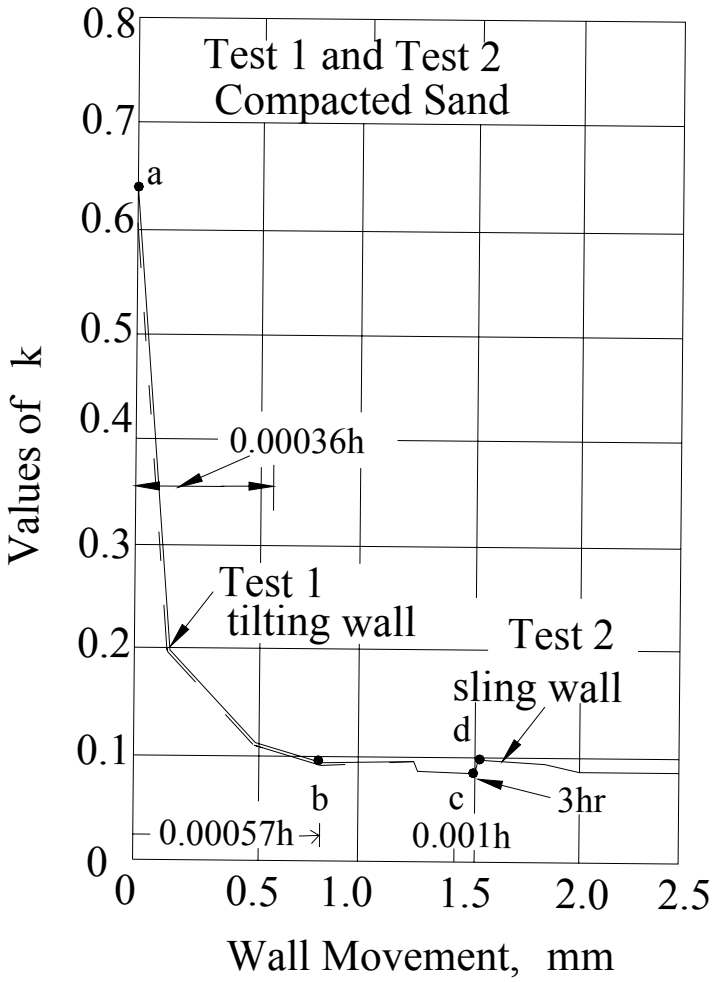

Fig. 2.10 Earth pressure coefficient K affected by yield of wall

(after Terzaghi, 1934)

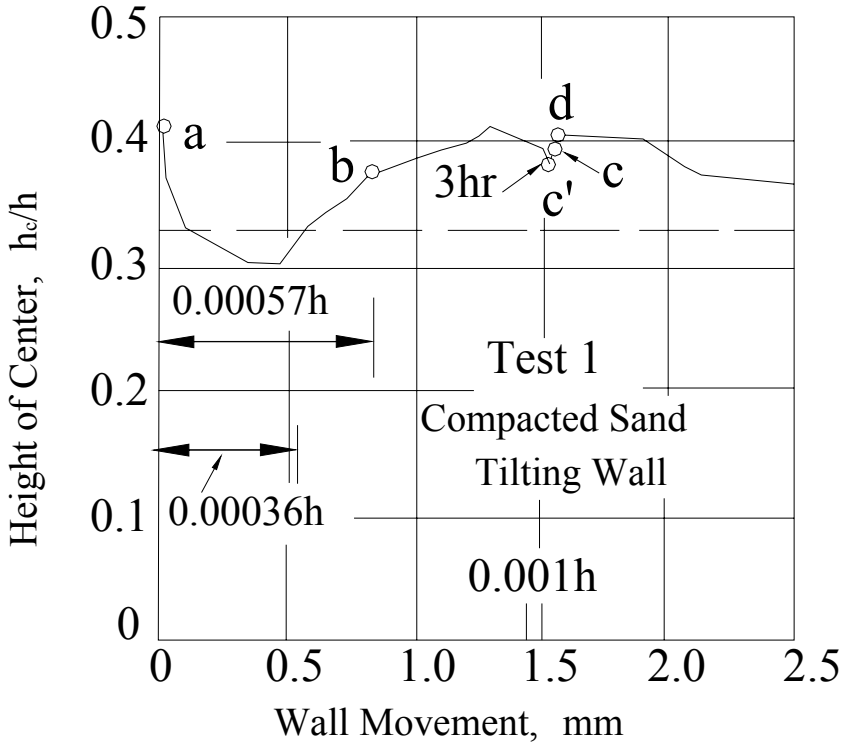

Fig. 2.11 Height of center of pressure in relation to yield of wall (after Terzaghi, 1934)

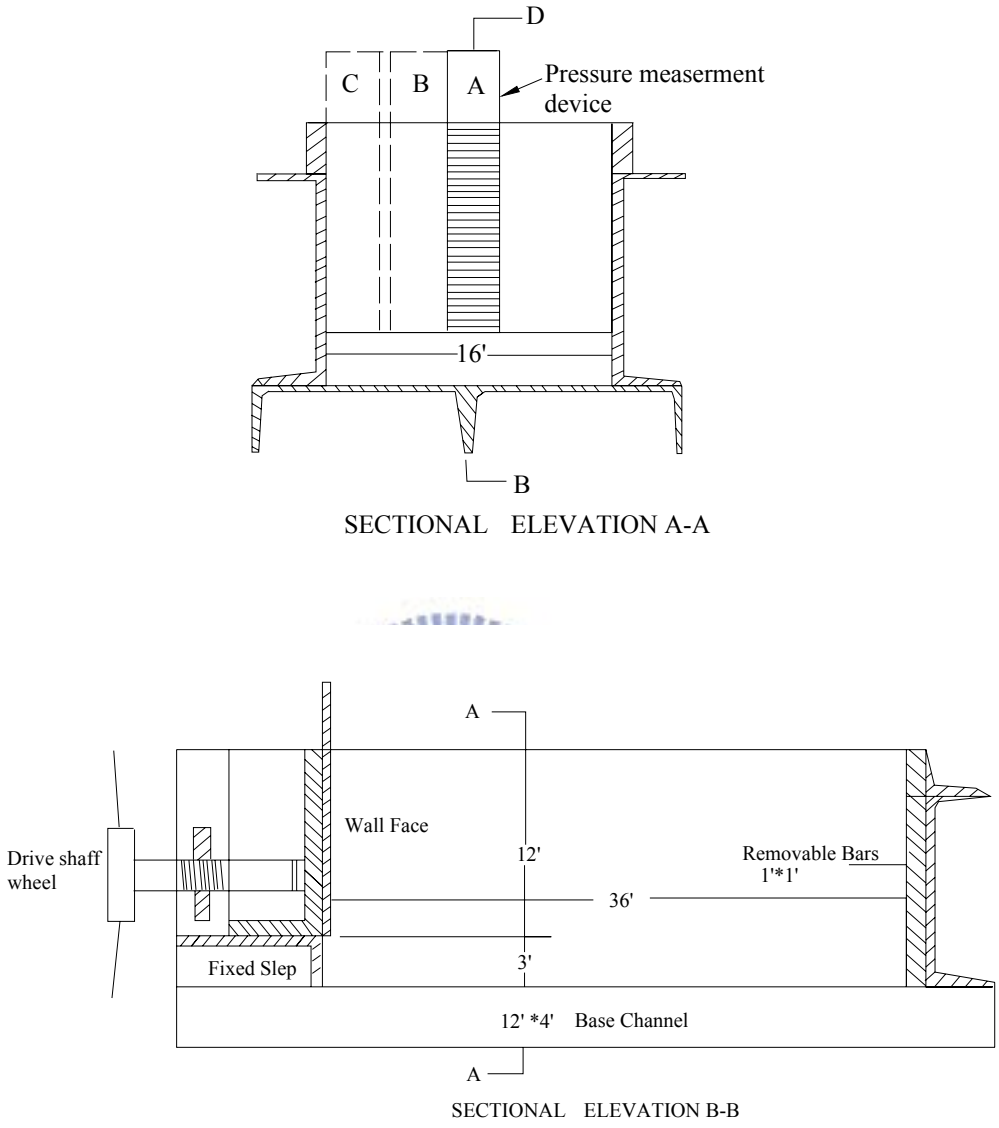

Fig. 2.12 University of Manchester model retaining wall

(after Mackey and Kirk, 1967)

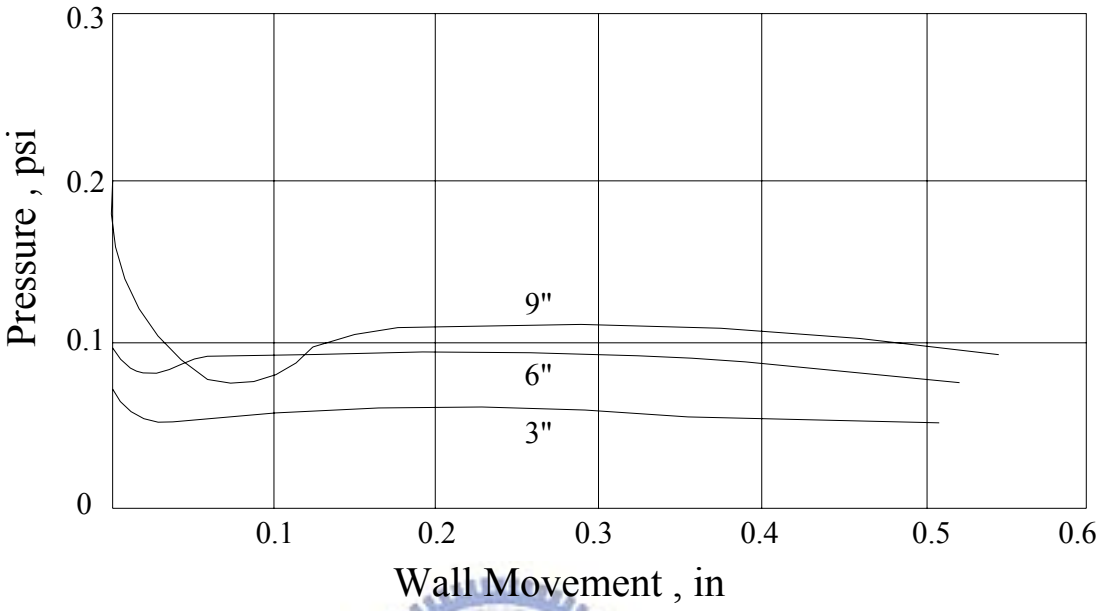

Fig. 2.13 Earth pressure with wall movement

(after Mackey and Kirk, 1967)

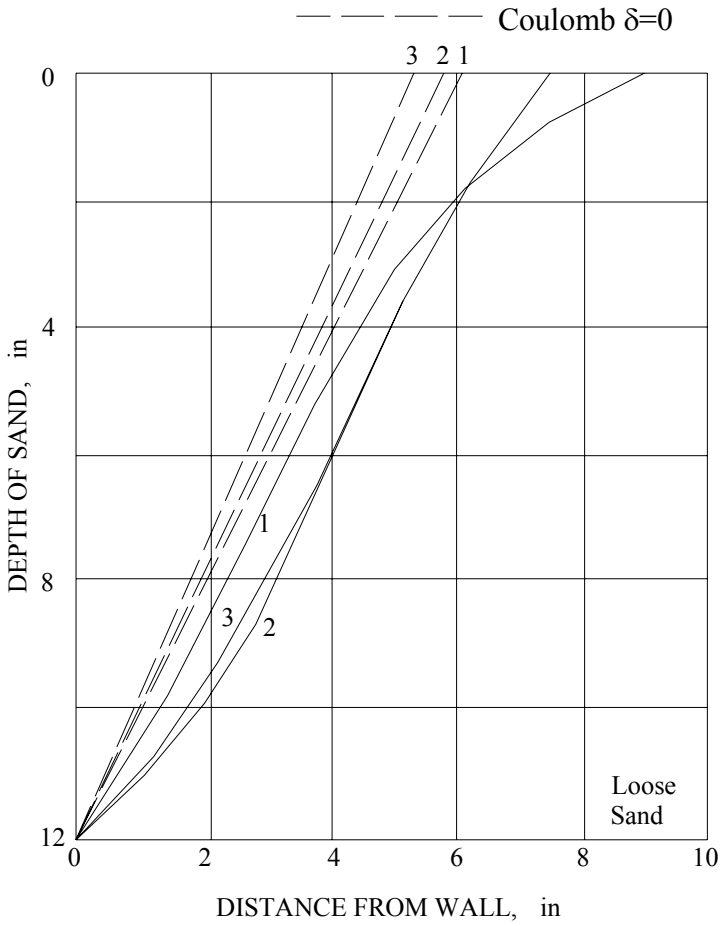

Sand 1: A uniformly graded fine sand
Sand 2: A medium graded sand
Sand 3: A uniformly graded coarse sand

Fig. 2.14 Failure surfaces (after Mackey and Kirk, 1967)

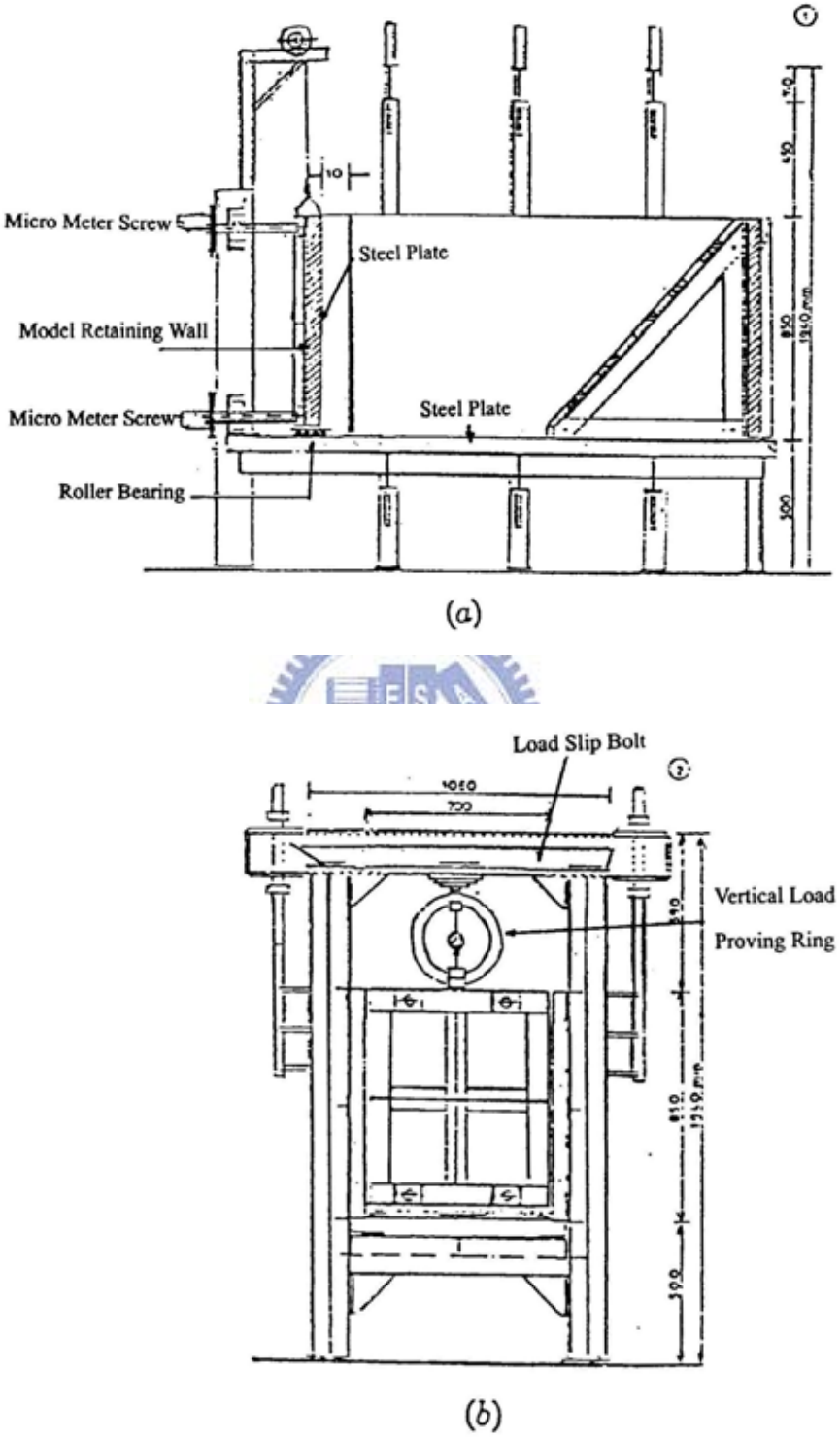

Fig. 2.15 College of Agriculture model retaining wall (after Bros, 1972)

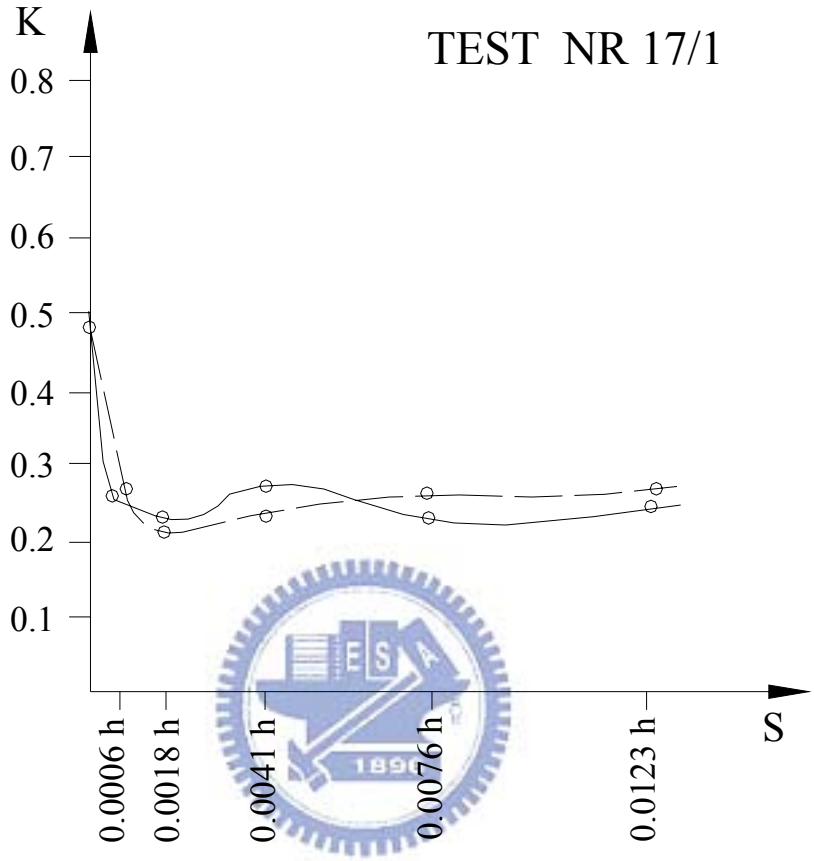

Fig. 2.16 Active earth pressure coefficient under T mode with wall movement (after Bros, 1972)

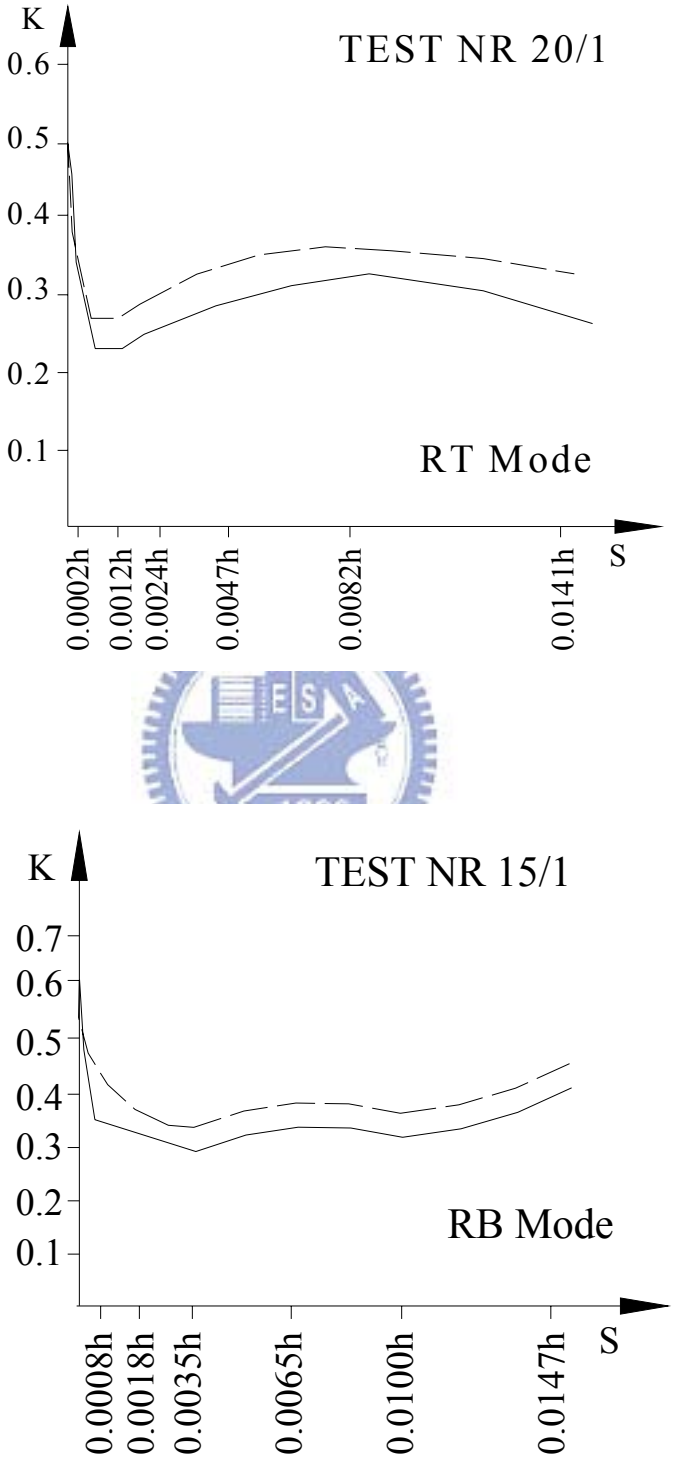

Fig. 2.17 Active earth pressure coefficient under both RT and RB mode with wall movement (after Bros, 1972)

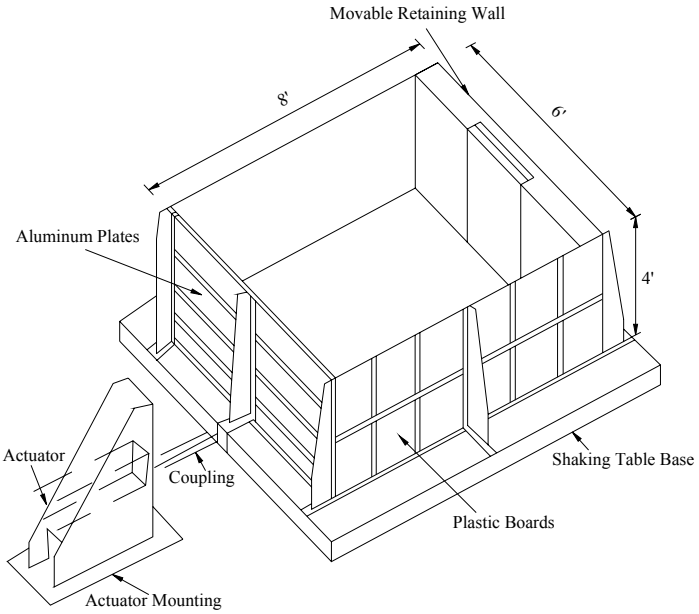

(a)

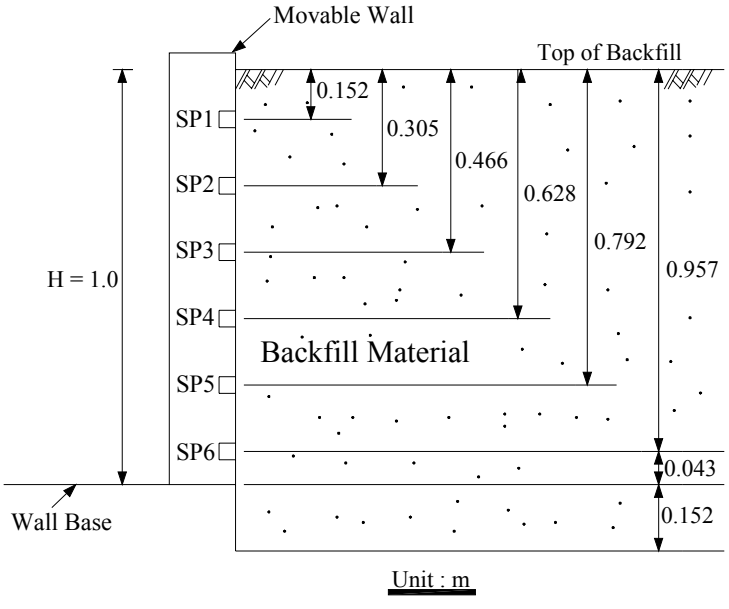

(b)

Fig. 2.18 Shaking table, soil box, and actuator (after Sherif et al., 1982)

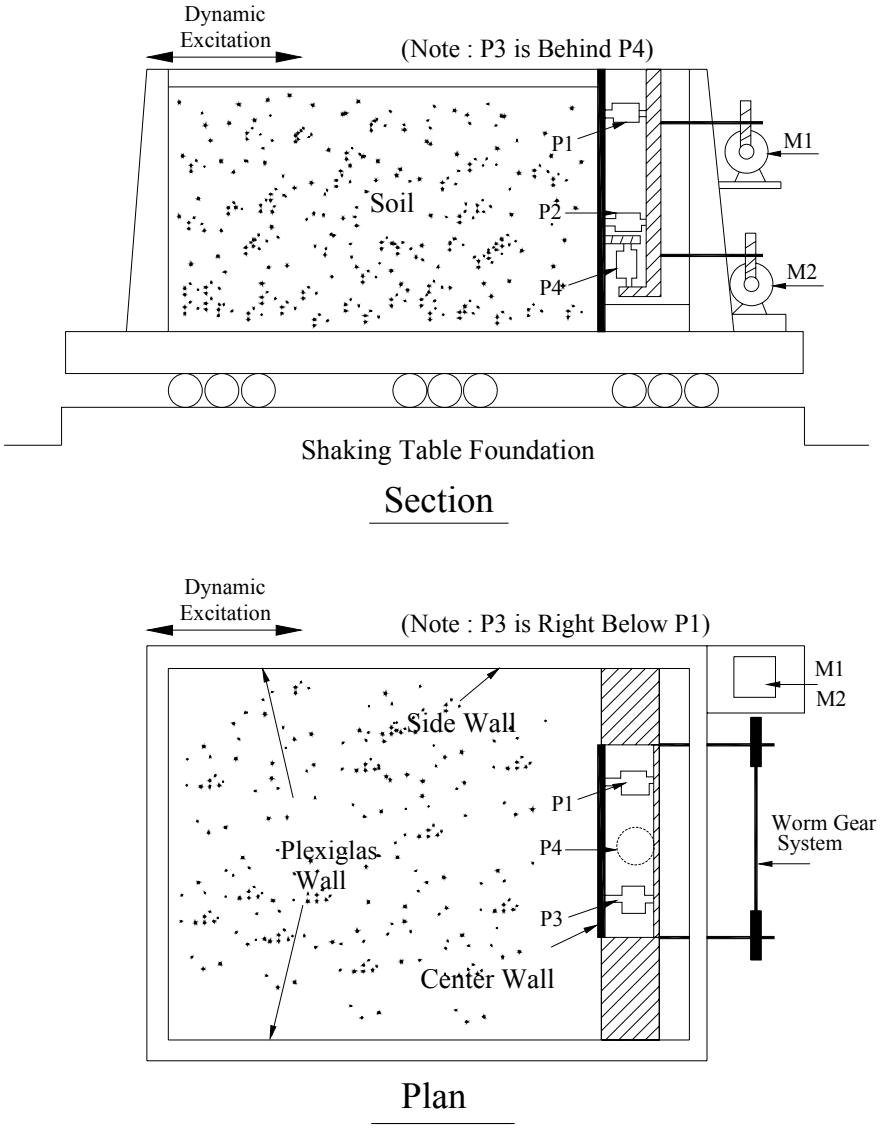

Fig. 2.19 Shaking table with movable retaining wall

(after Sherif et al., 1982)

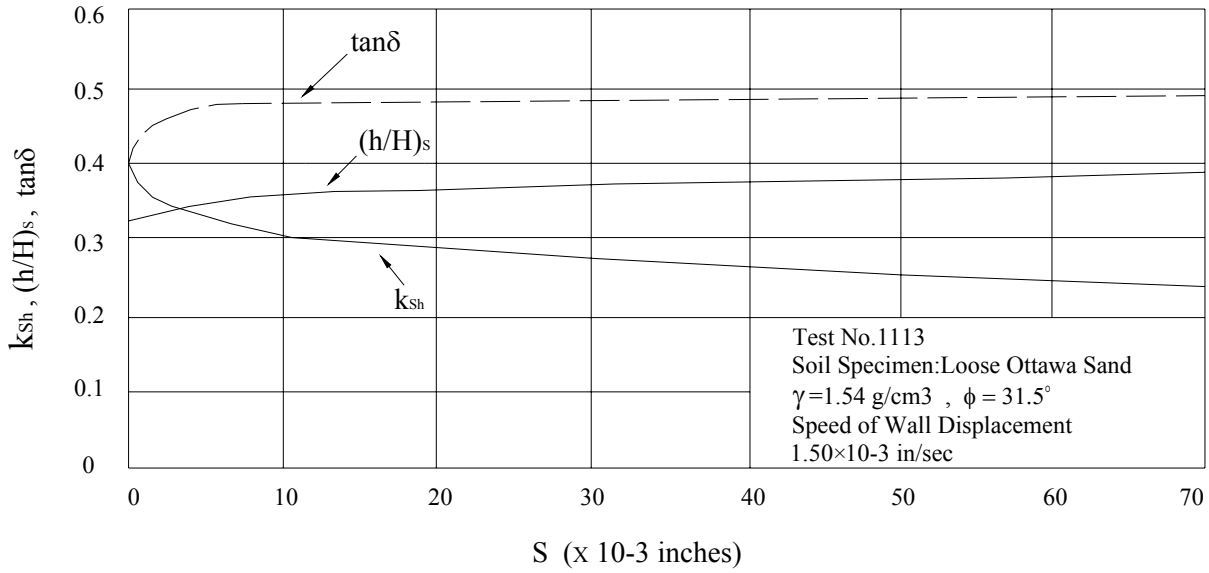

Fig. 2.20 Ksh, (h/H)s, and tanδ versus wall displacement S

(after Sherif et al., 1982)

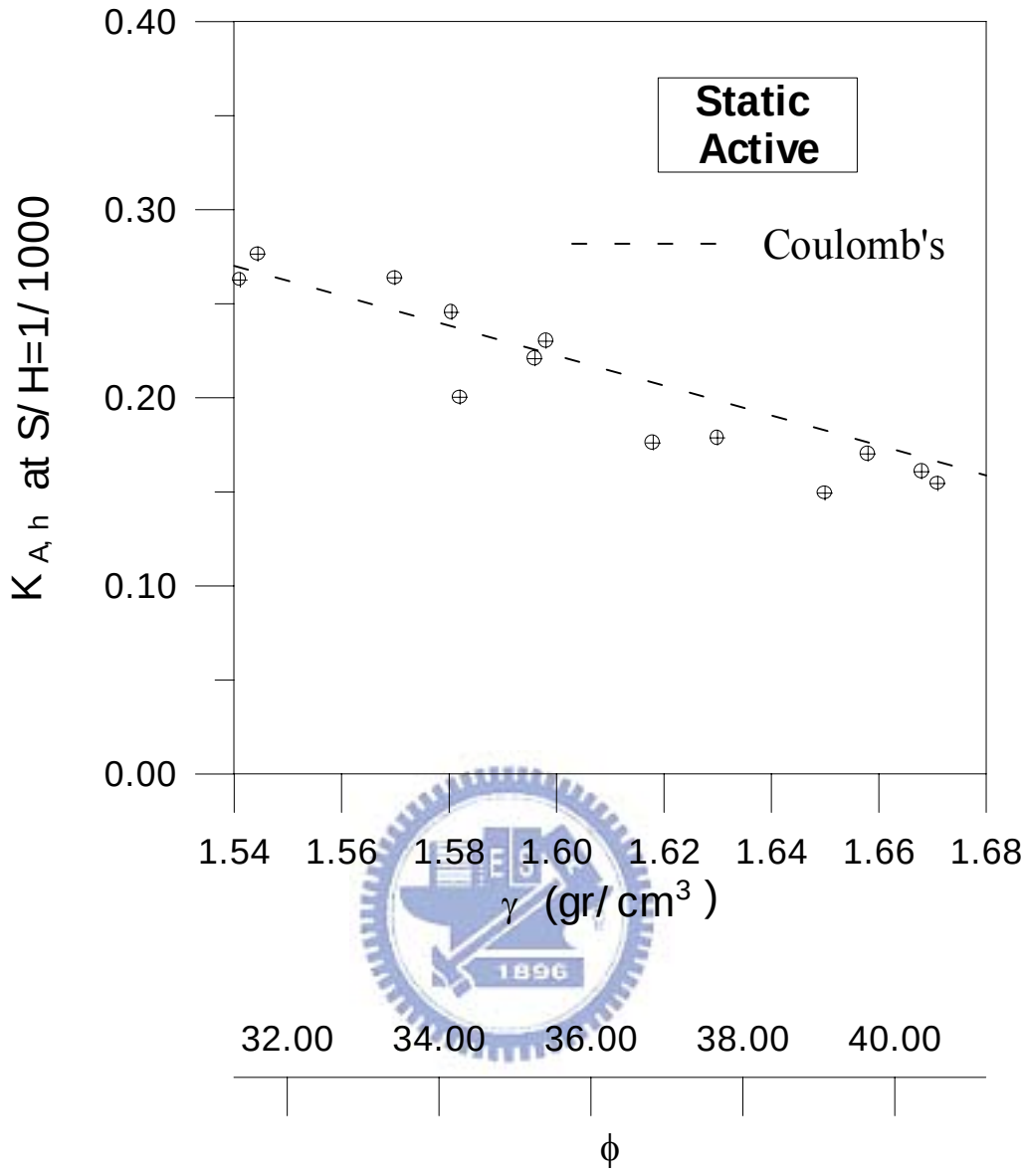

Fig. 2.21 Experimental K_{Sah} values at S /H=0.001 versus soil density (after Sherif et al., 1982)

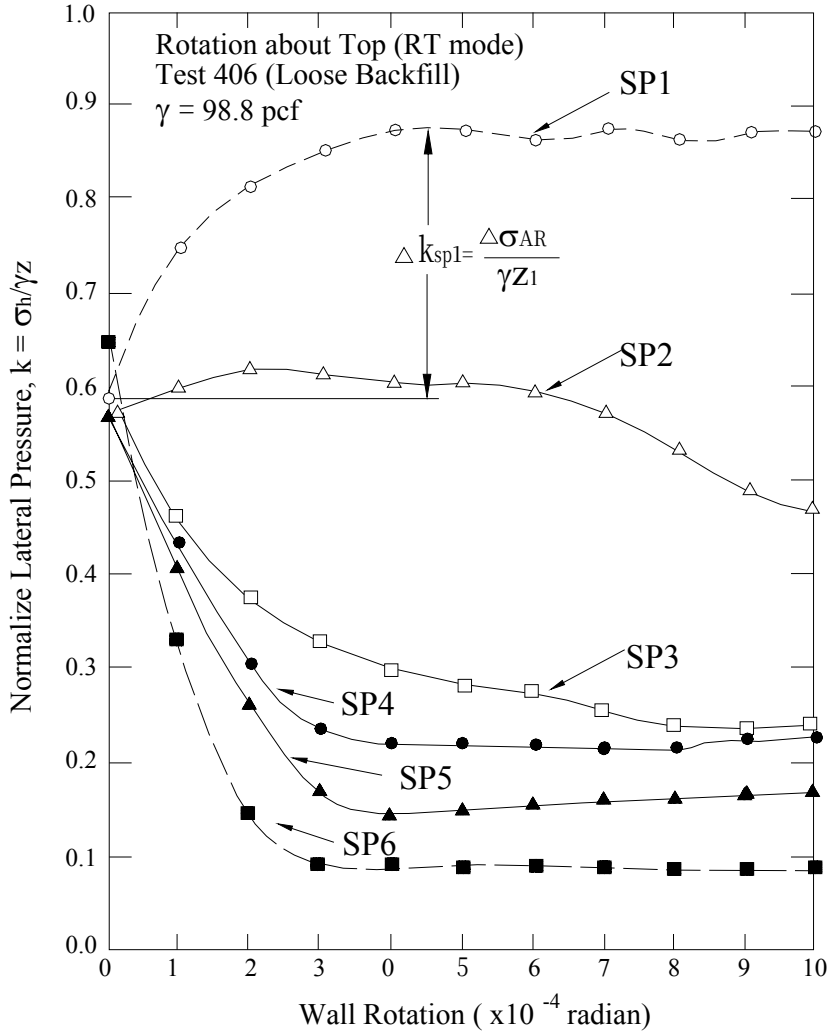

Fig. 2.22 Change of normalized lateral pressure with wall rotation about top (loose backfill) (after Fang and Ishibashi, 1986)

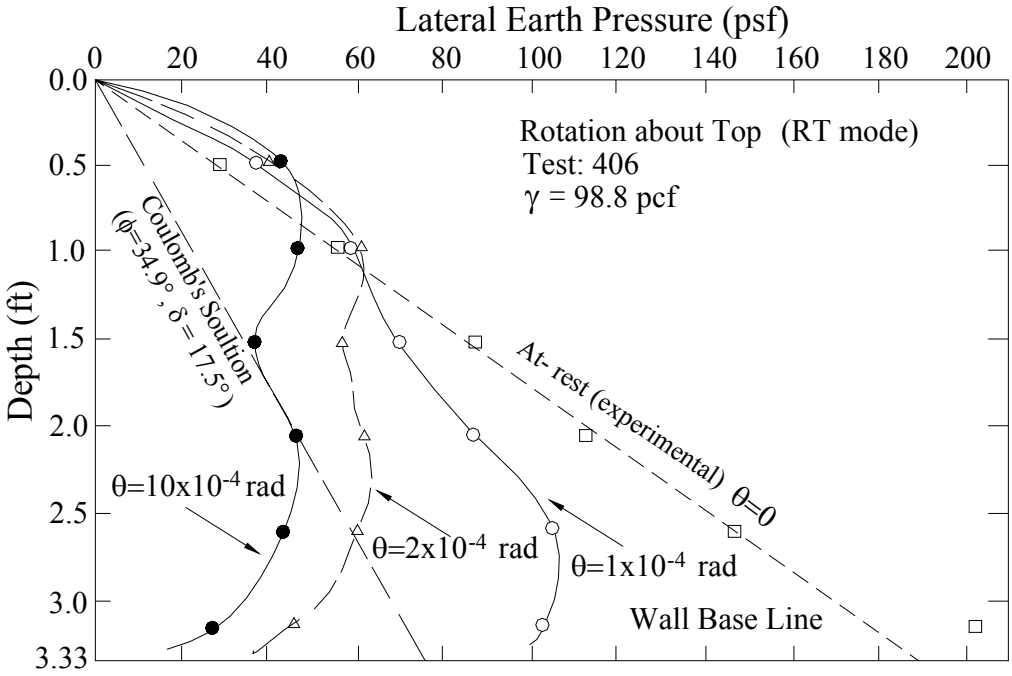

Fig. 2.23 Distributions of horizontal earth pressure at different wall rotation (rotation about top) (after Fang and Ishibashi, 1986)

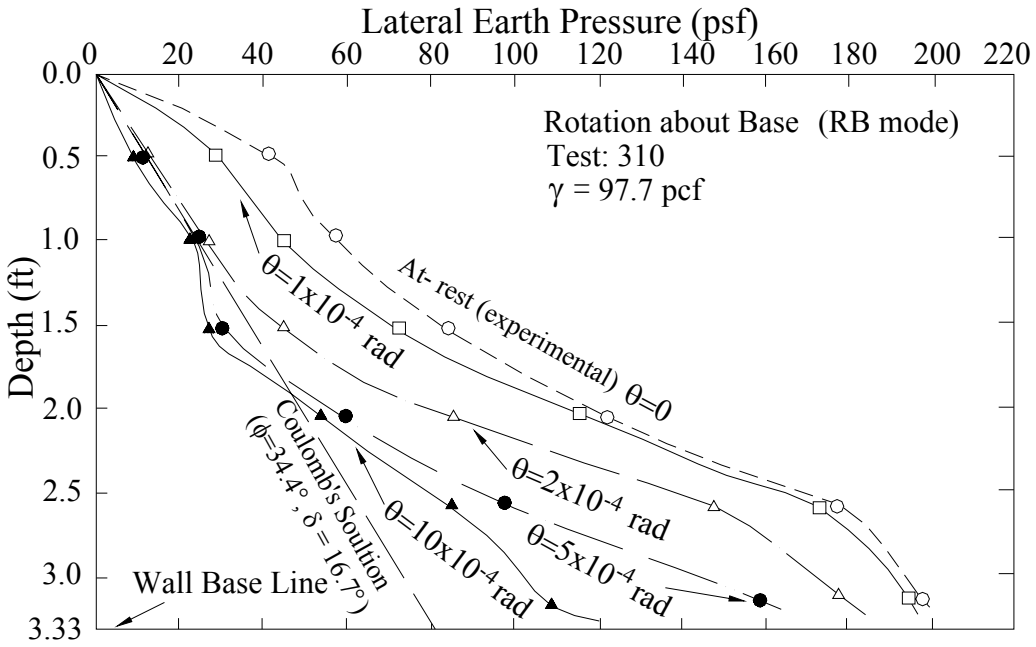

Fig. 2.24 Distributions of horizontal earth pressure at different wall rotation (rotation about base) (after Fang and Ishibashi, 1986)

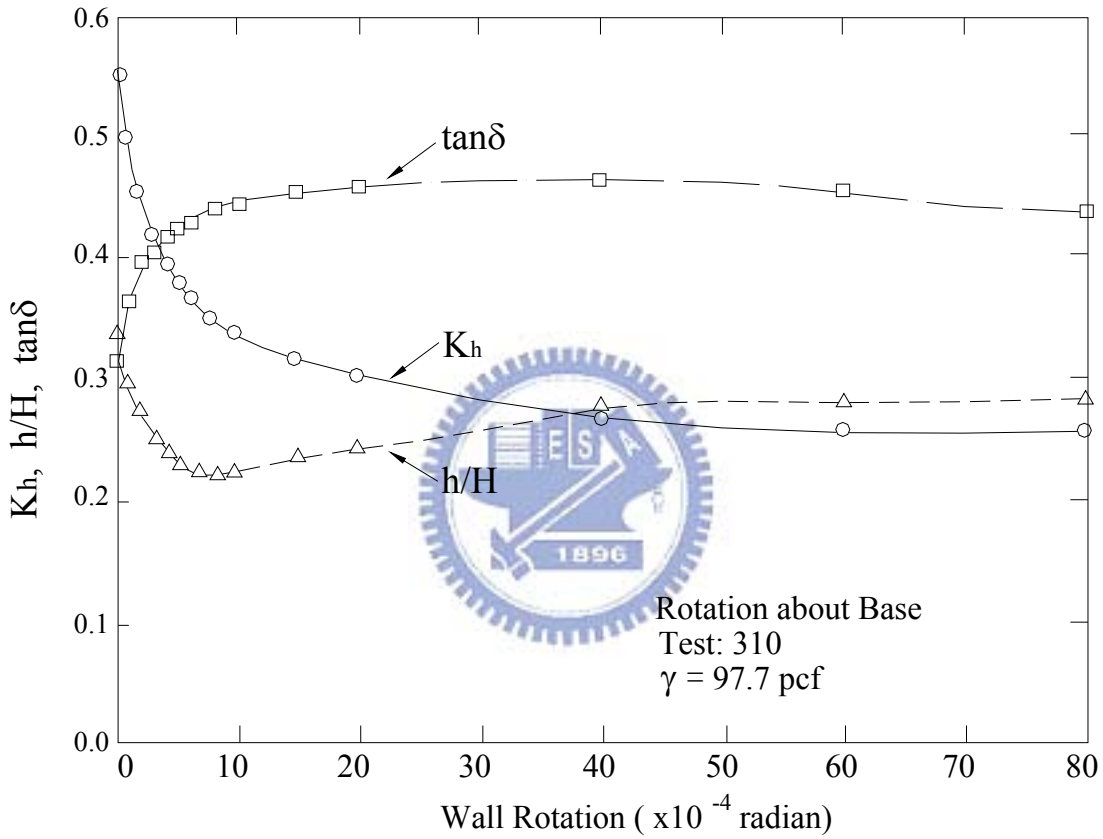

Fig. 2.25 Horizontal earth pressure coefficient Kh, relative height of resultant pressure application h/H, and coefficient of wall friction tan δ Versus wall rotation(rotation about base) (after Fang and Ishibashi. 1986)

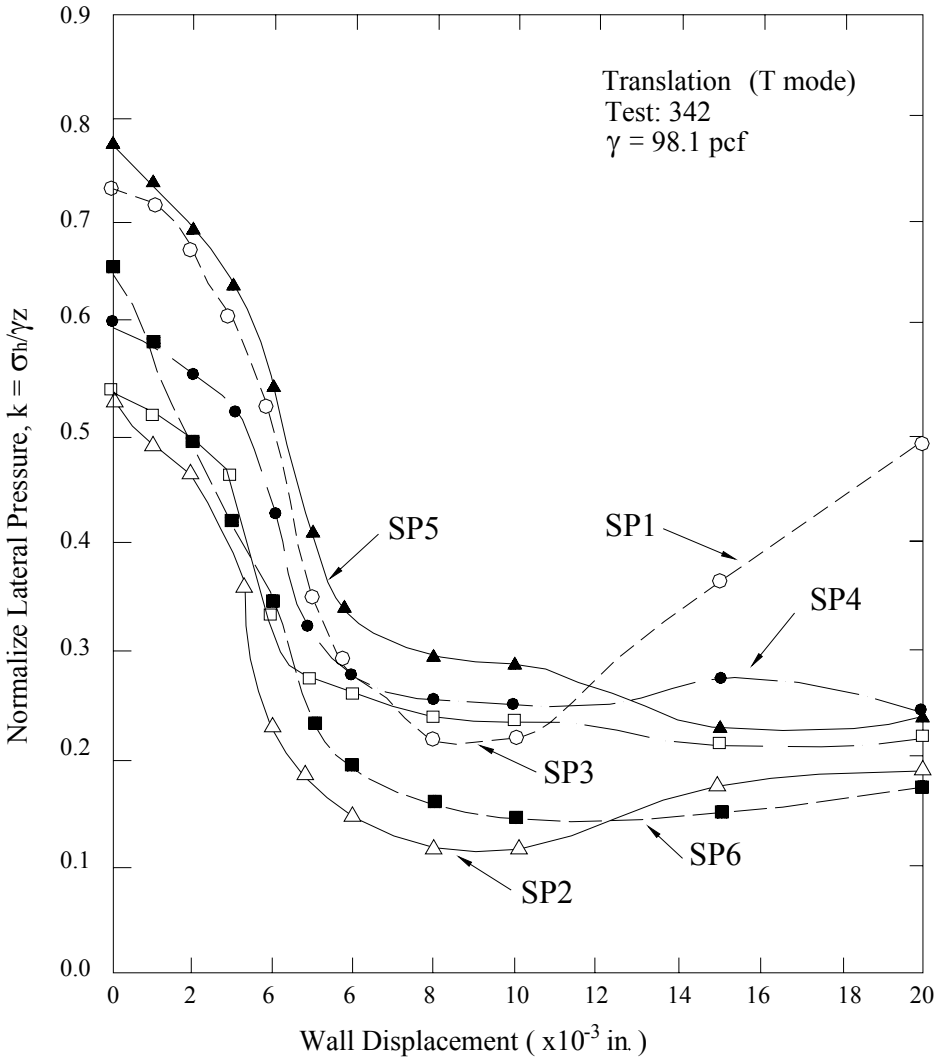

Fig. 2.26 Change of normalized lateral pressure with translation wall displacement (after Fang and Ishibashi, 1986)

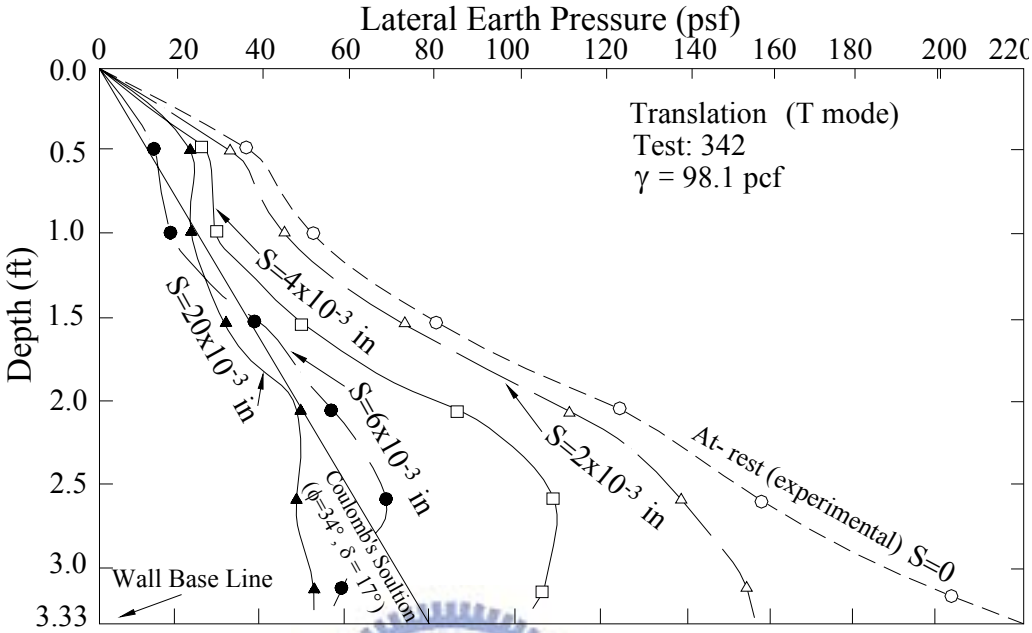

Fig. 2.27 Distributions of horizontal earth pressure at different wall displacement (after Fang and Ishibashi, 1986)

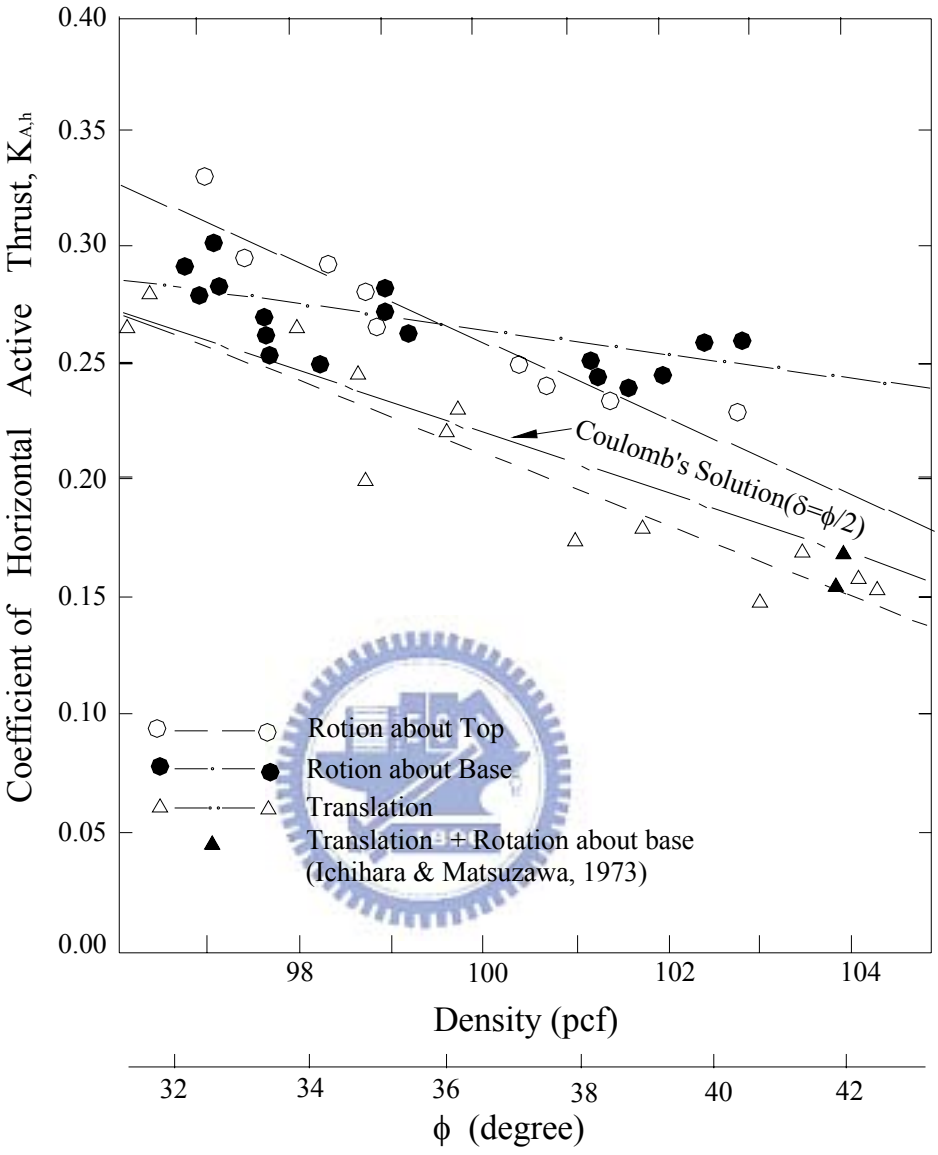

Fig. 2.28 Coefficient of horizontal active thrust as a function of soil density (after Fang and Ishibashi, 1986)

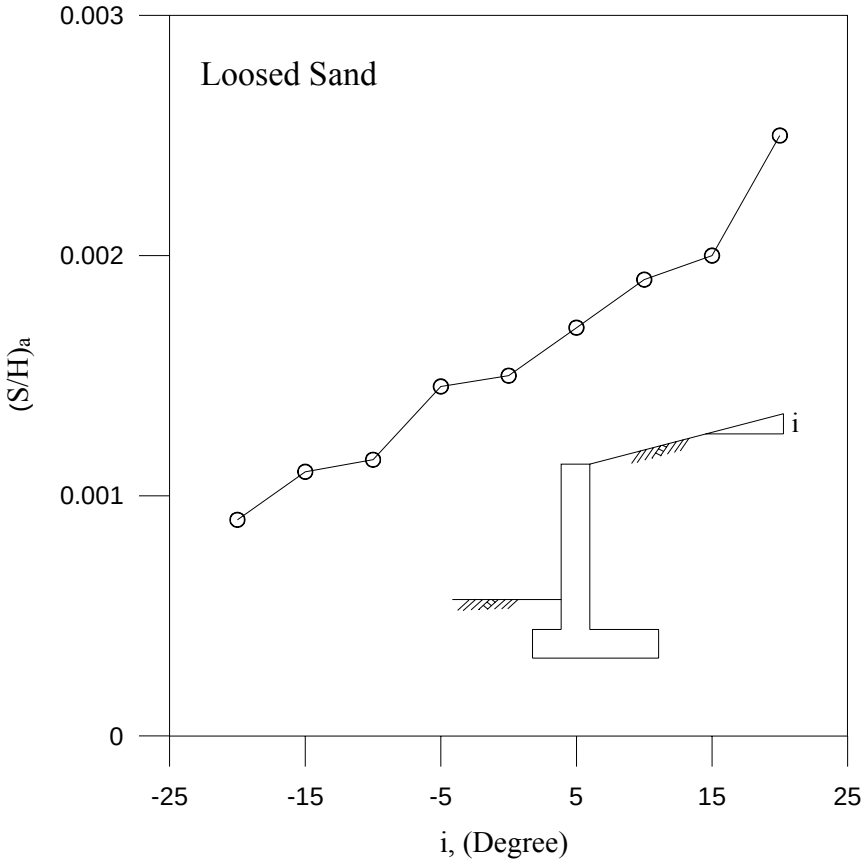

Fig. 2.29 $(S/H)_a$ versus backfill inclination (after Fang et al., 1997)

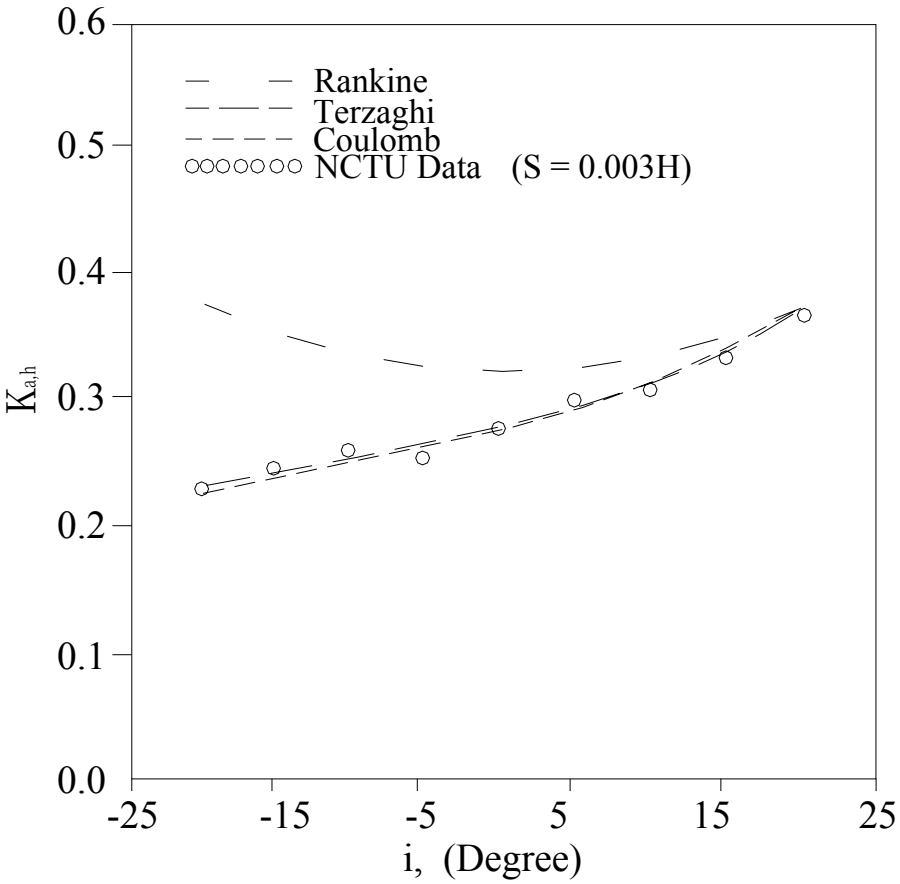

Fig. 2.30 Active earth pressure coefficient $K_{a,h}$ versus backfill inclination (after Fang et al., 1997)

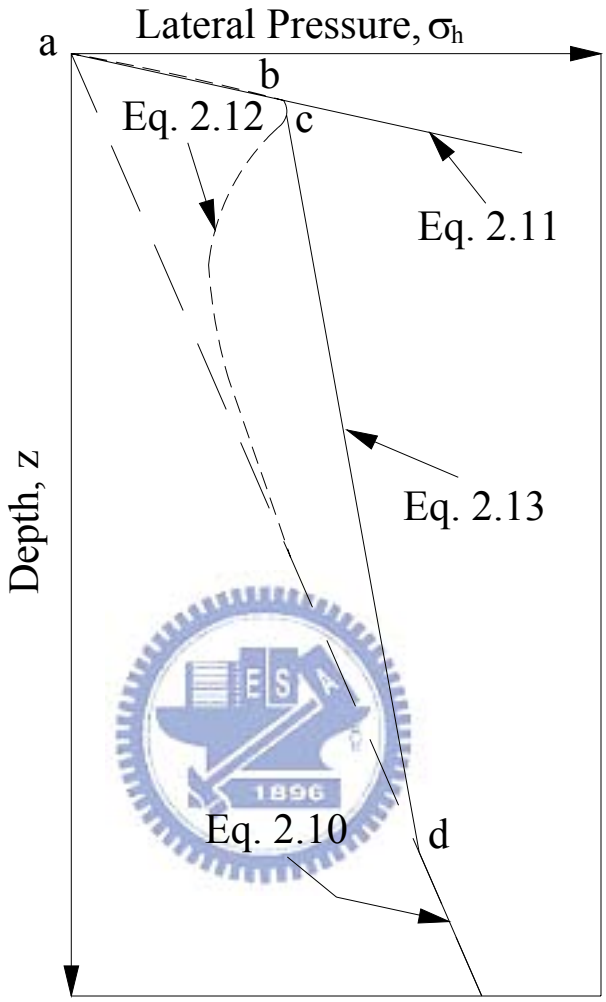

Fig. 2.31 Hand-calculation for estimating σ_h

(after Peck and Mesri, 1987)

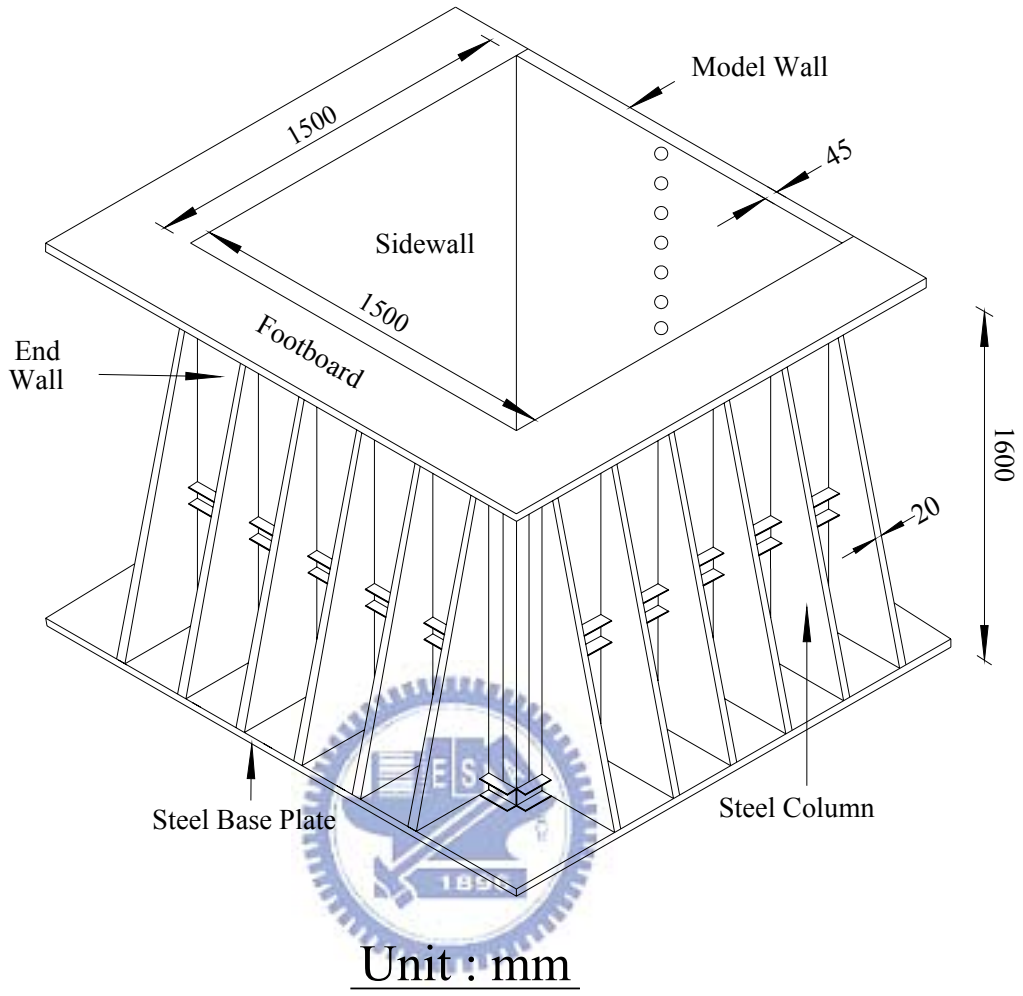

Fig. 2.32 National Chiao Tung Univ. non-yielding retaining wall facility

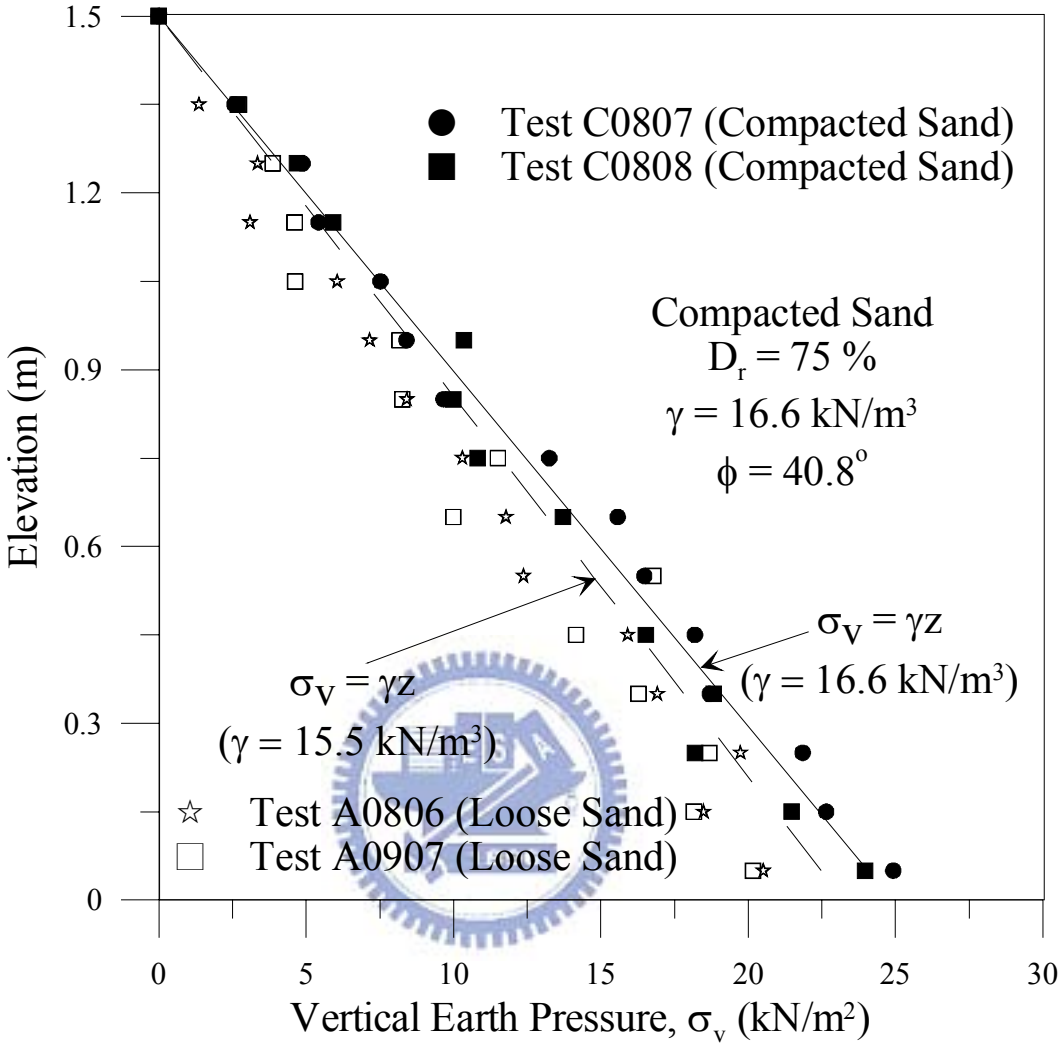

Fig. 2.33 Distribution of vertical earth pressure mearsured in soil mass (after Chen, 2003)

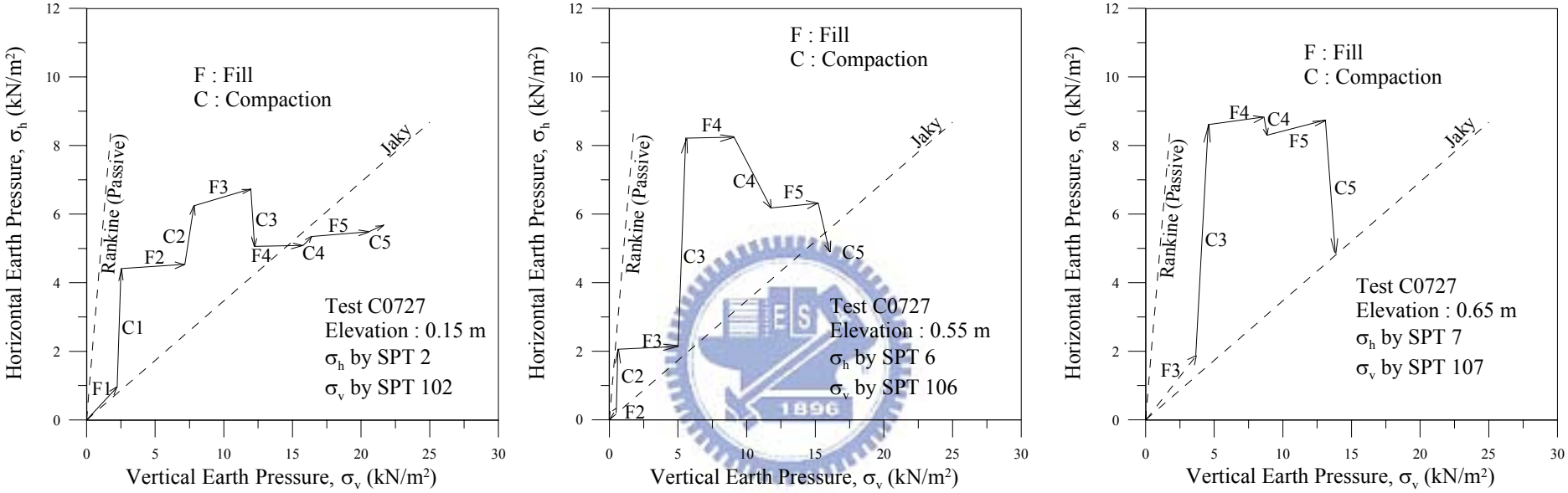

Fig. 2.34 Stress path of a soil element under compaction (after Chen, 2003)

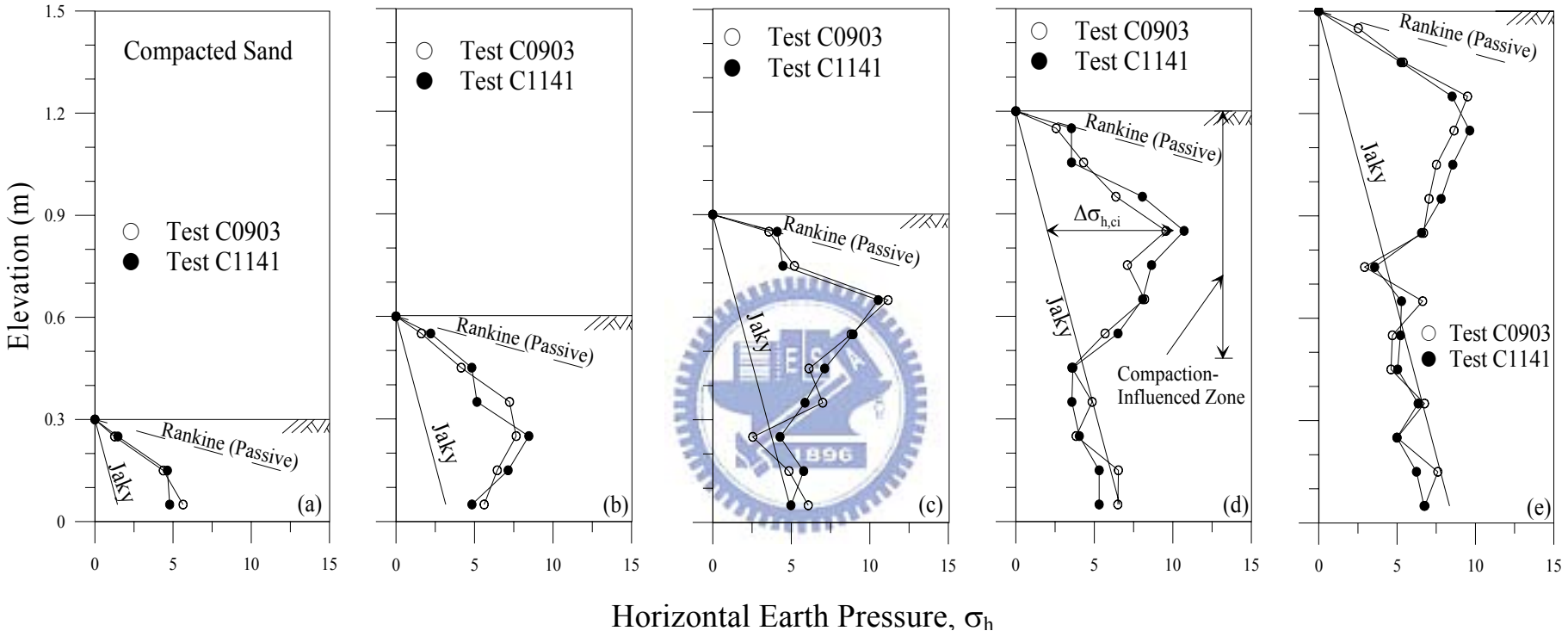

Fig. 2.35 Distribution of horizontal earth pressure after compaction (after Chen, 2003)

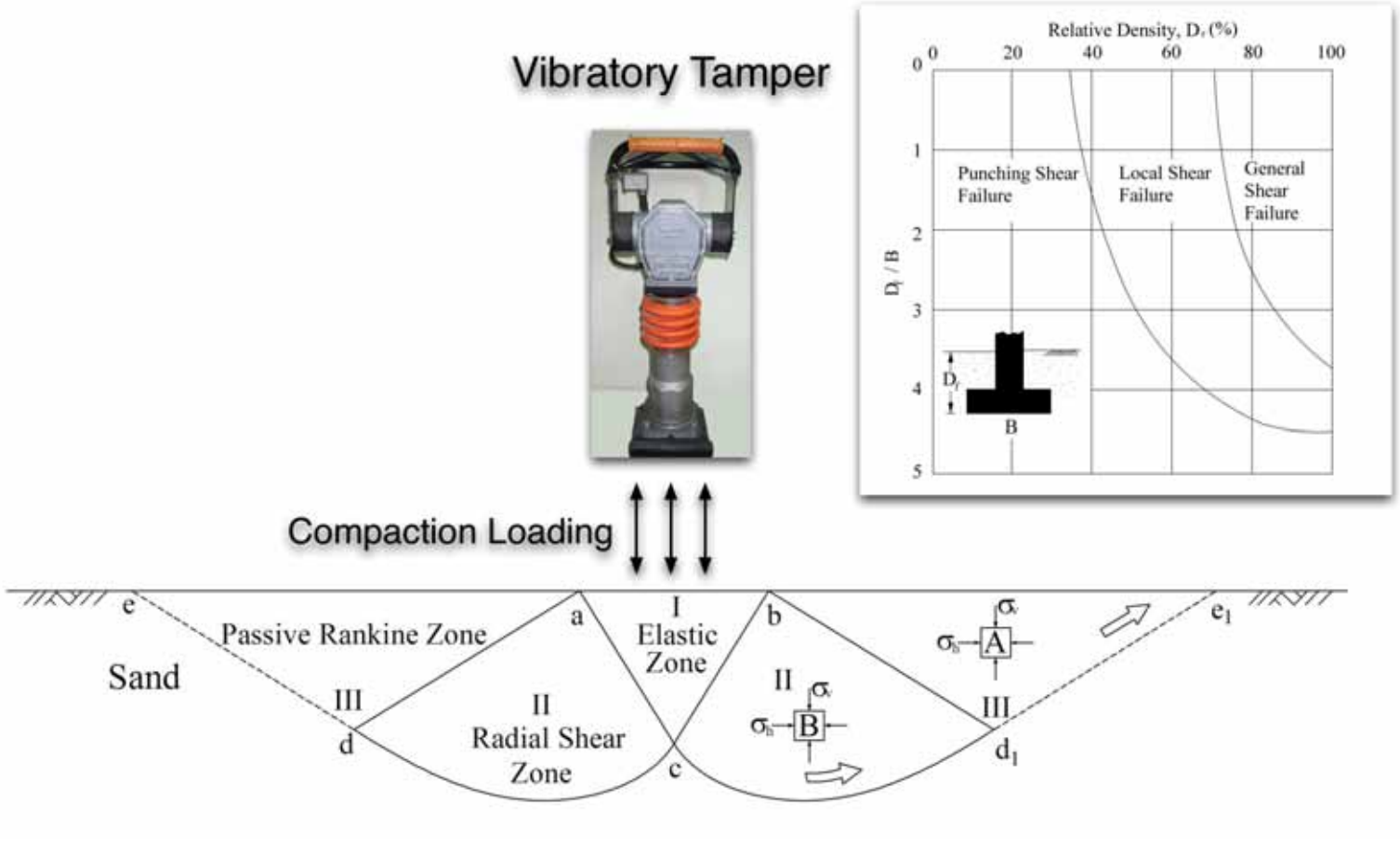

Fig. 2.36 (a) Bearing capacity failure in soil due to compaction; (b) Modes of bearing capacity failure in sand (Chen, 2003)

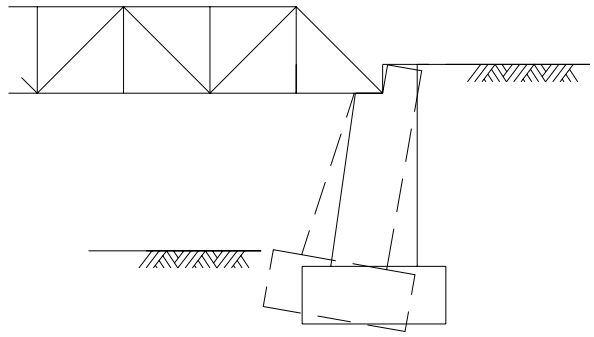

(a)

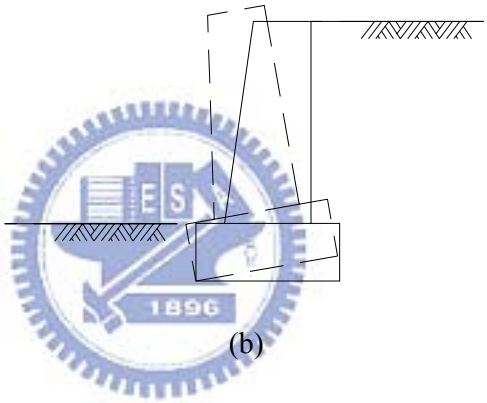

(b)

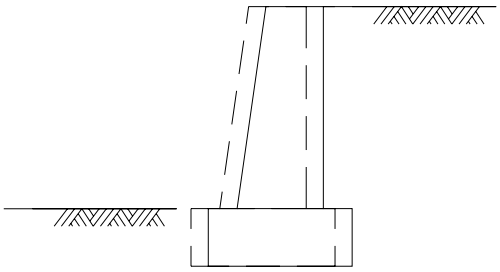

(c)

Fig. 3.1 Active wall movement modes, (a) Rotation about wall top (RT mode); (b) Rotation about wall base (RB mode); (c) Translation (T mode) (after Huang, 2003)

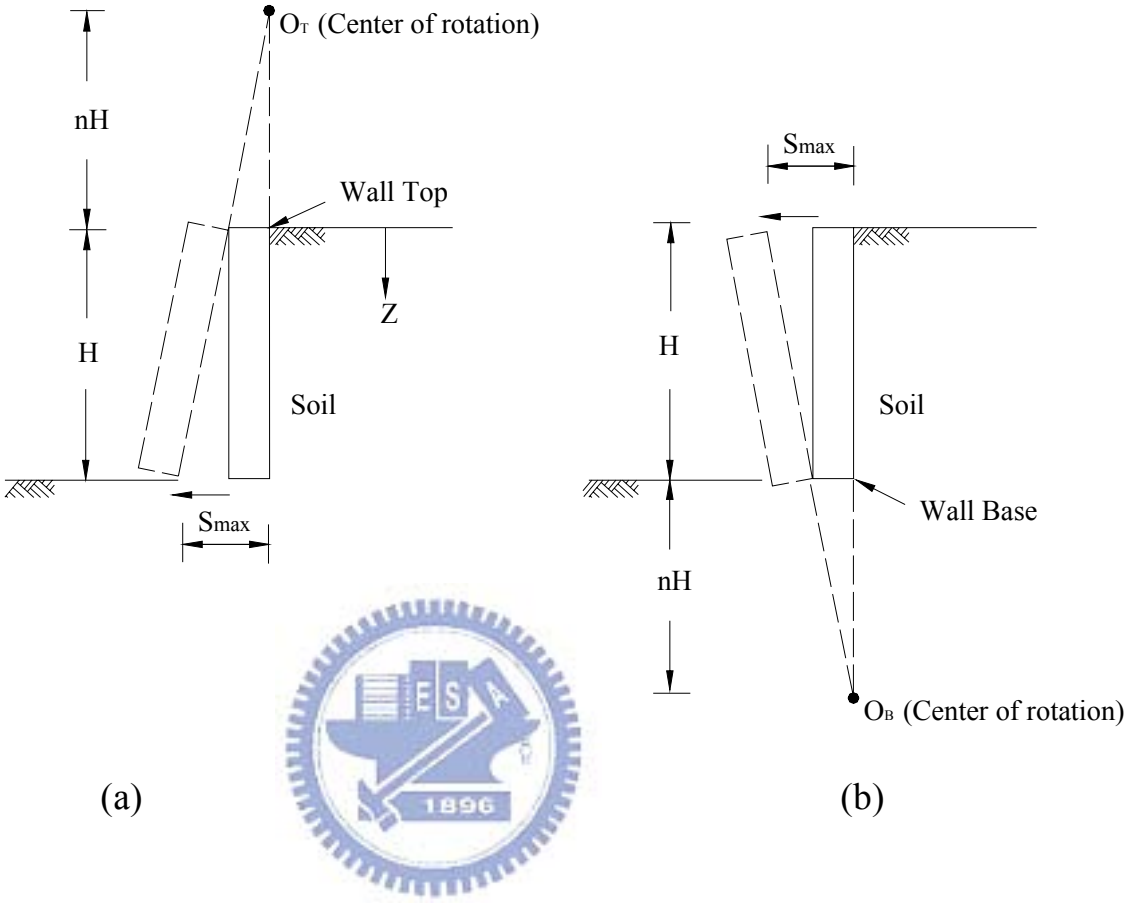

Fig. 3.2 (a) Rotation about a point above wall top (RTT mode);

(b) Rotation about a point below wall base (RBT mode)

(after Huang, 2003)

Fig. 3.3 Steel interface plate (2100 mm × 1497mm)

(after Wang, 2005)

Fig. 3.4 Supporting frame (after Chen, 2005)

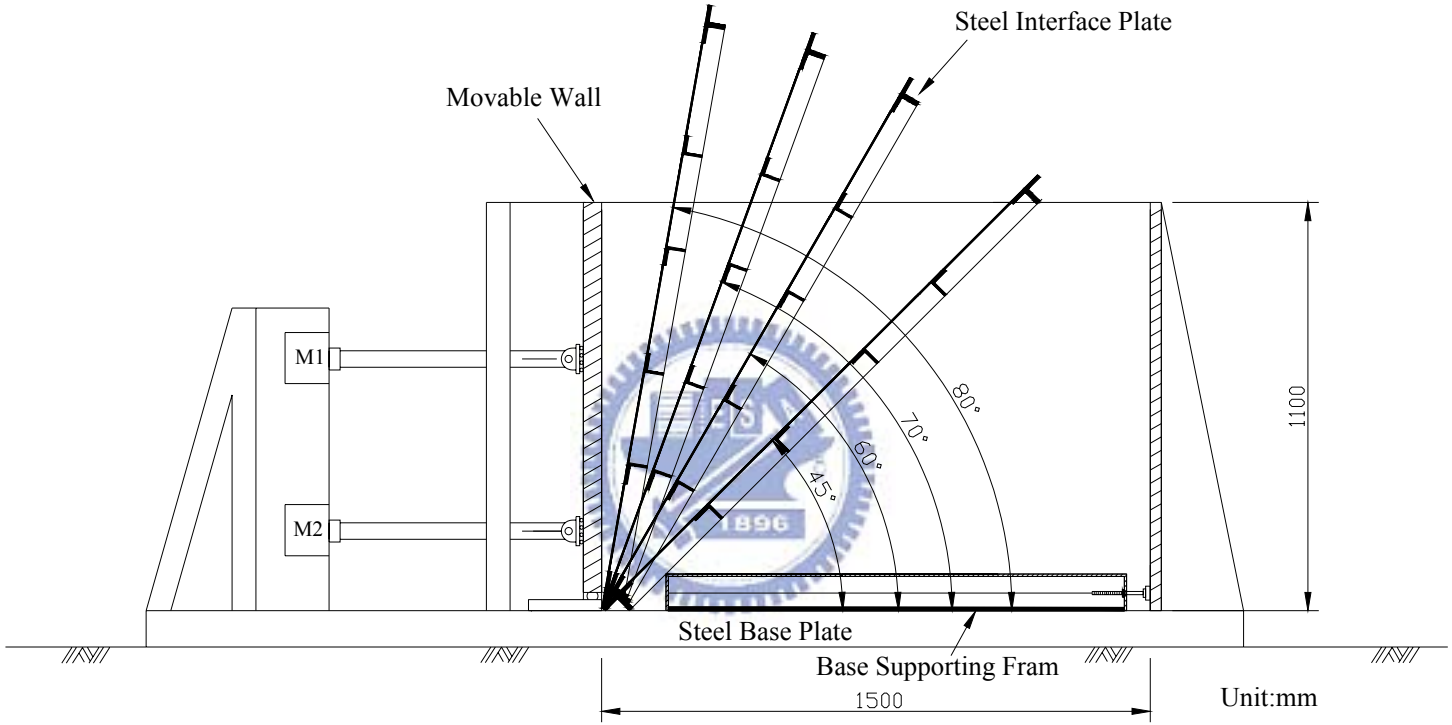

Fig. 3.5 Different interface inclinations

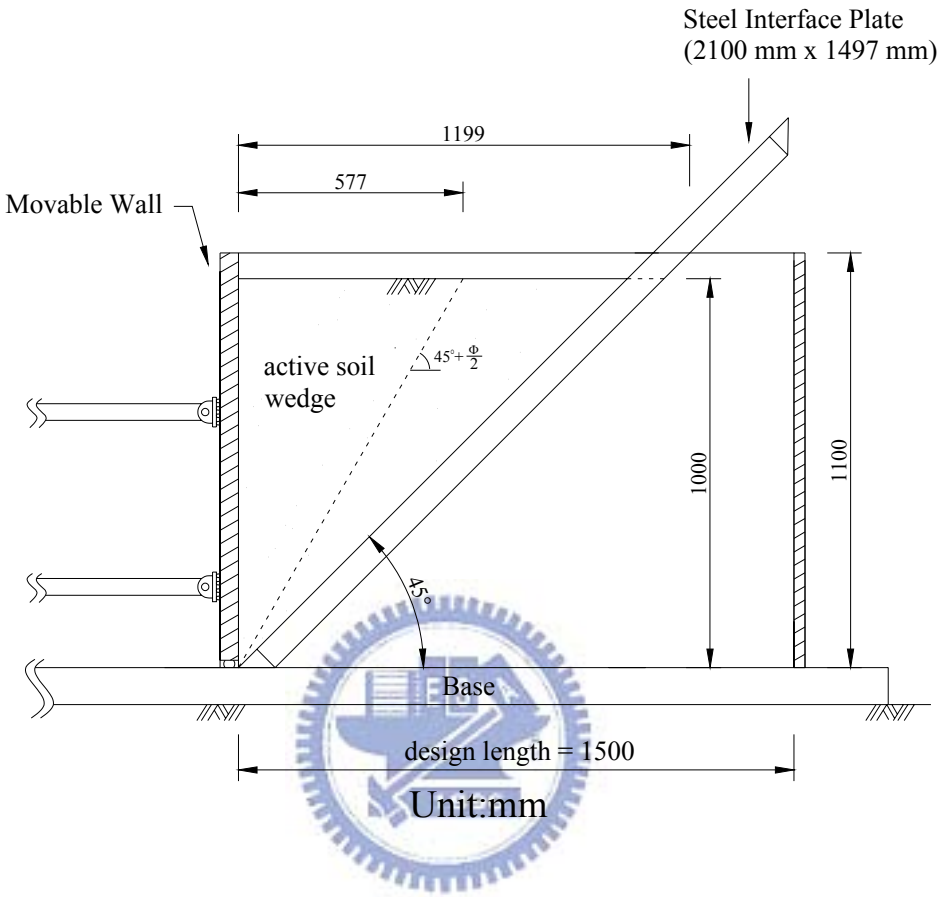

Fig. 3.6 Critical condition for d = 0 mm and $\alpha = 45°$

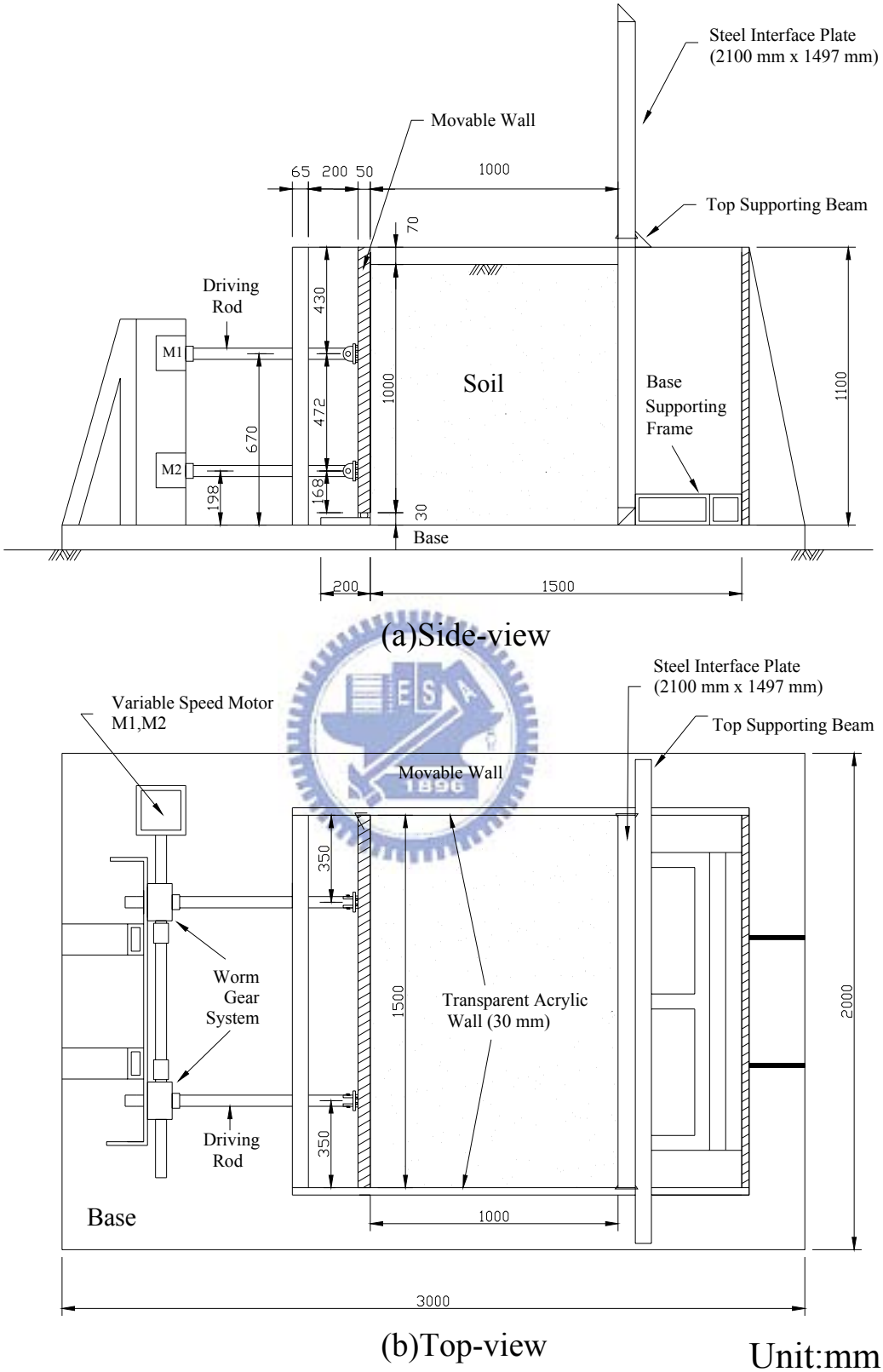

Fig. 3.7 NCTU K_A model retaining wall

Fig. 3.8 Top view of NCTU K_A model retaining wall

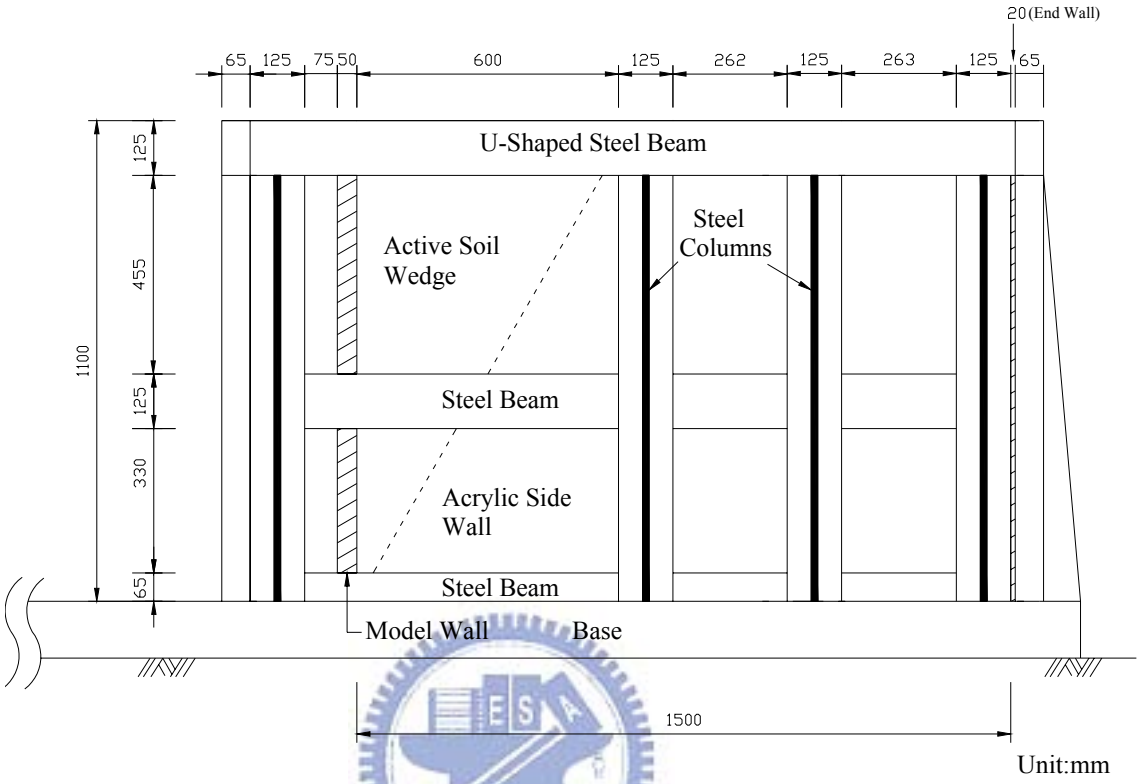

Fig. 3.9 Side wall reinforcment

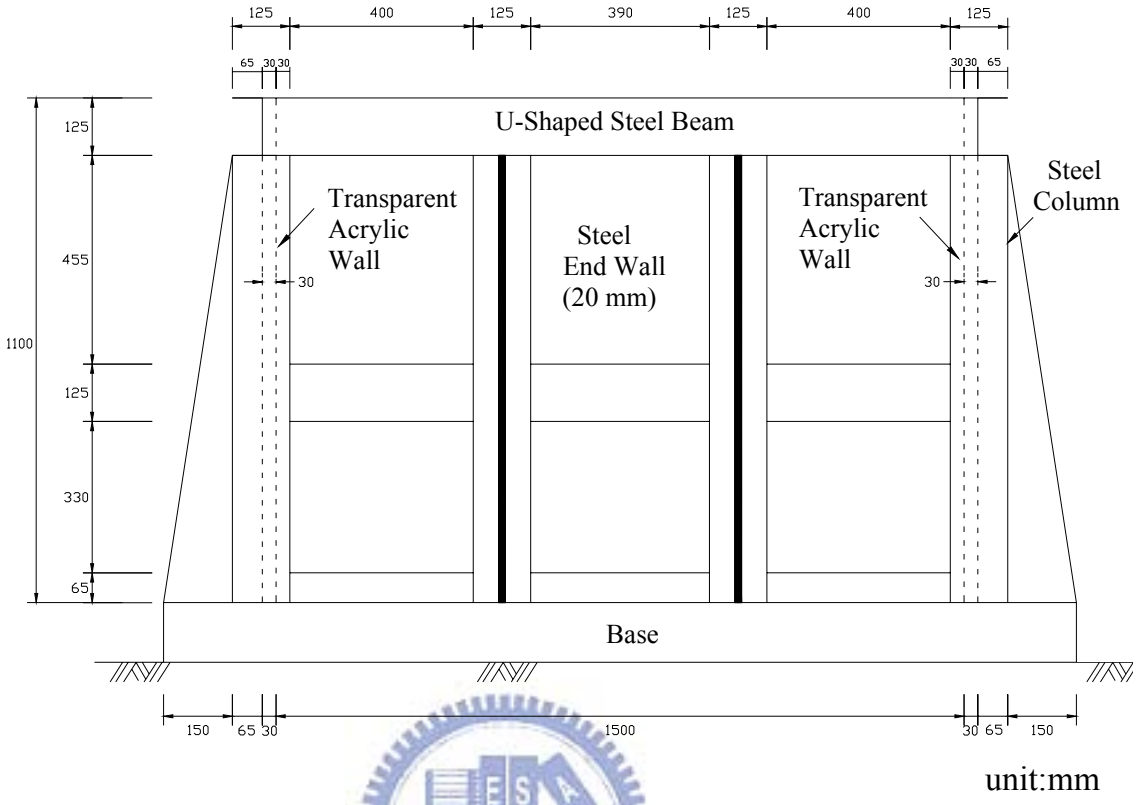

Fig. 3.10 End wall reinforcement

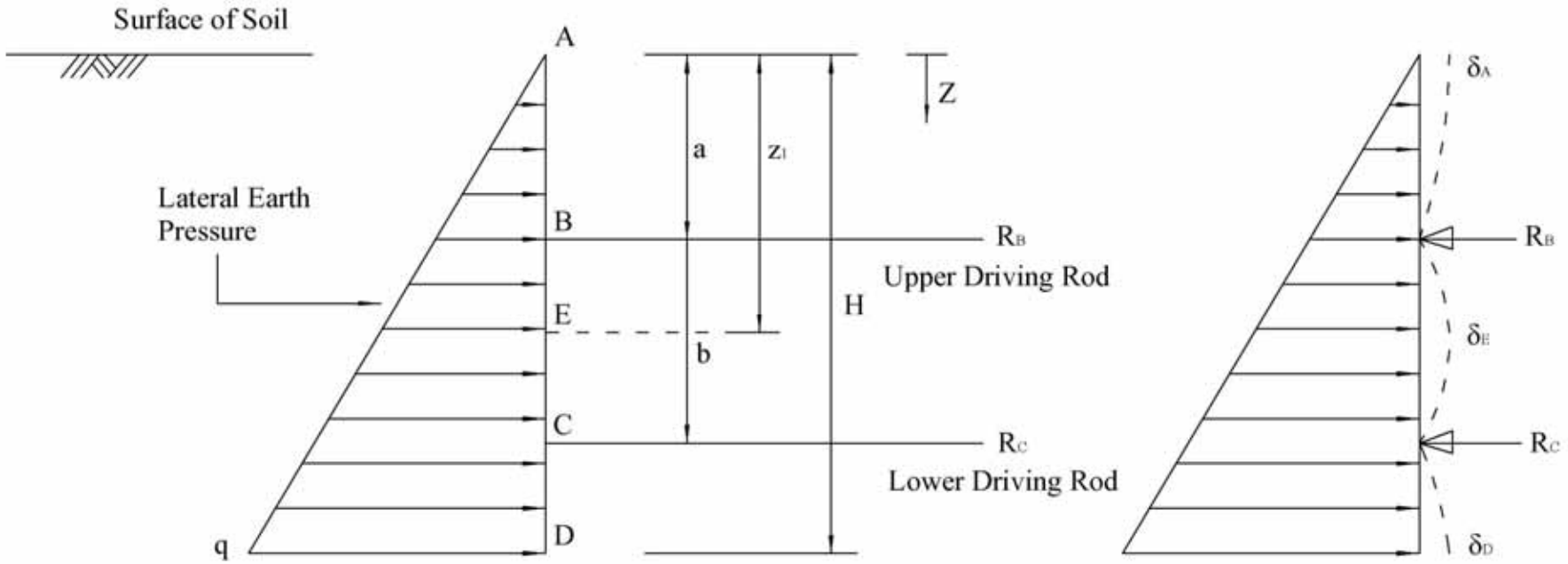

Fig. 3.11 Determine positions of wall driving rods(side -view)

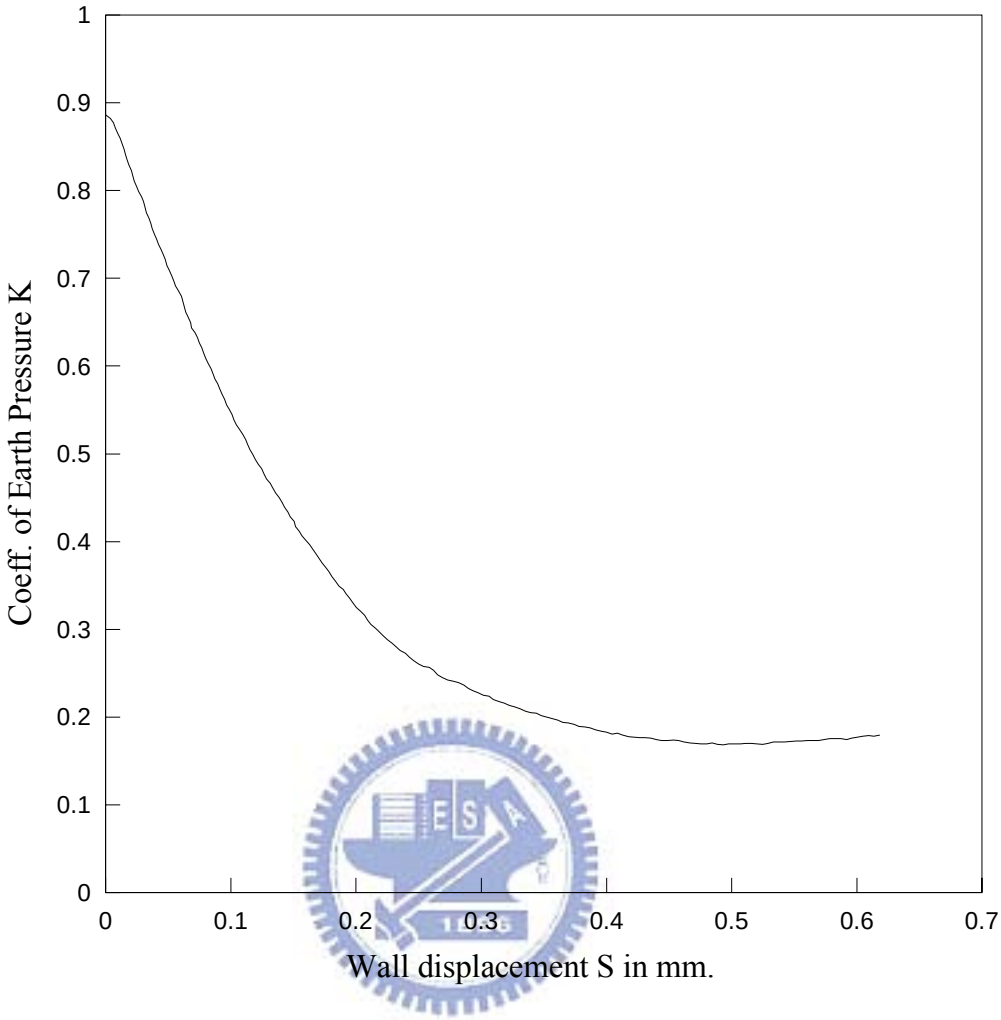

Fig. 3.12 Relationship of the coefficient of earth pressure, K, and the mean wall displacement, S (after Ichihara and Matsuzawa, 1973)

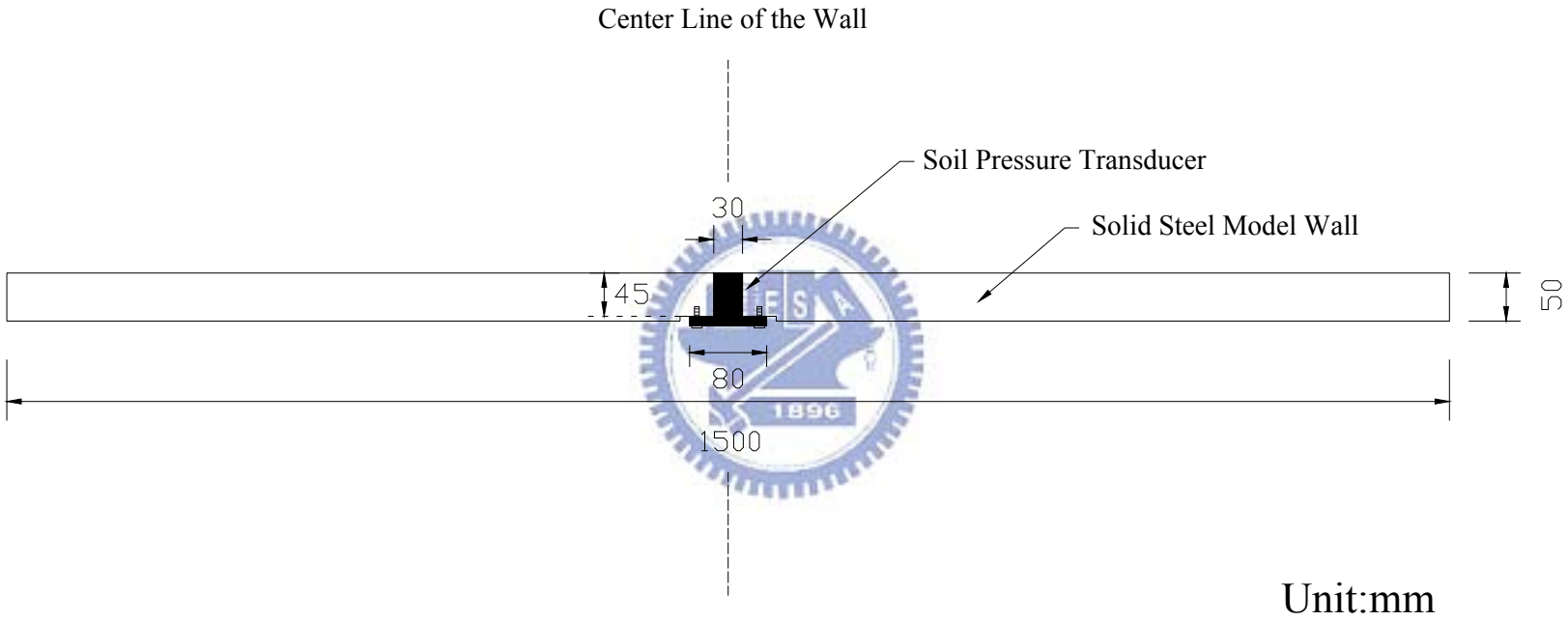

Fig. 3.13 Typical cross-section of the beam

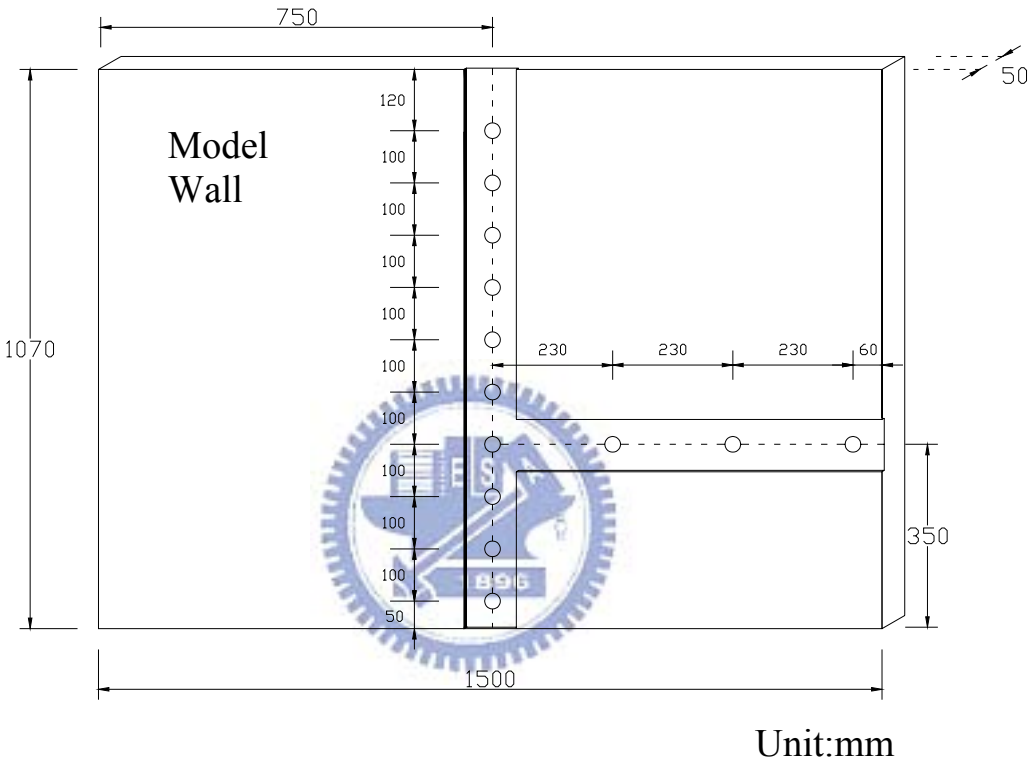

Fig. 3.14 Dimensions of model retaining wall

(a) front view

(b) rear view

Fig. 3.15 Model retaining wall

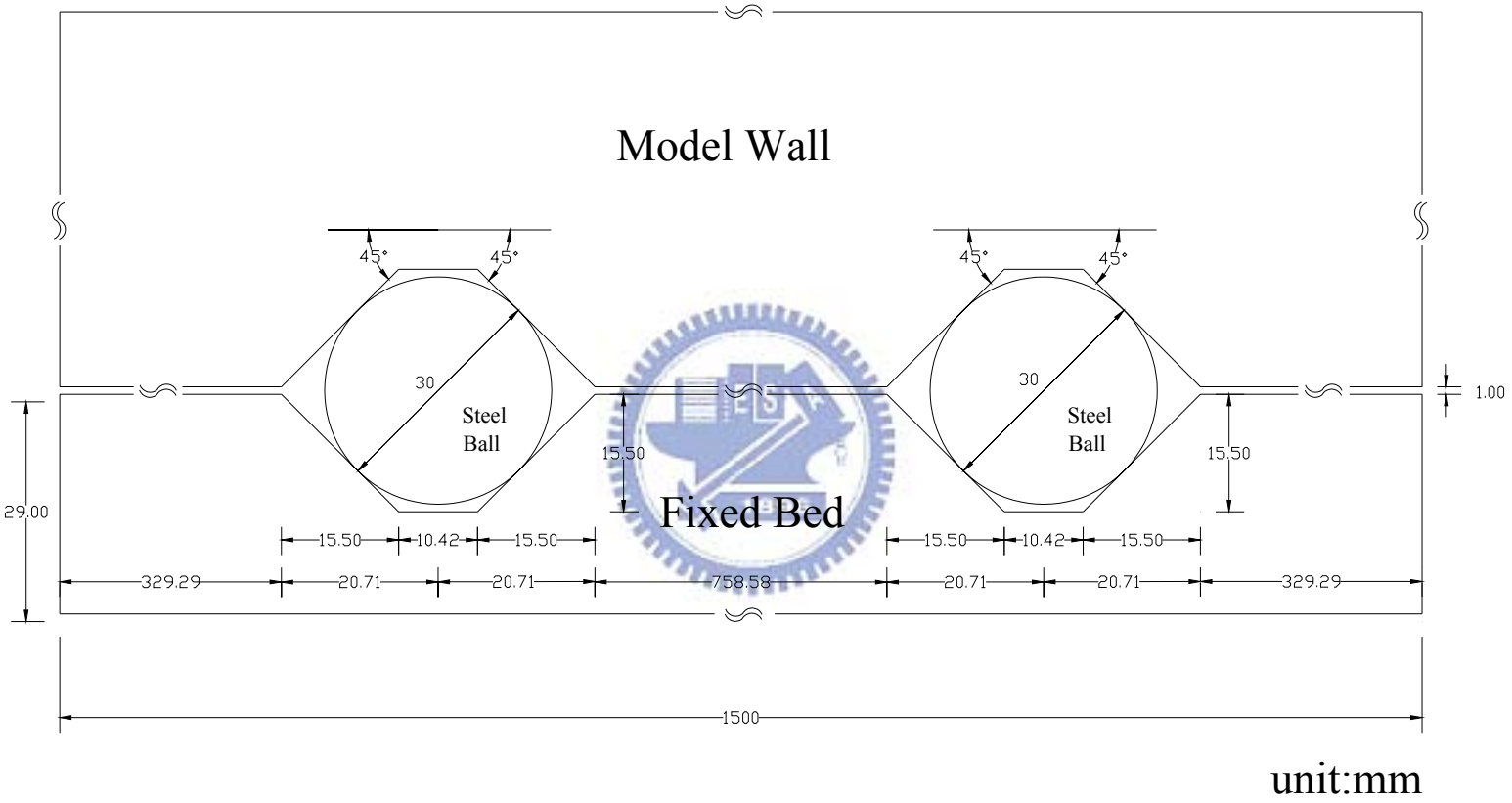

Fig. 3.16 Design of roller supports and unidirectional notches

Fig. 3.17 roller supports and unidirectional notches

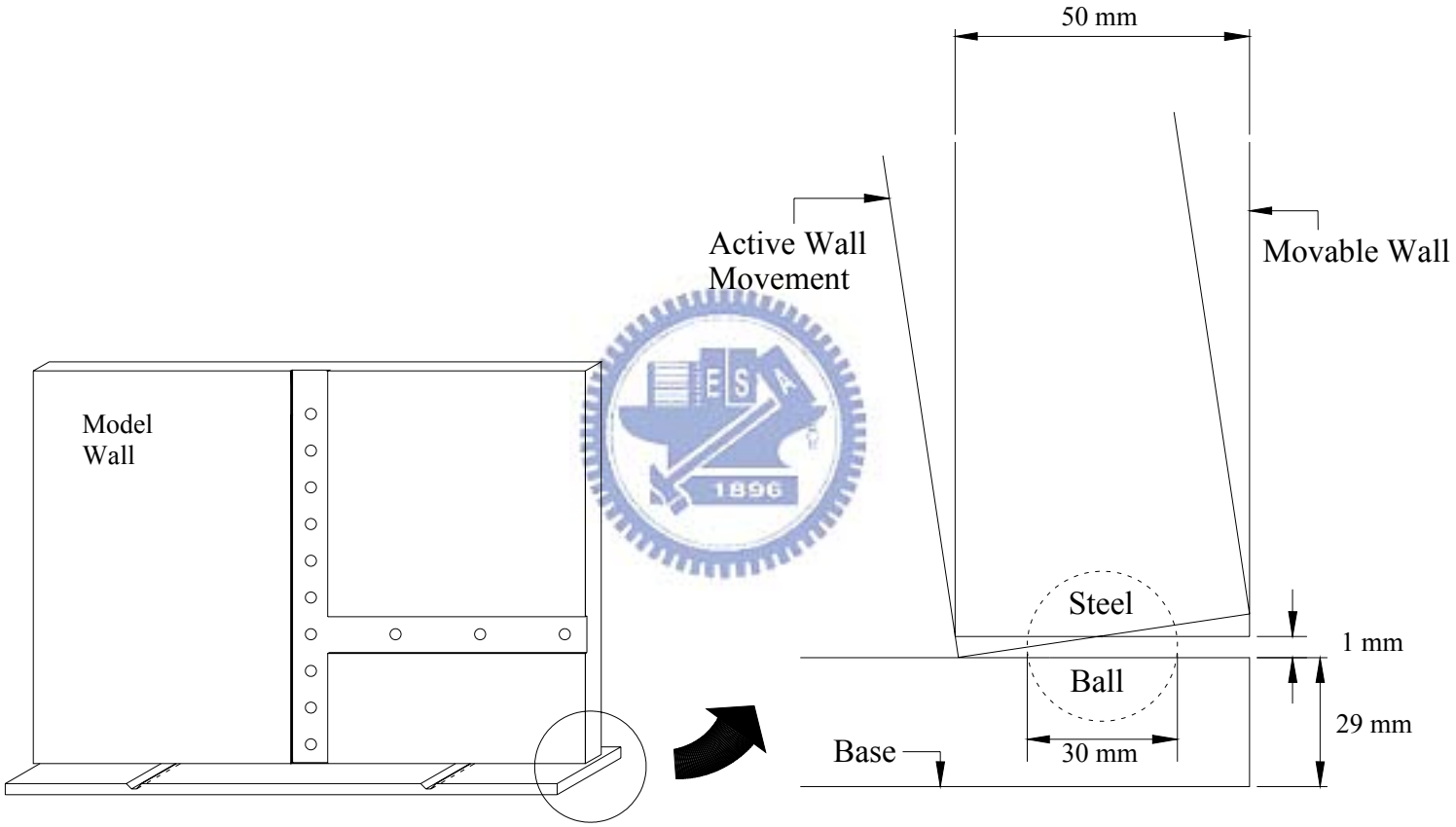

Fig. 3.18 Gap between model wall and fixed bed

Fig. 3.19 Soil pressure transducer (Kyowa PGM-0.2KG)

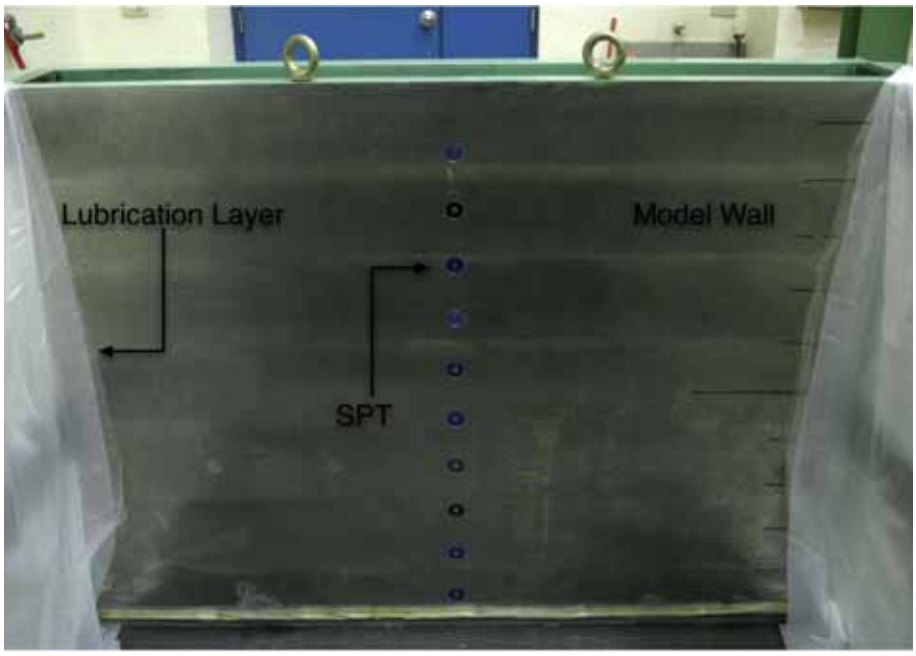

(a) front view

(b) rear view

Fig. 3.20 arrangement of soil pressure transducers

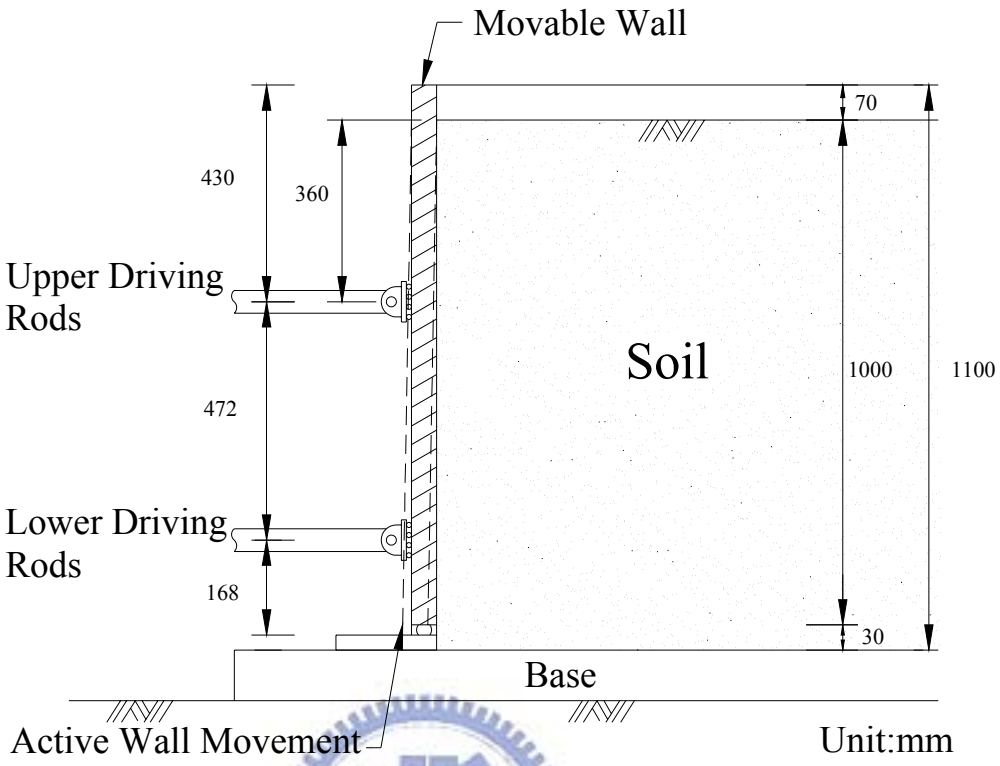

Fig. 3.21 Geometry of the wall rotation about the top

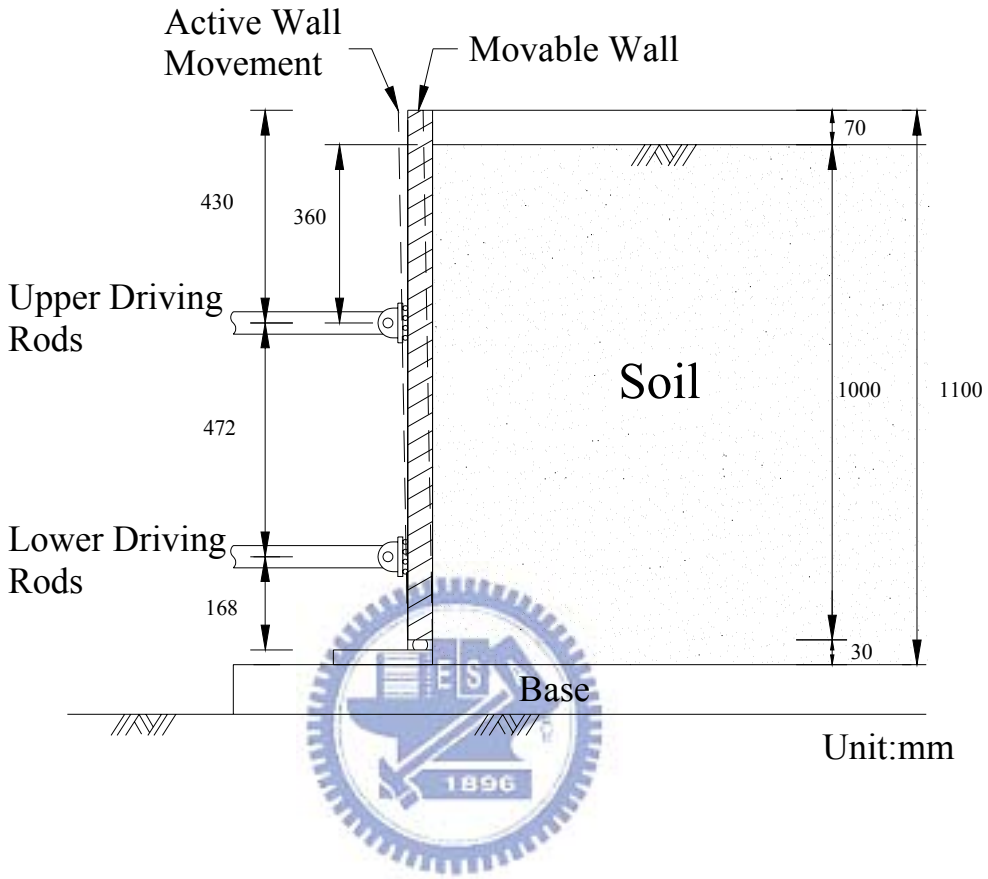

Fig. 3.22 Geometry of the wall rotation about the base

Fig. 3.23 Acrylic cover to protect driving system

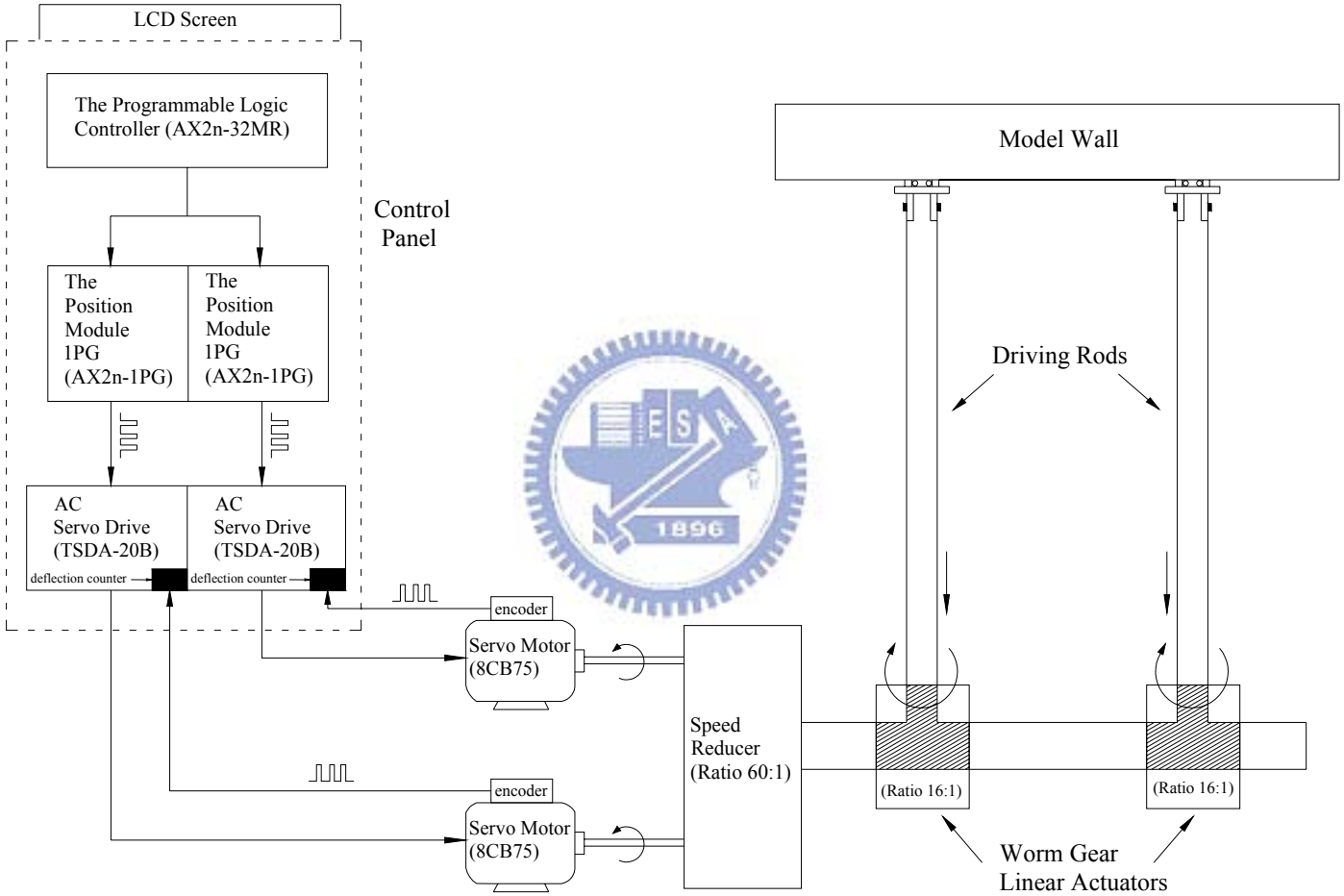

Fig. 3.24 Wall-driving system

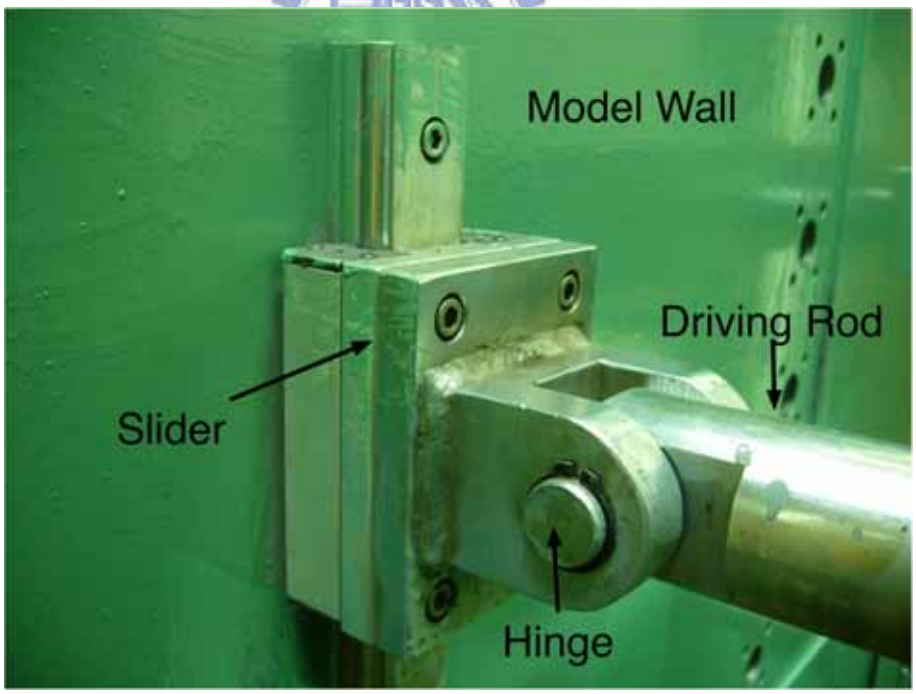

Fig. 3.25 Hinge-and-slider

Fig. 3.26 Servo motor of driving system

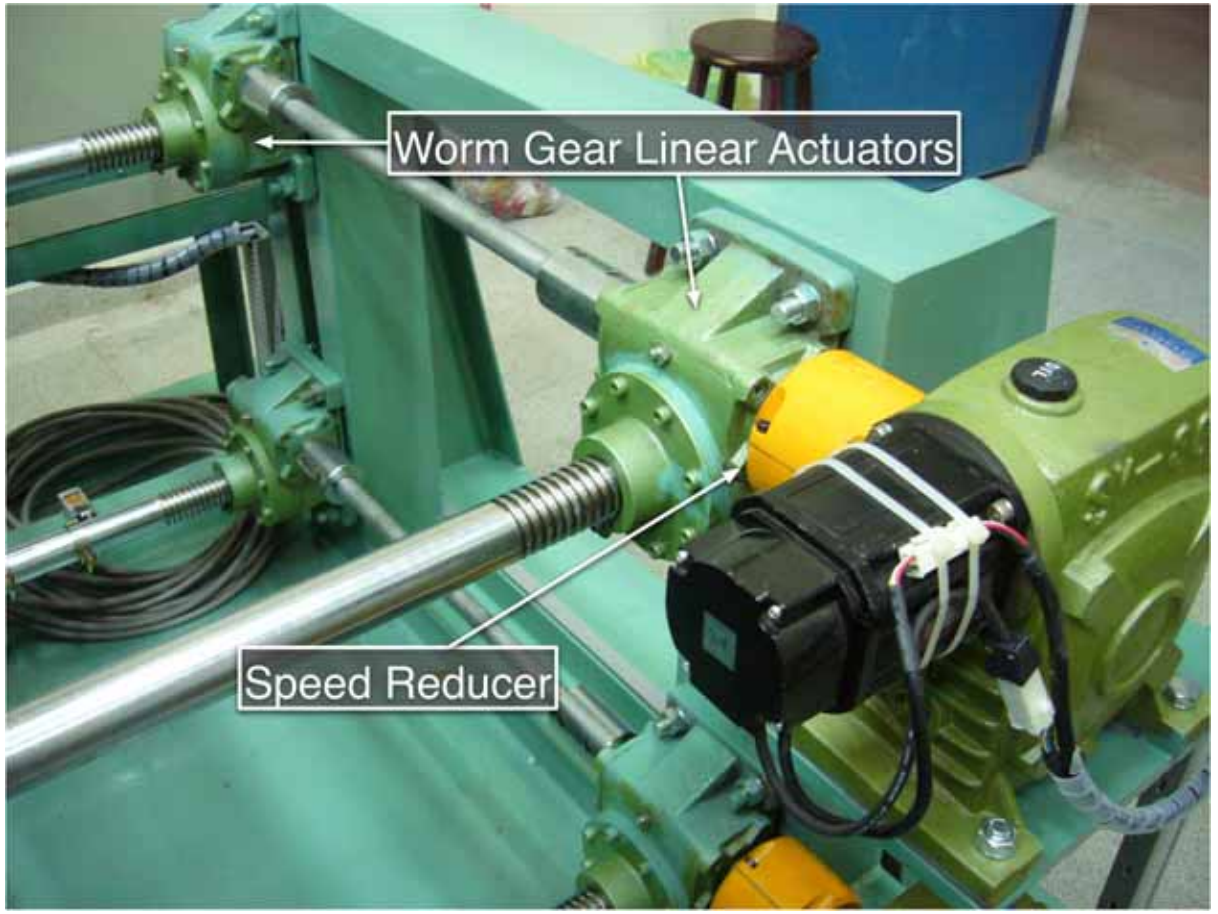

Fig. 3.27 Speed reducer and worm gear linear actuators of driving system

(a) Outward appearance

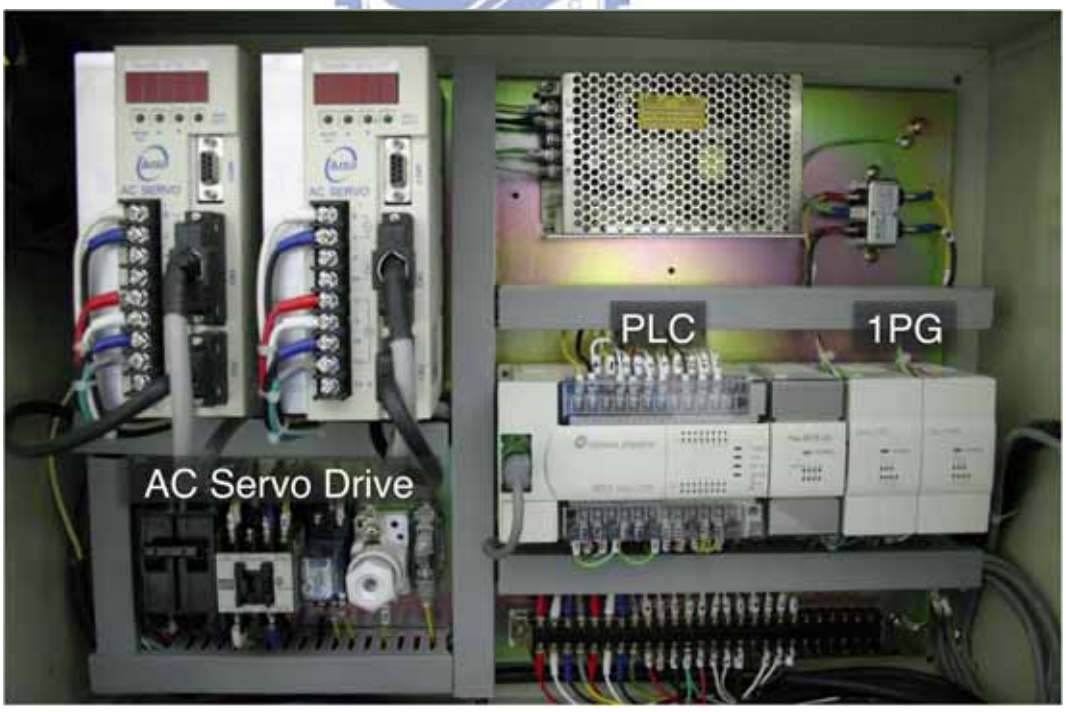

(b) Instrumentation inside the control panel

Fig. 3.28 Control panel of wall driving system

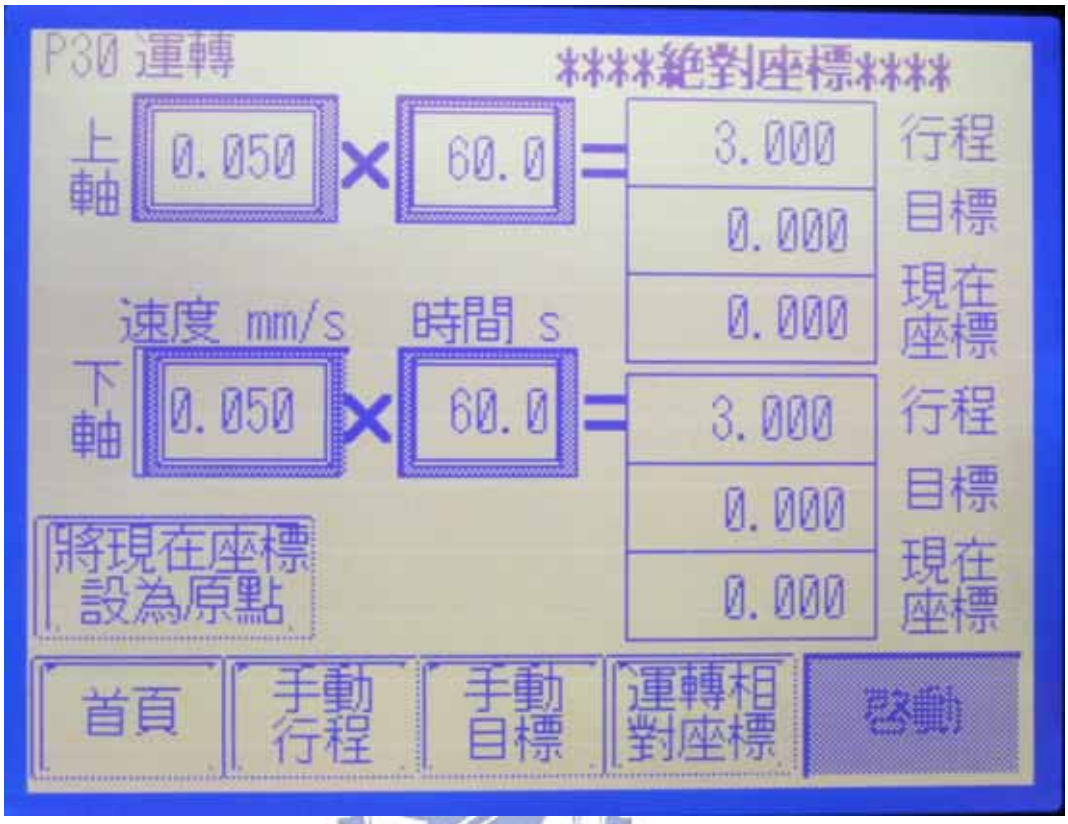

Fig. 3.29 Touch control LCD display

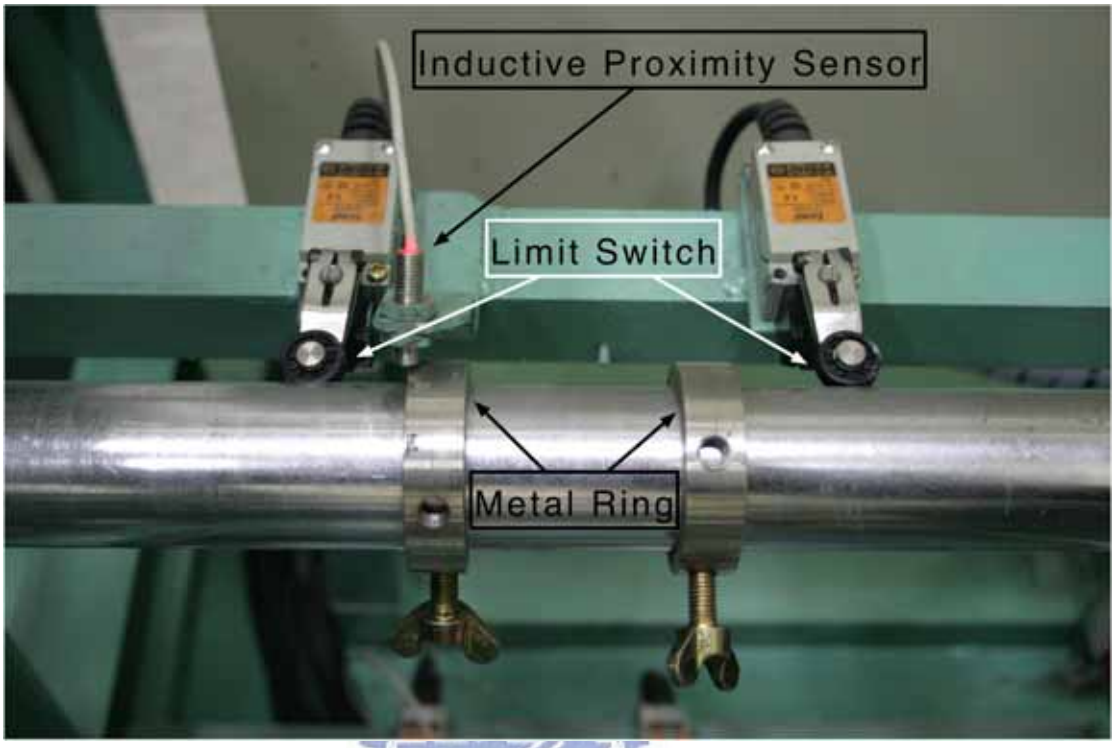

Fig. 3.30 Inductive proximity switch and limit switch

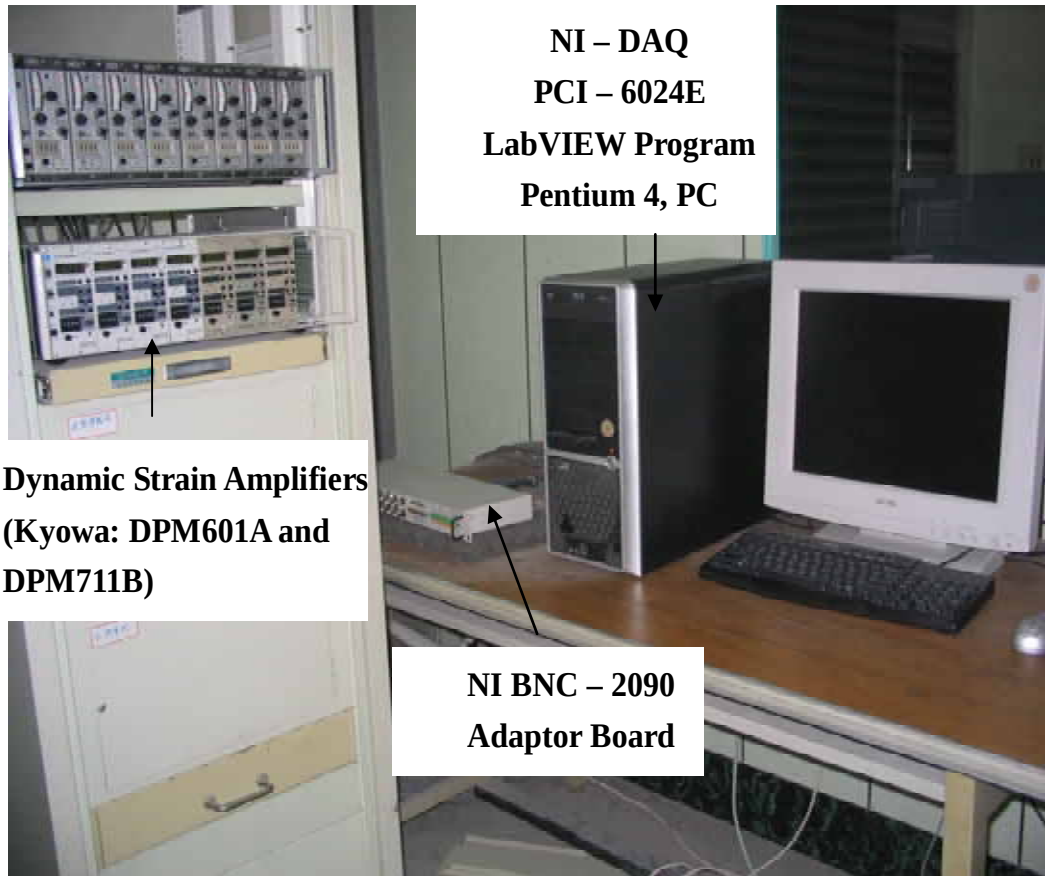

Fig. 3.31 Data acquisition system

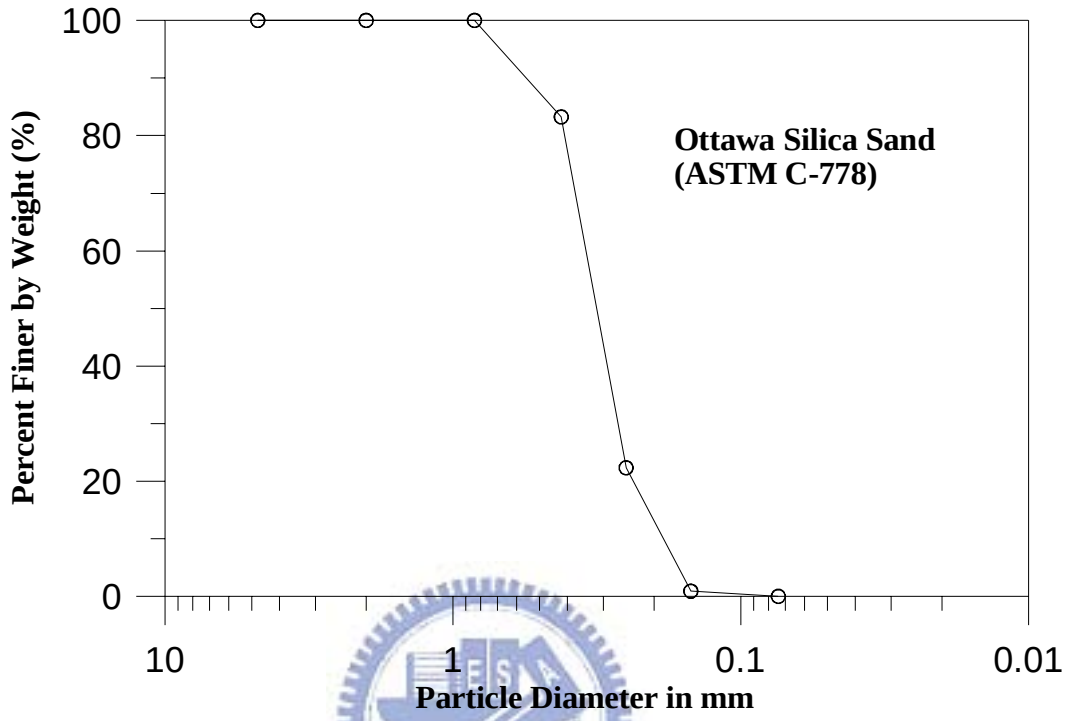

Fig. 4.1 Grain size distribution of Ottwa sand

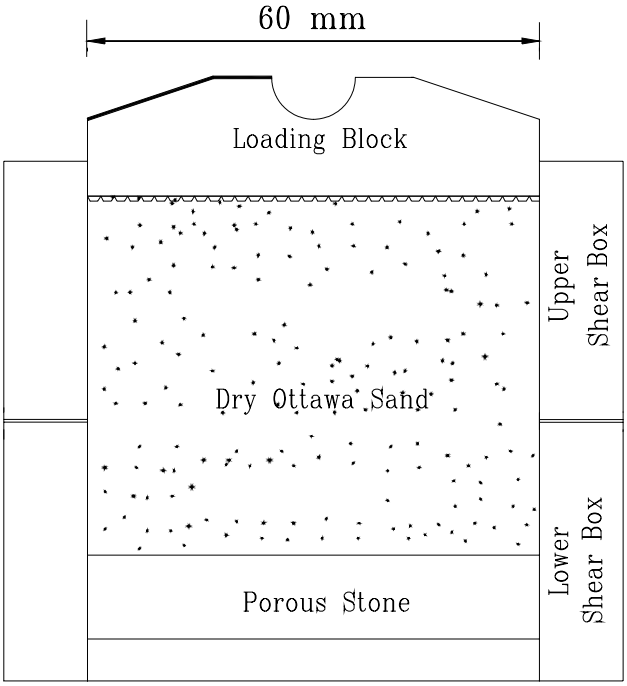

Fig. 4.2 Shear box of direct shear test device (after Wu, 1992)

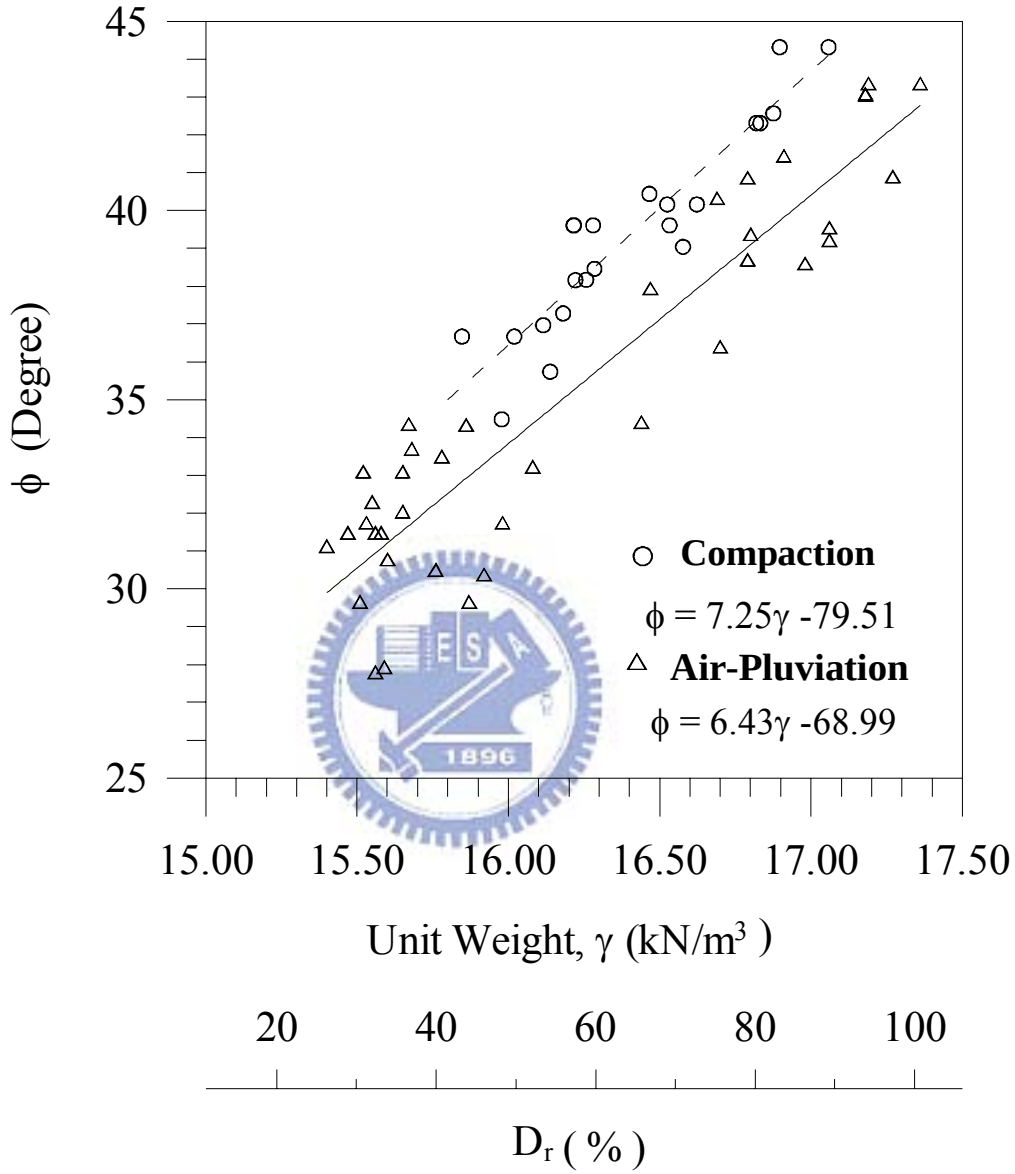

Fig. 4.3 Relationship between unit weight γ and internal friction angle ϕ (after Chang, 2000)

Fig 4.4 Pluviation of the Ottawa sand into soil bin

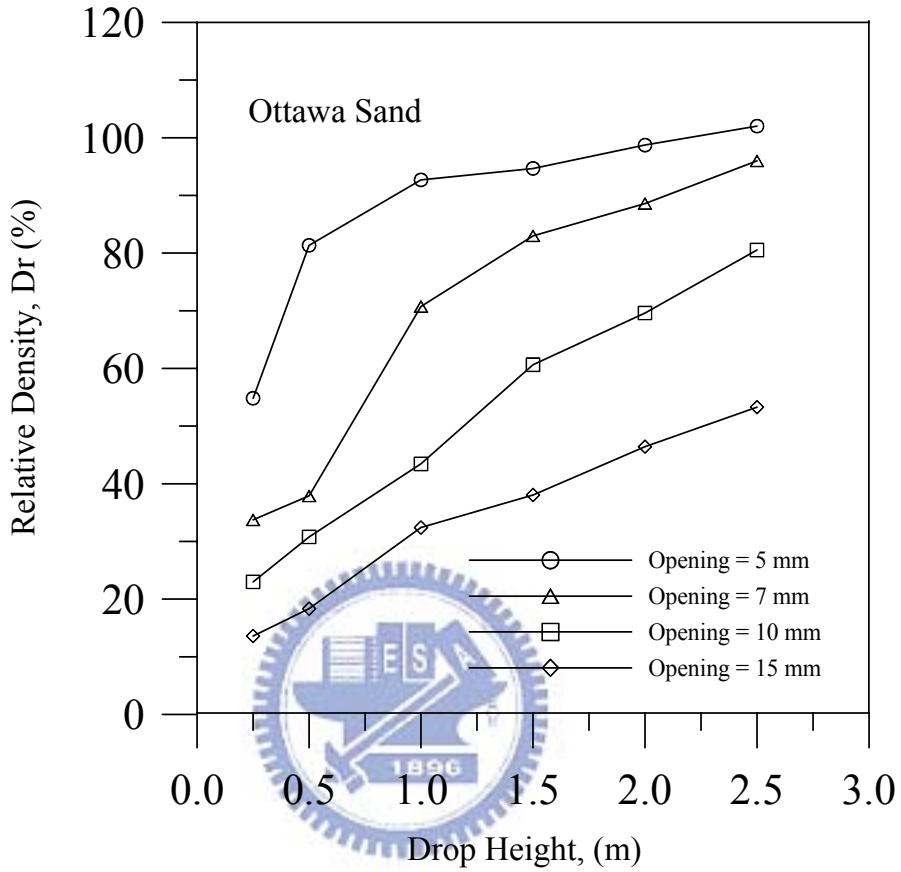

Fig. 4.5 Relationship between relation density and drop height (after Ho, 1999)

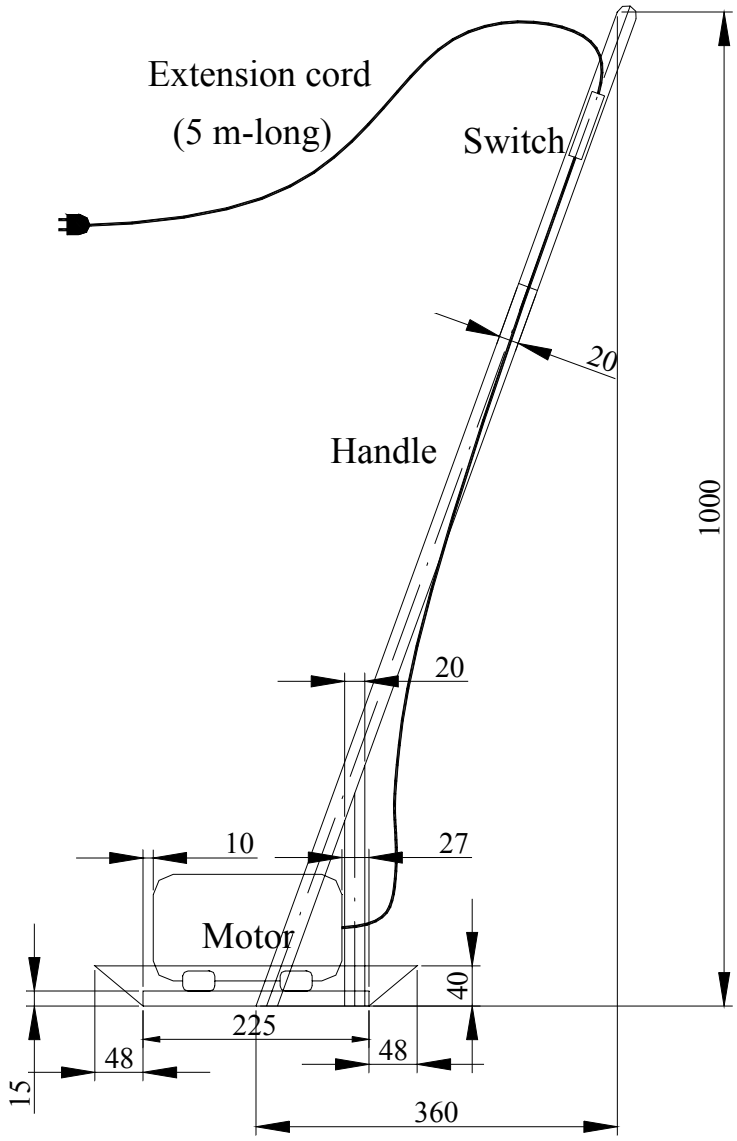

unit :mm

Fig. 4.6 Side-view of vibratory soil compactor

Fig. 4.7 Square vibratory soil compactor

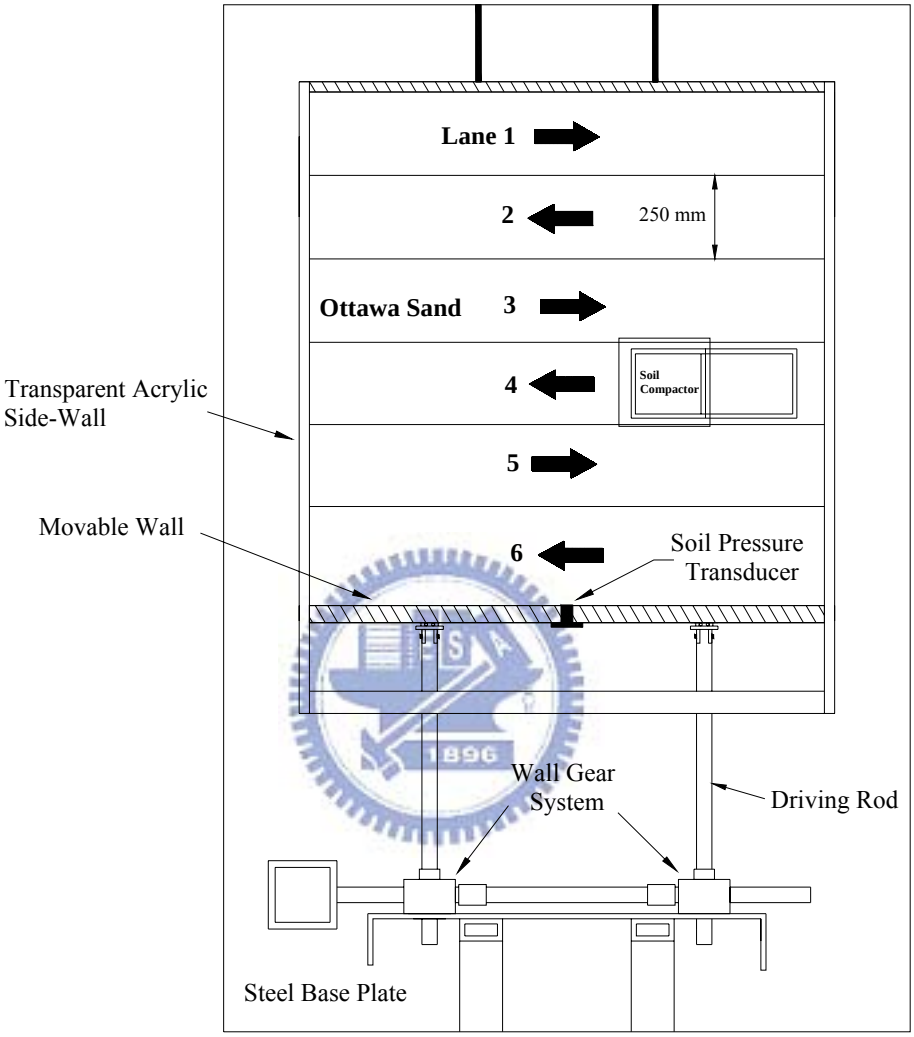

Fig. 4.8 Backfill compacted with square compactor in 6 lanes

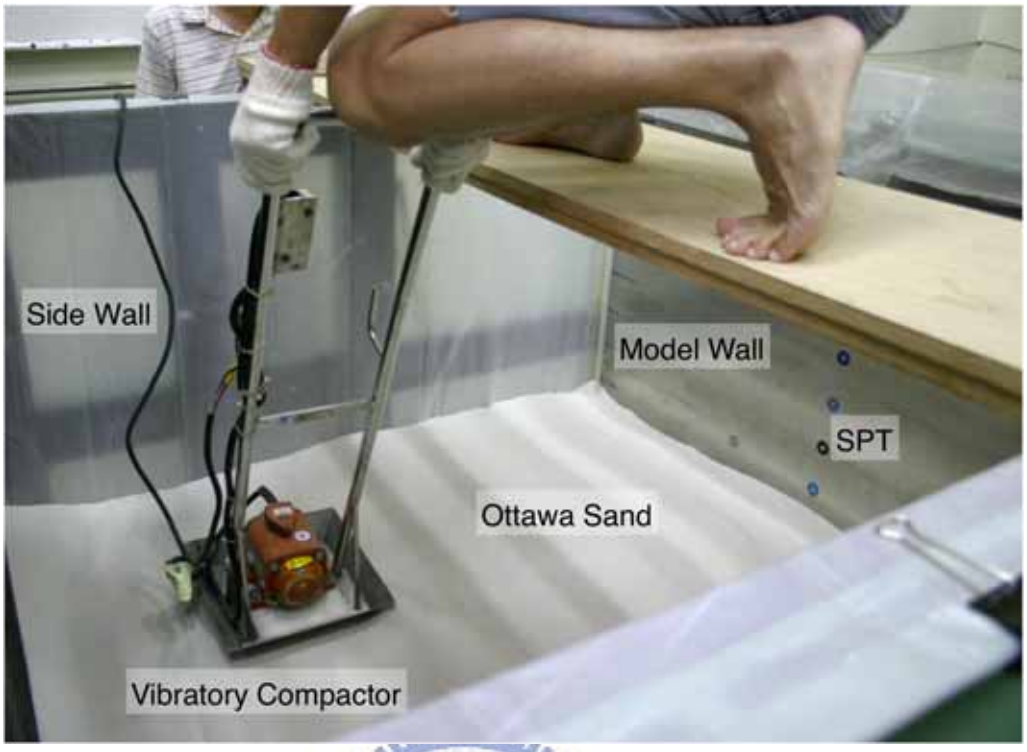

(a) Compaction at H = 0.2 m

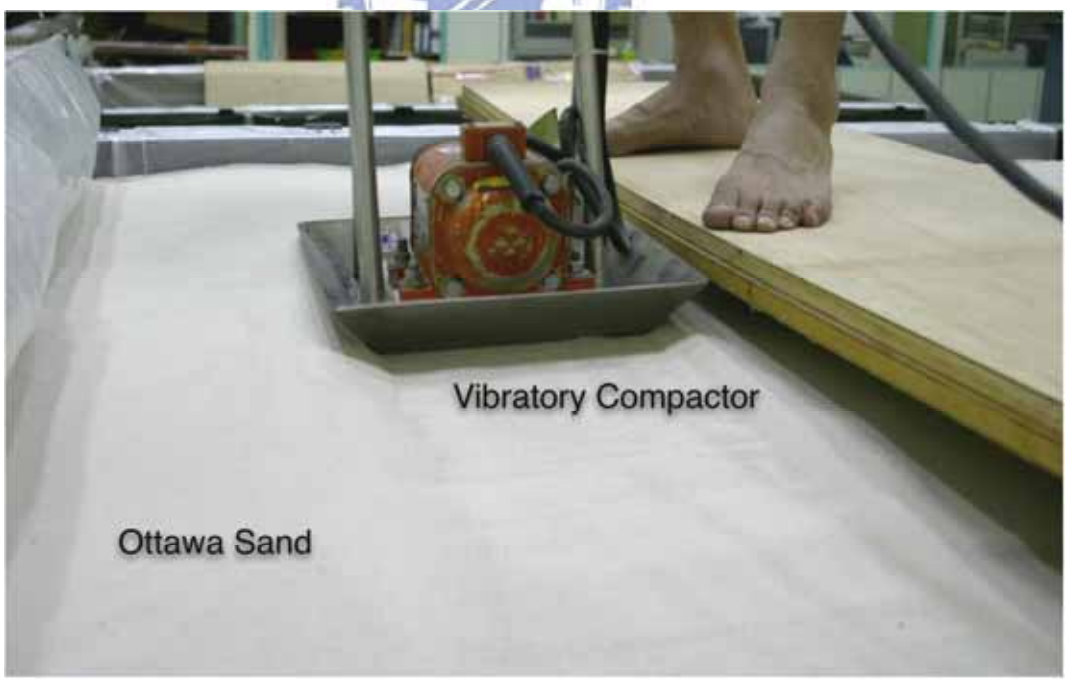

(b) Compaction at H= 1 m

Fig. 4.9 Compaction of backfill with square compactor

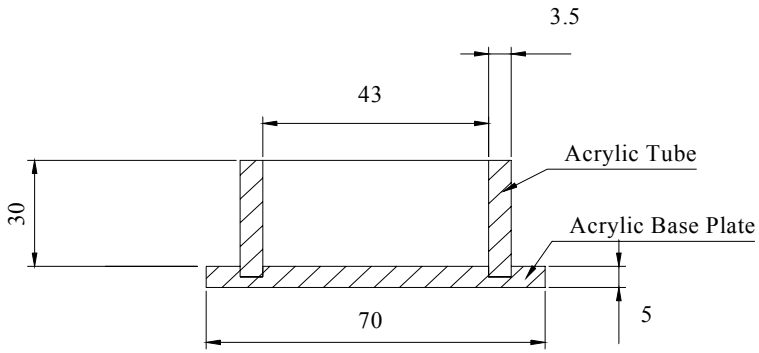

Side-view

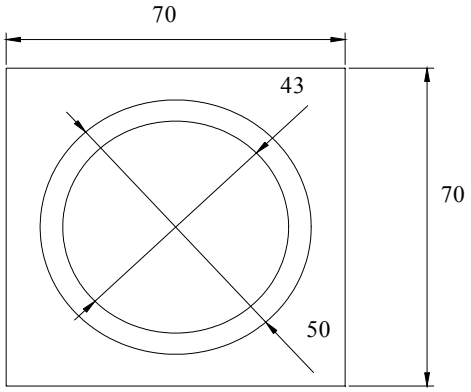

Top-view

unit : mm

Fig. 4.10 Soil-density control cup

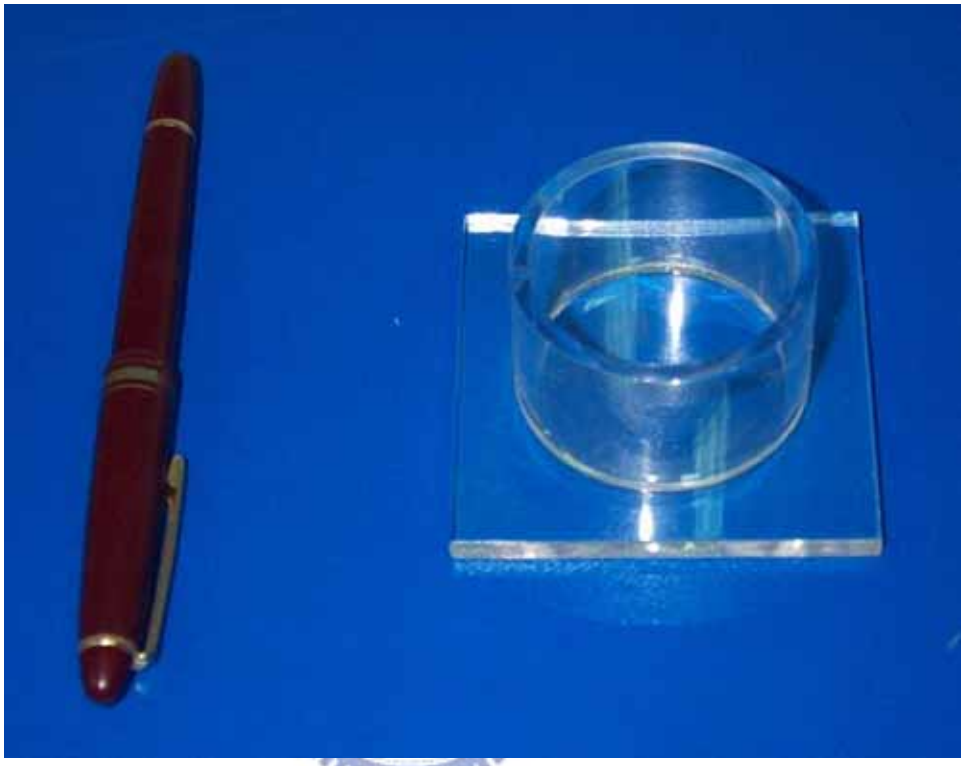

Fig. 4.11 Soil-density cup

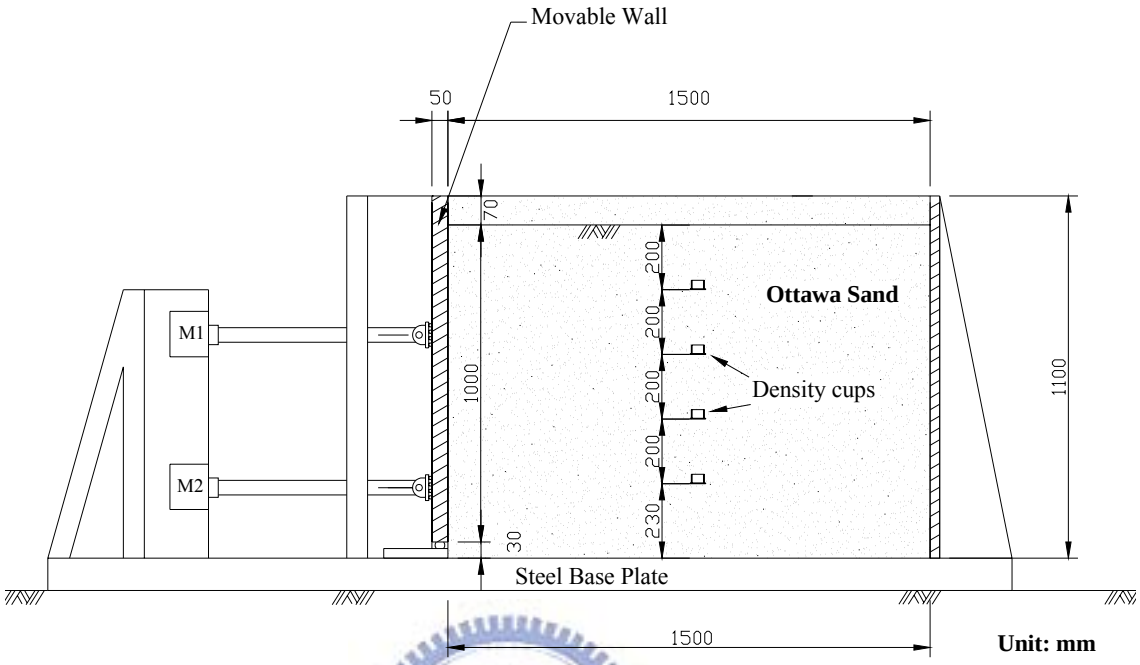

Fig. 4.12 Soil density cups buried at the different elevations

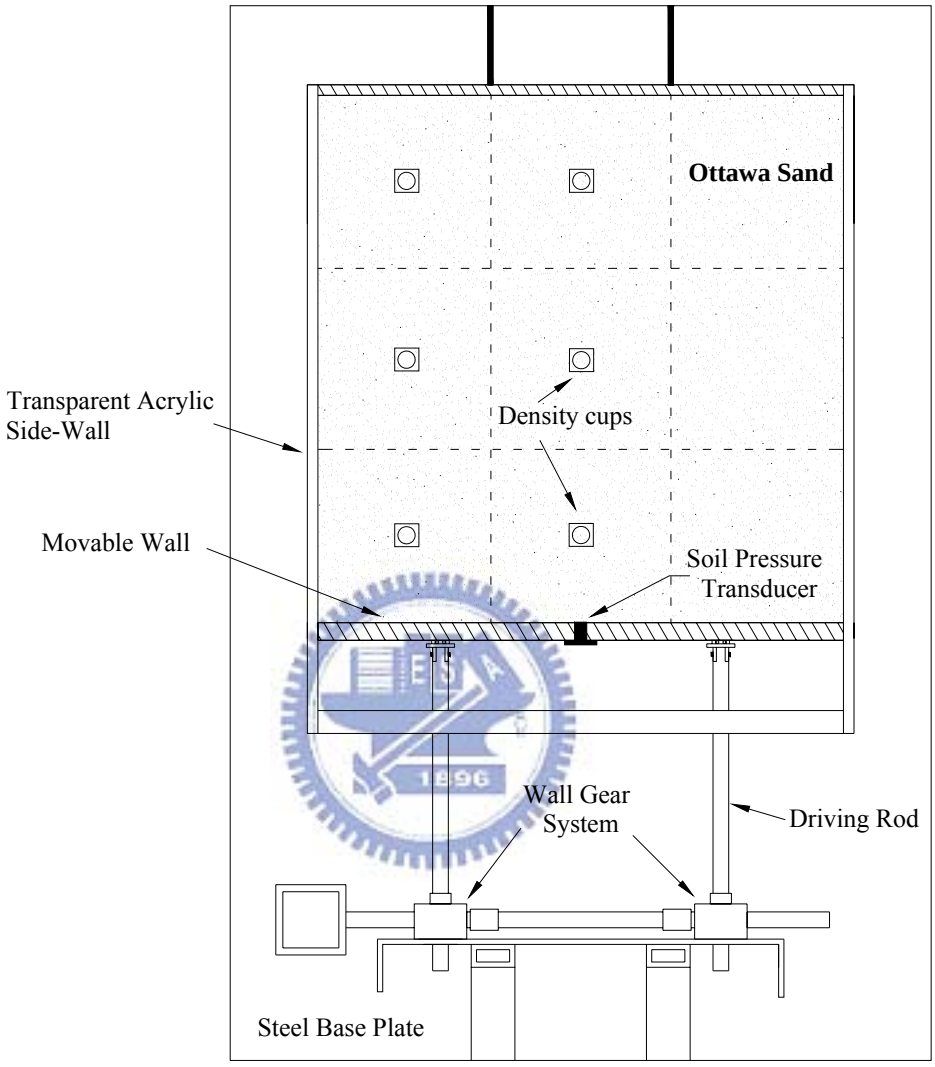

Fig 4.13 Locations of soil density cups at the elevation

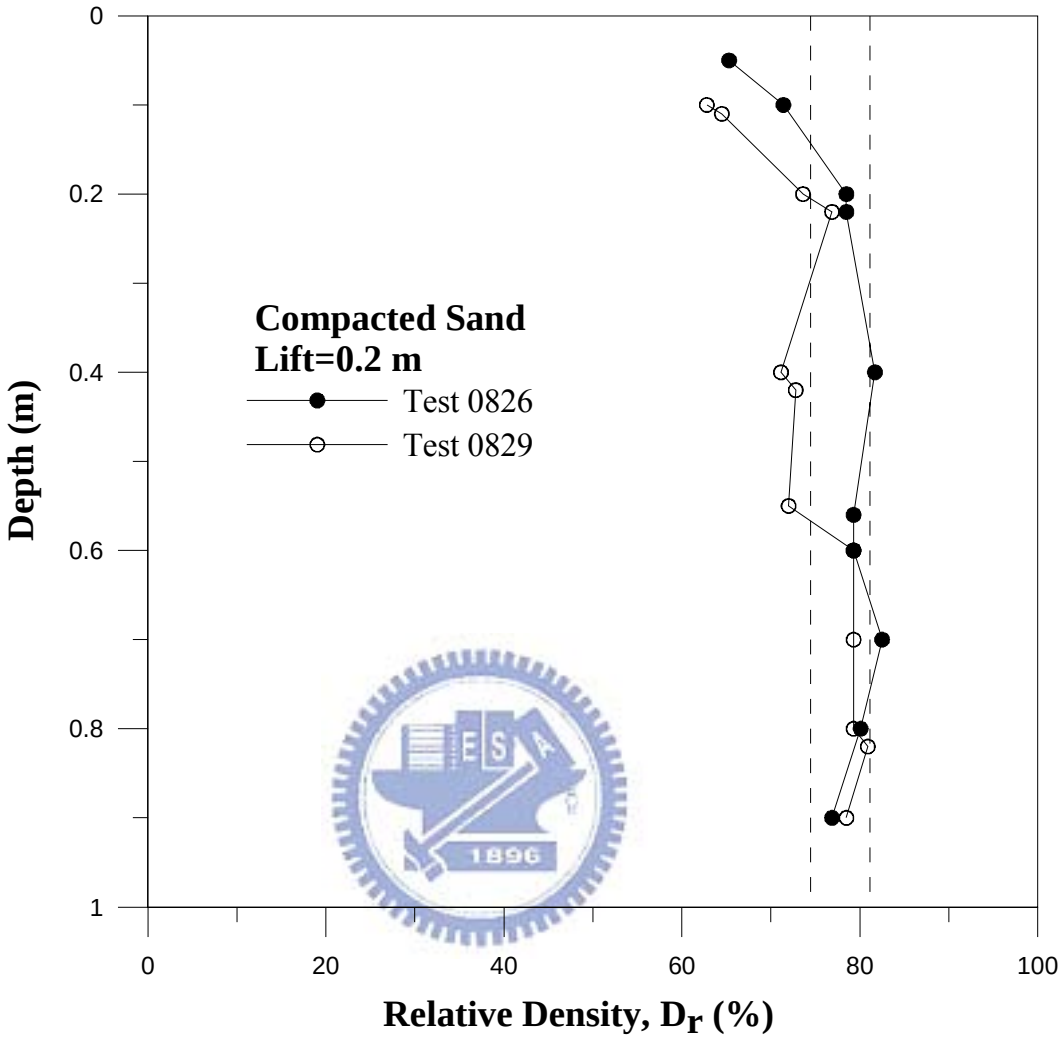

Fig. 4.14 Distribution of soil density compacted with square compactor

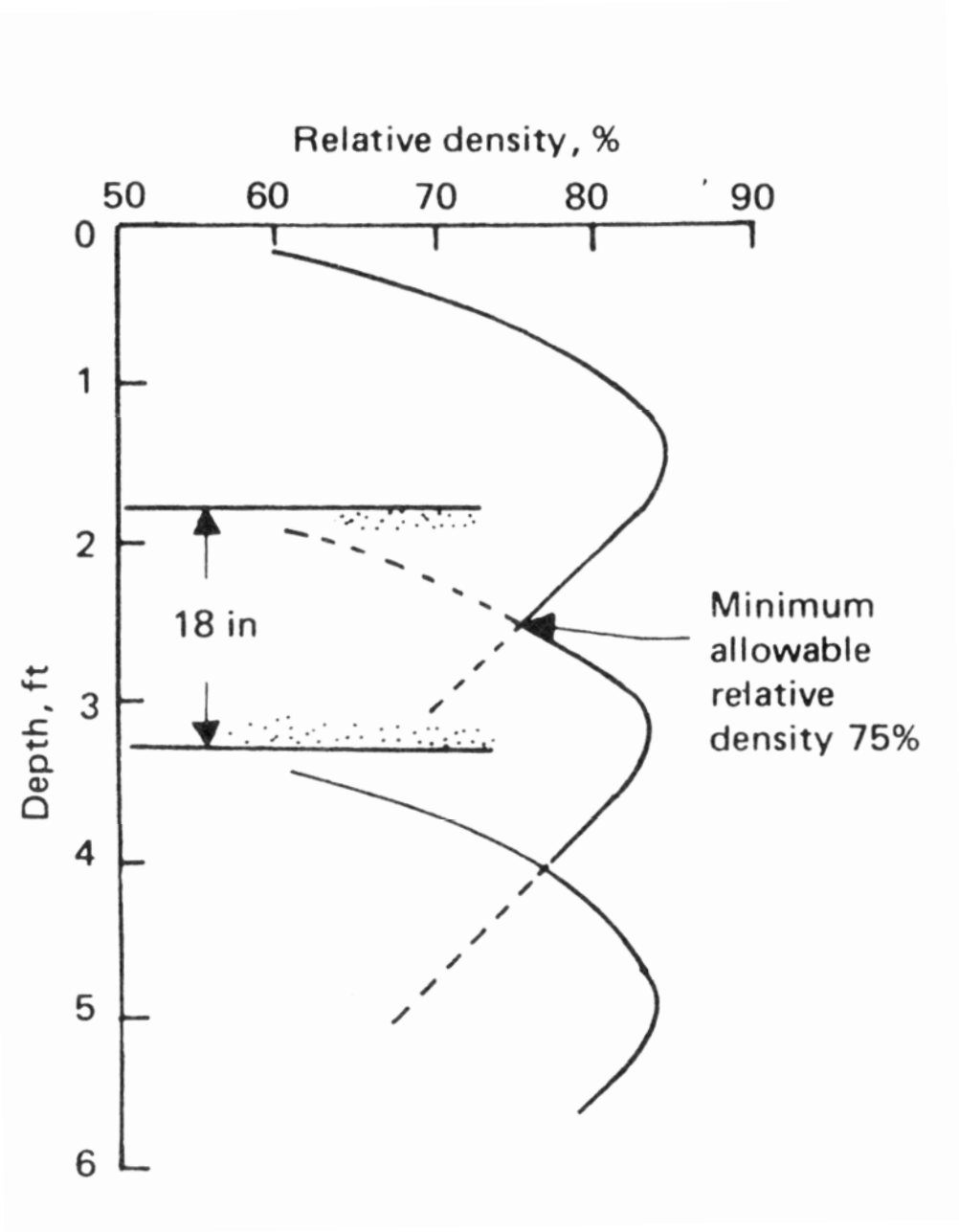

Fig. 4.15 Relative density vs. Depth relation for vibratory roller compaction (after D'Appolonia et al., 1969)

Fig. 4.16 Lubrication layer on the side wall

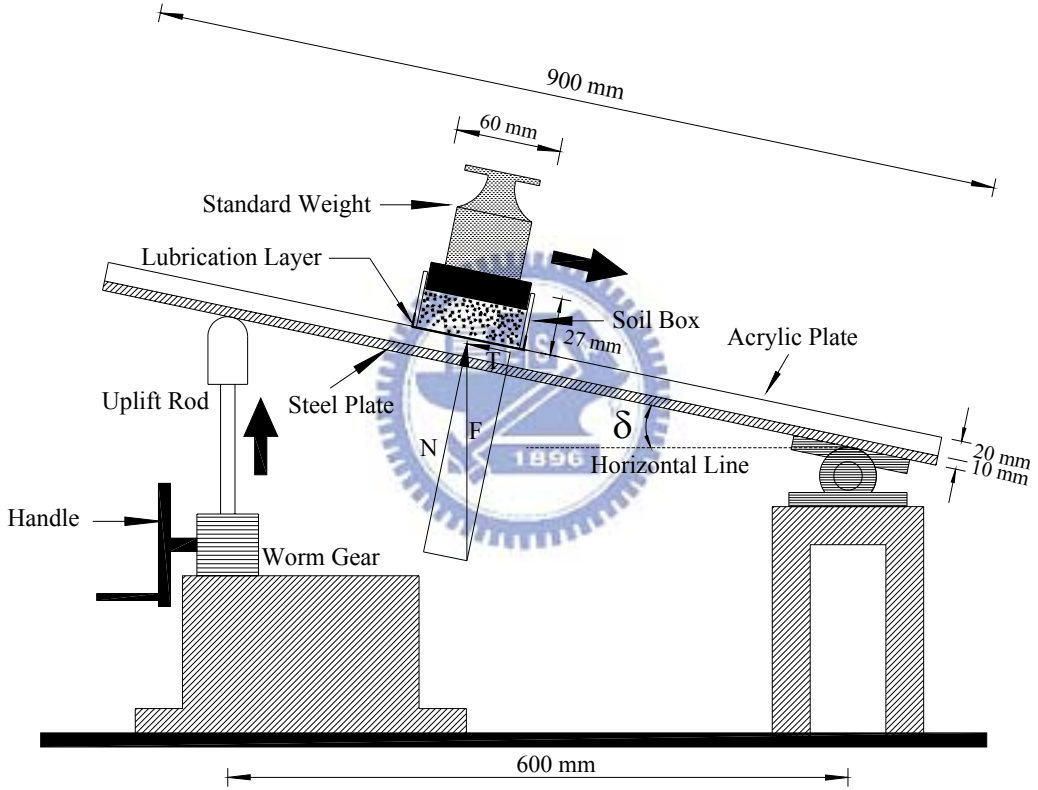

Fig. 4.17 Schematic diagram of sliding block test (after Fang et al., 2004)

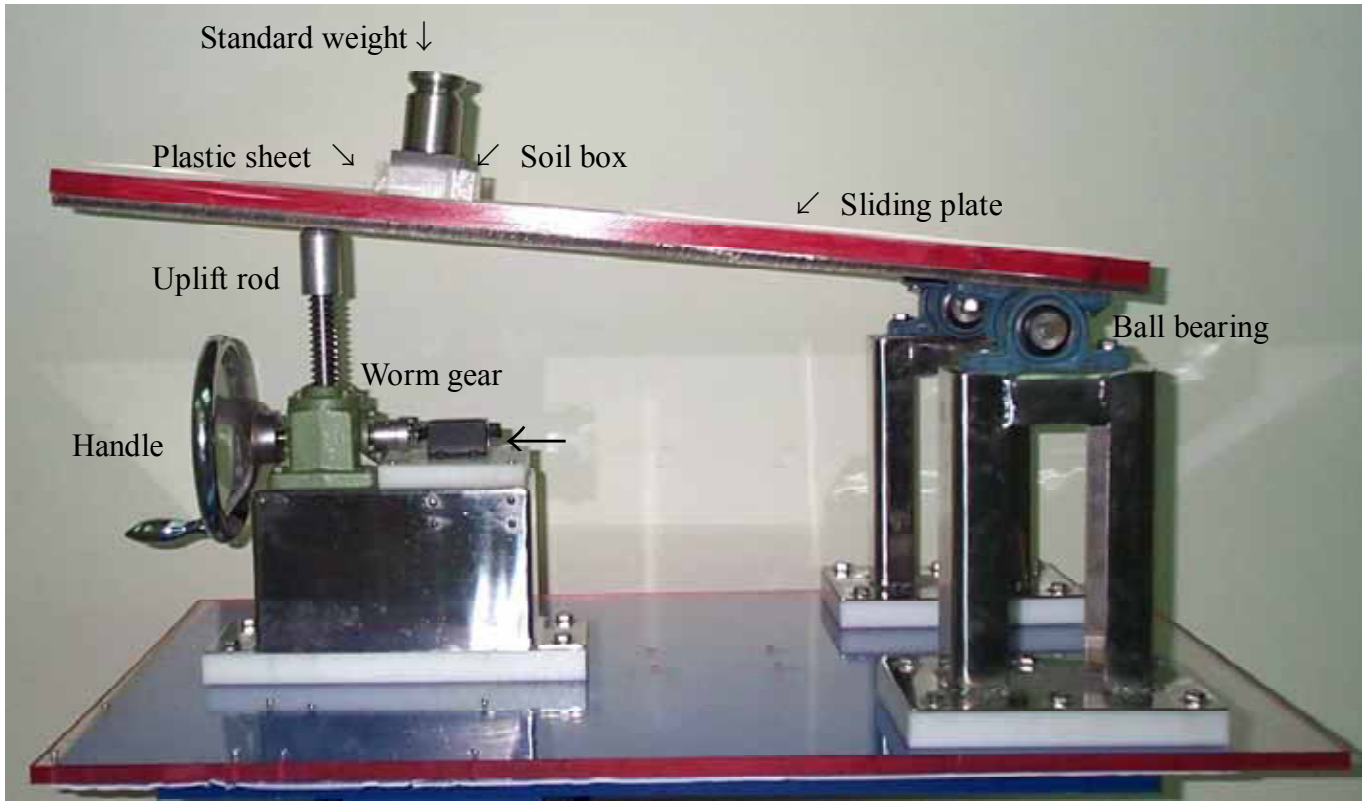

Fig.4.18 Sliding block test apparatus (after Fang et al., 2004)

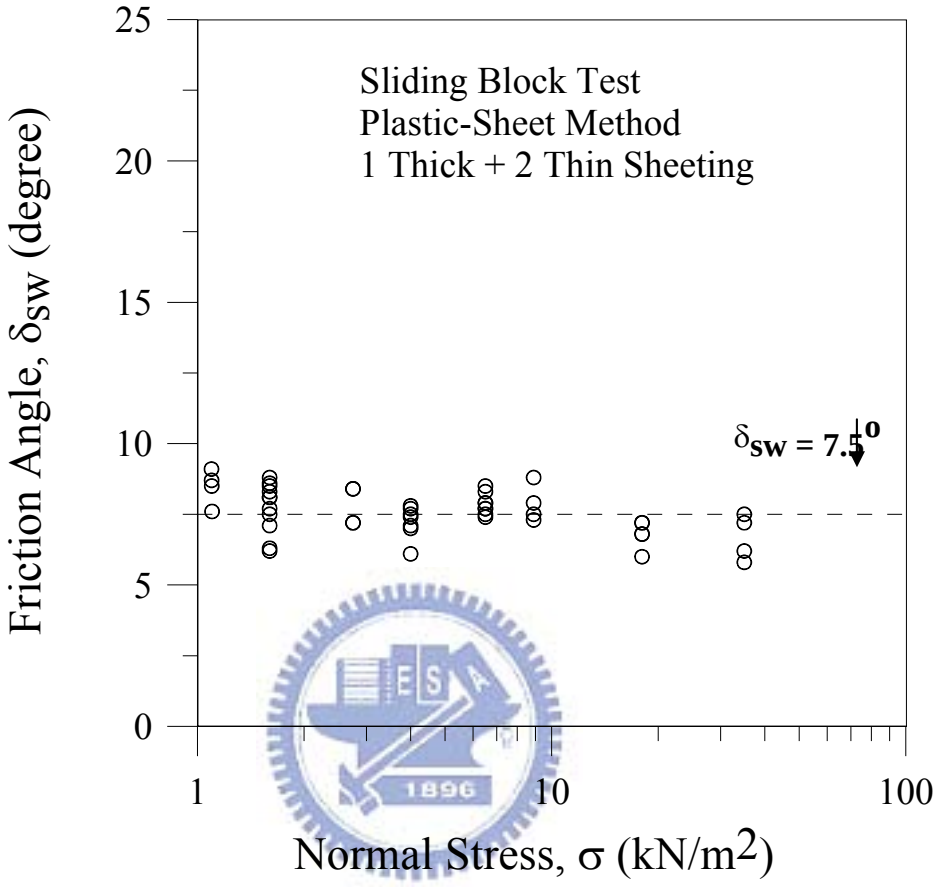

Fig. 4.19 Variation of interface friction angle with normal stress

(after Fang et al., 2004)

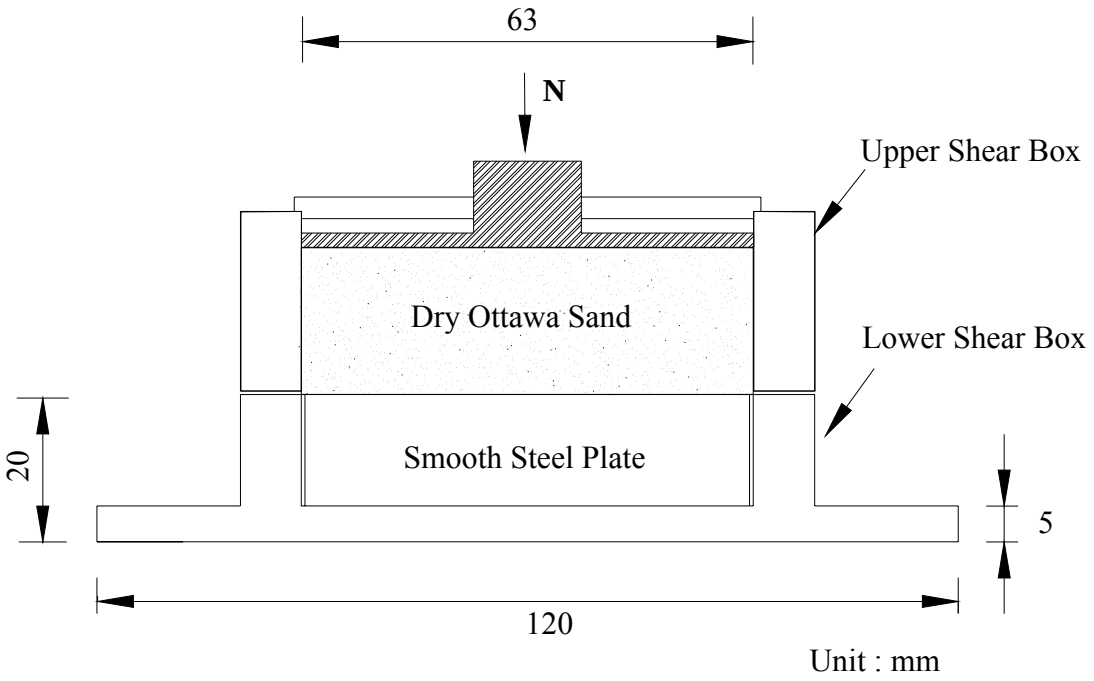

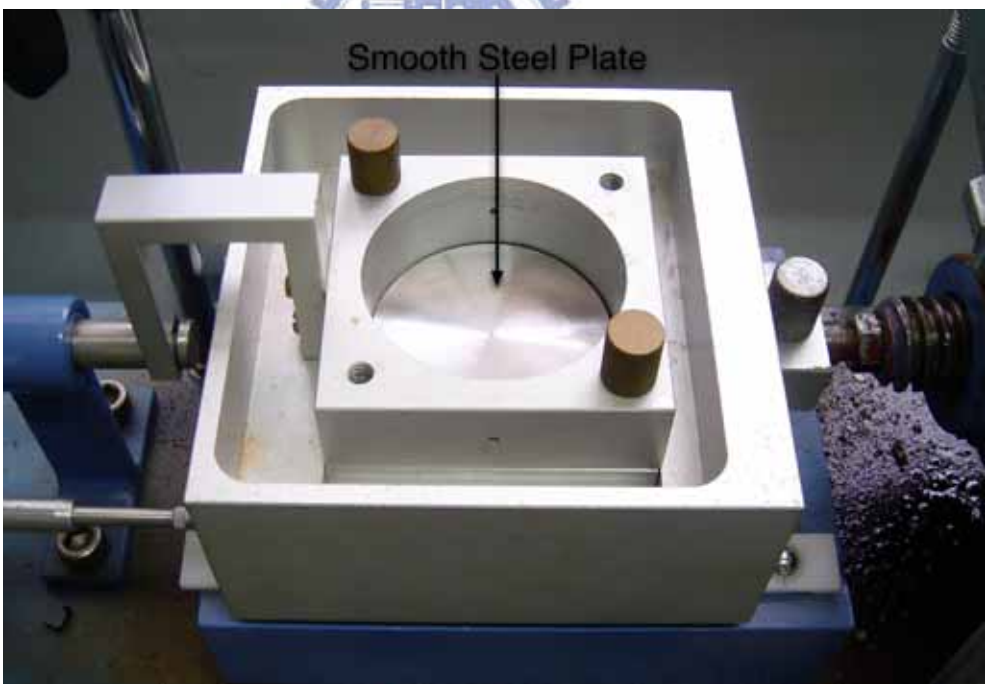

Fig. 4.20 Direct shear test arrangement to determine wall friction angle

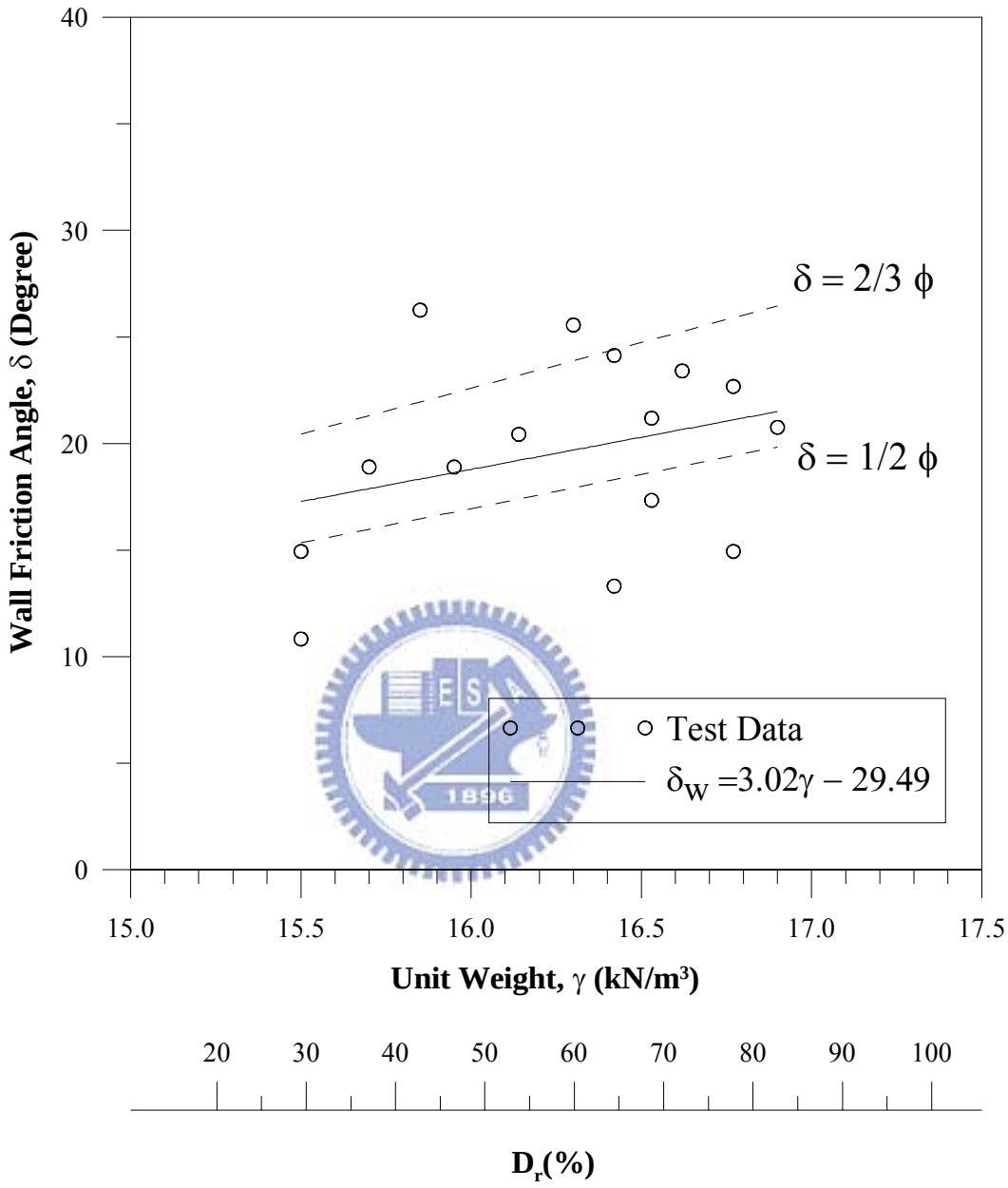

Fig. 4.21 Relationship between unit weight γ and wall friction angle δ_w

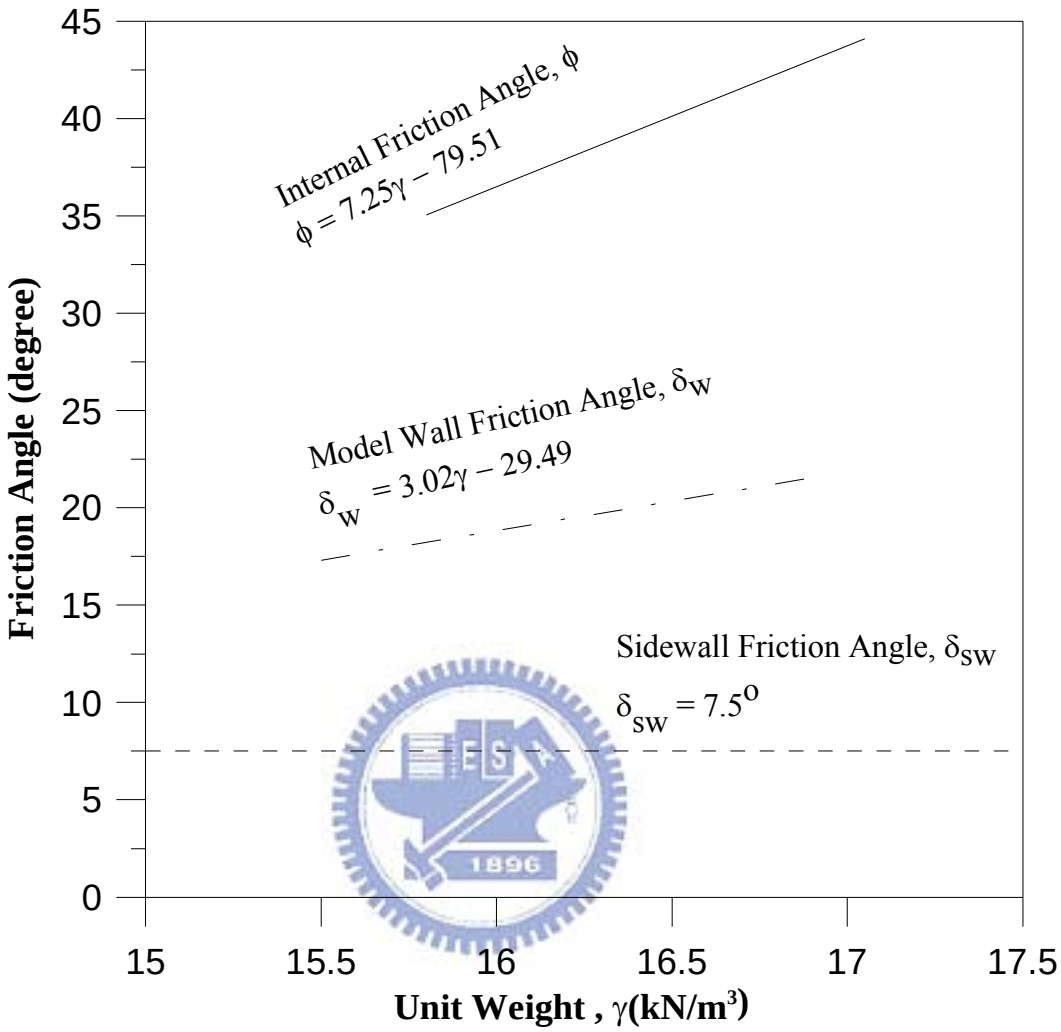

Fig. 4.22 Relationship between unit weight γ and different friction angles

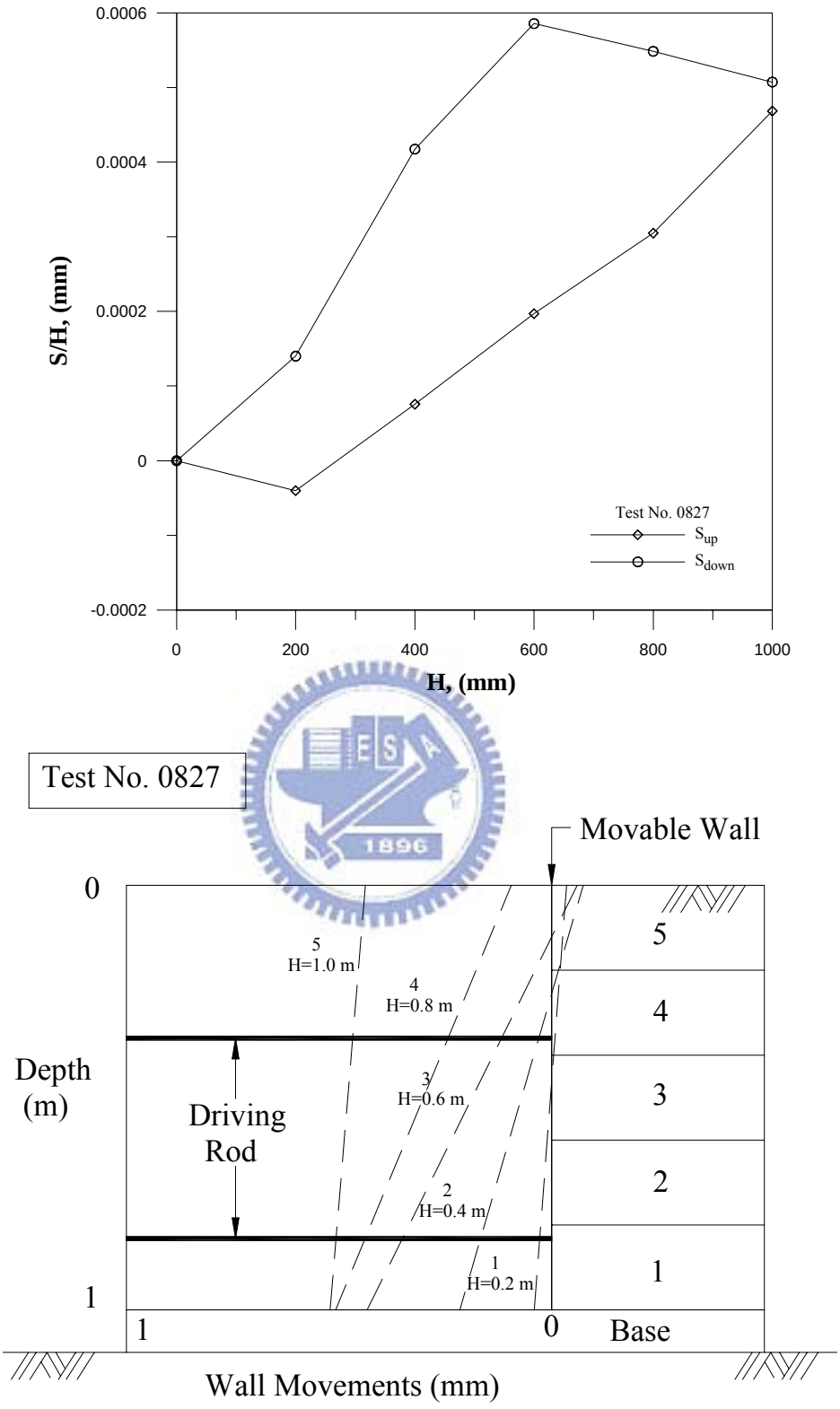

Fig. 5.1 Variation of wall movements during compaction of backfill

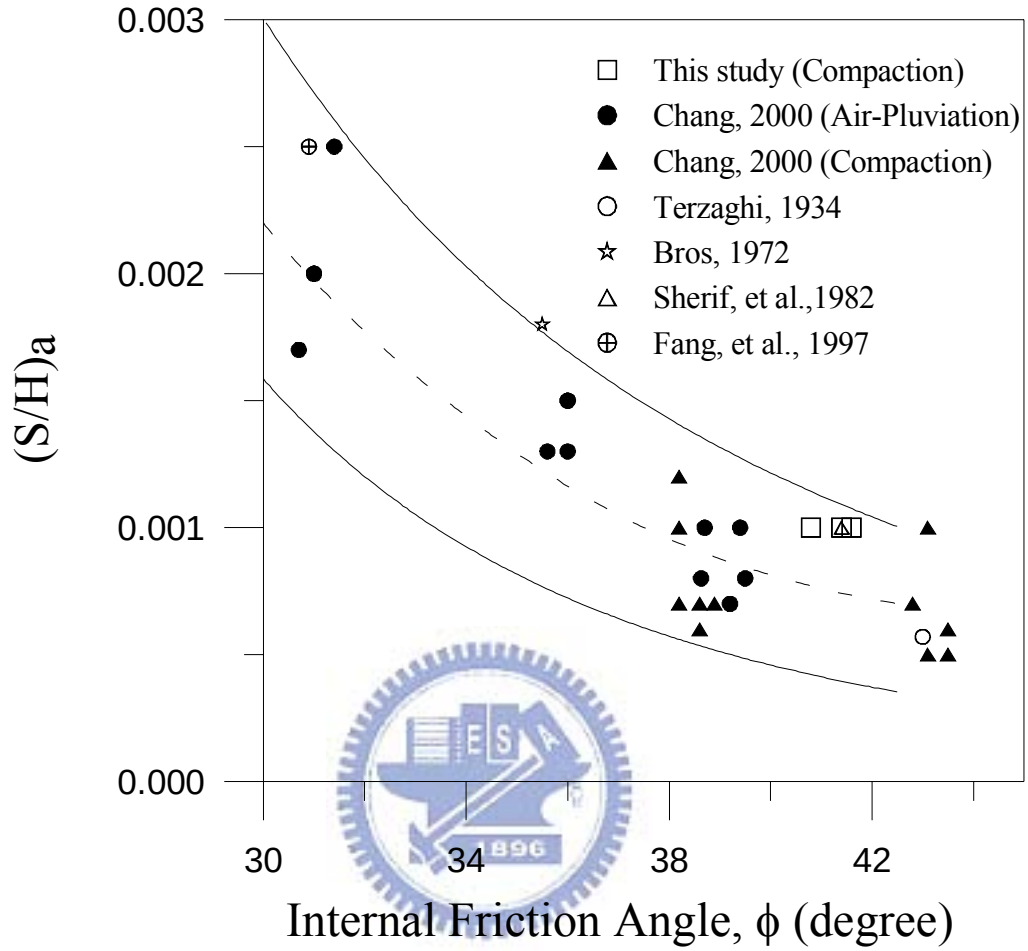

Fig. 5.2 Variation of $(S/H)_a$ for backfill with different internal friction angle

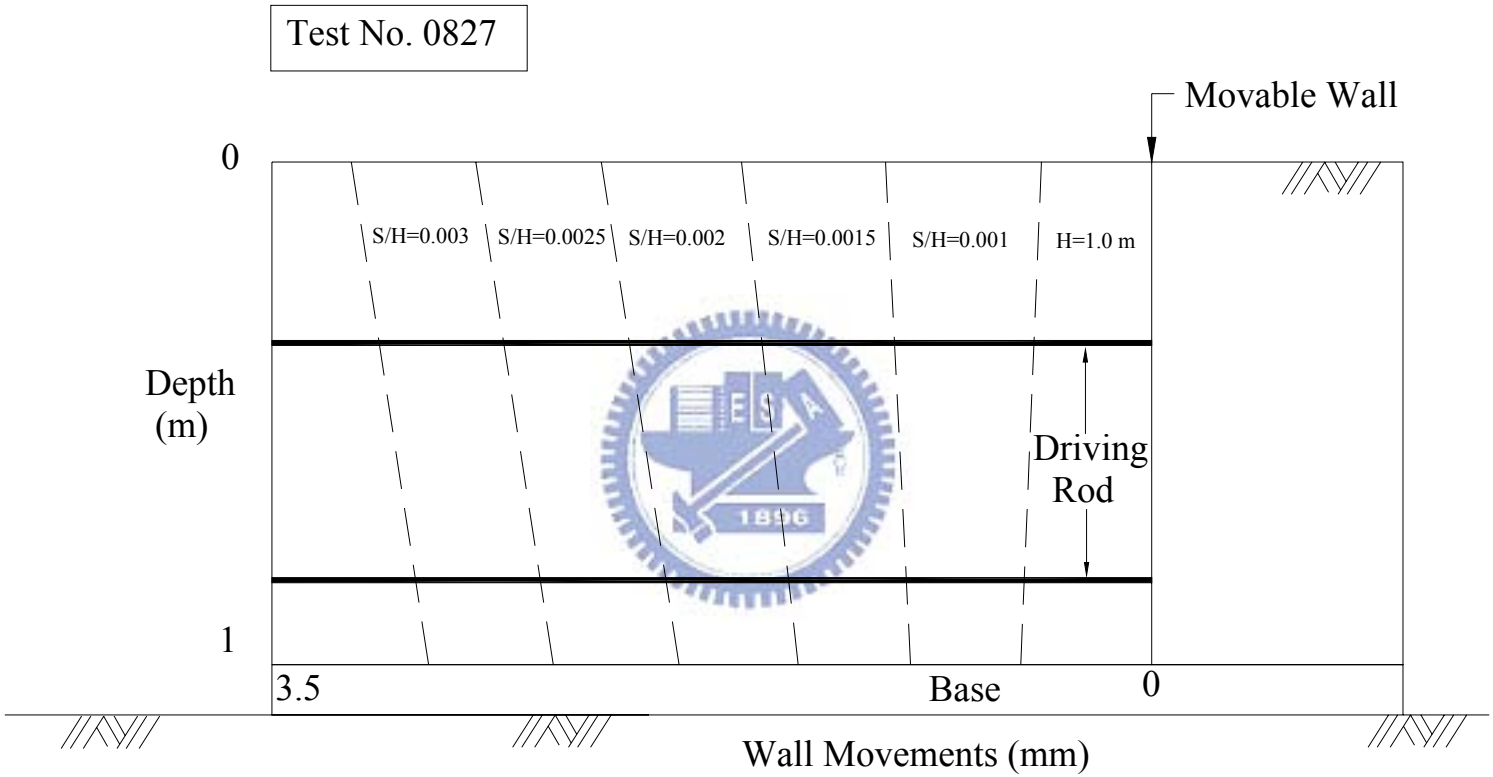

Fig. 5.3 Wall movement for T mode (Test 0827)

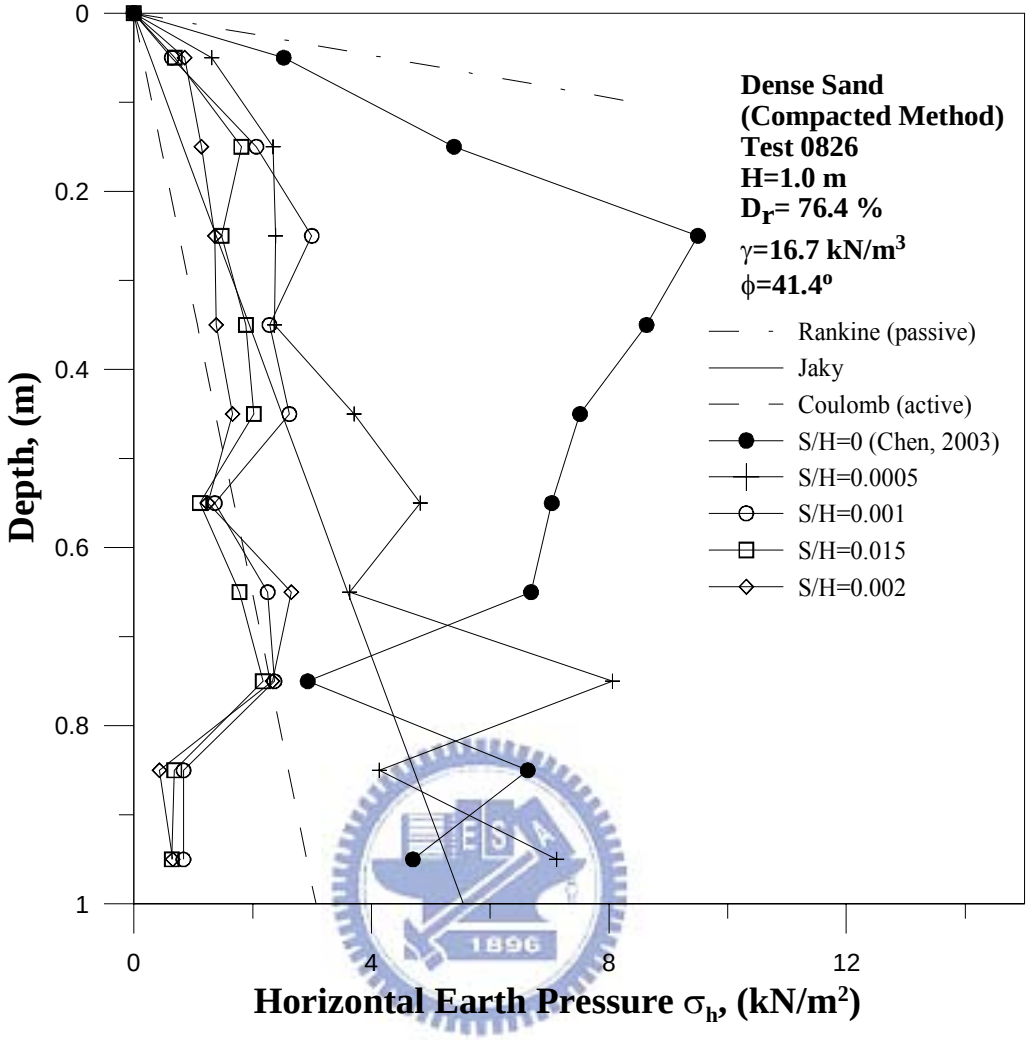

Fig. 5.4 Distribution of horizontal earth pressure (Test 0826)

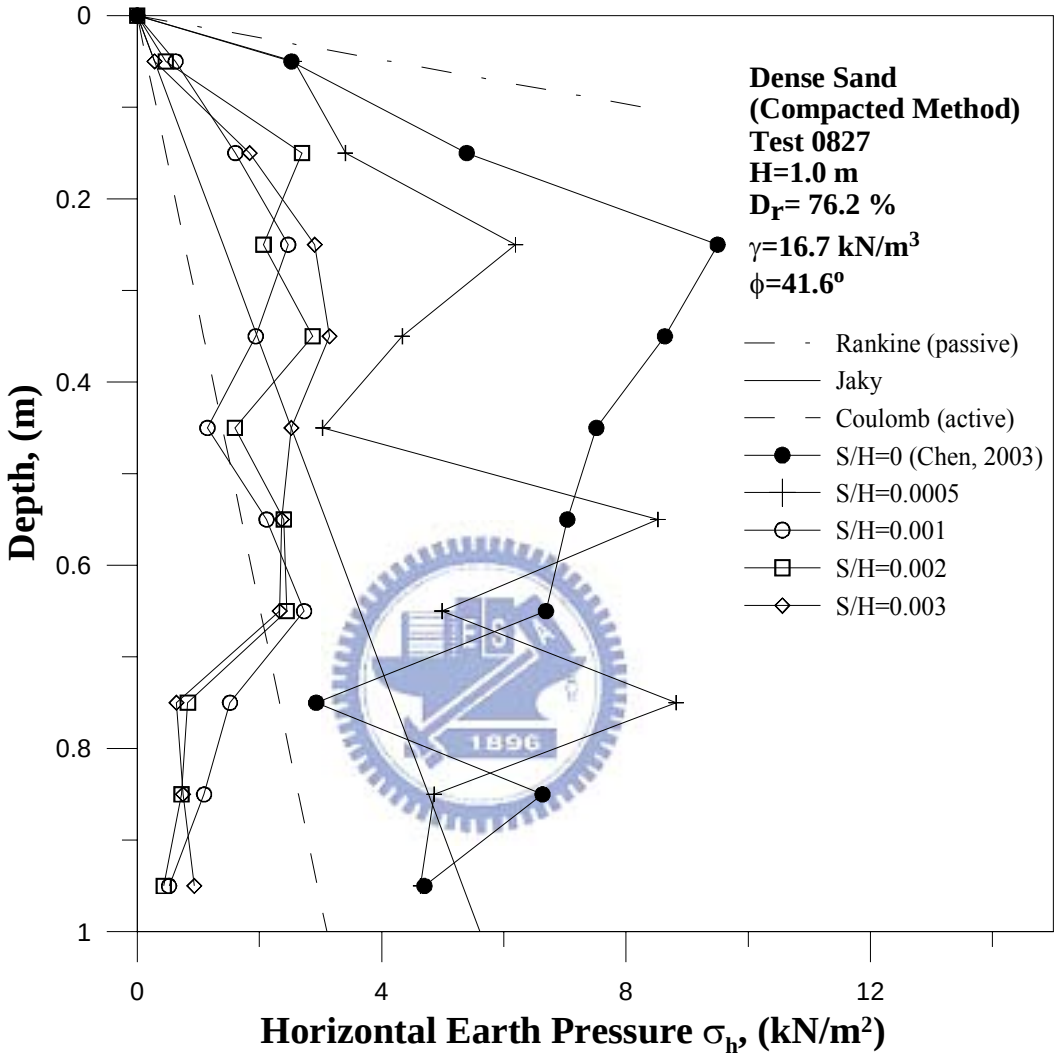

Fig. 5.5 Distribution of horizontal earth pressure (Test 0827)

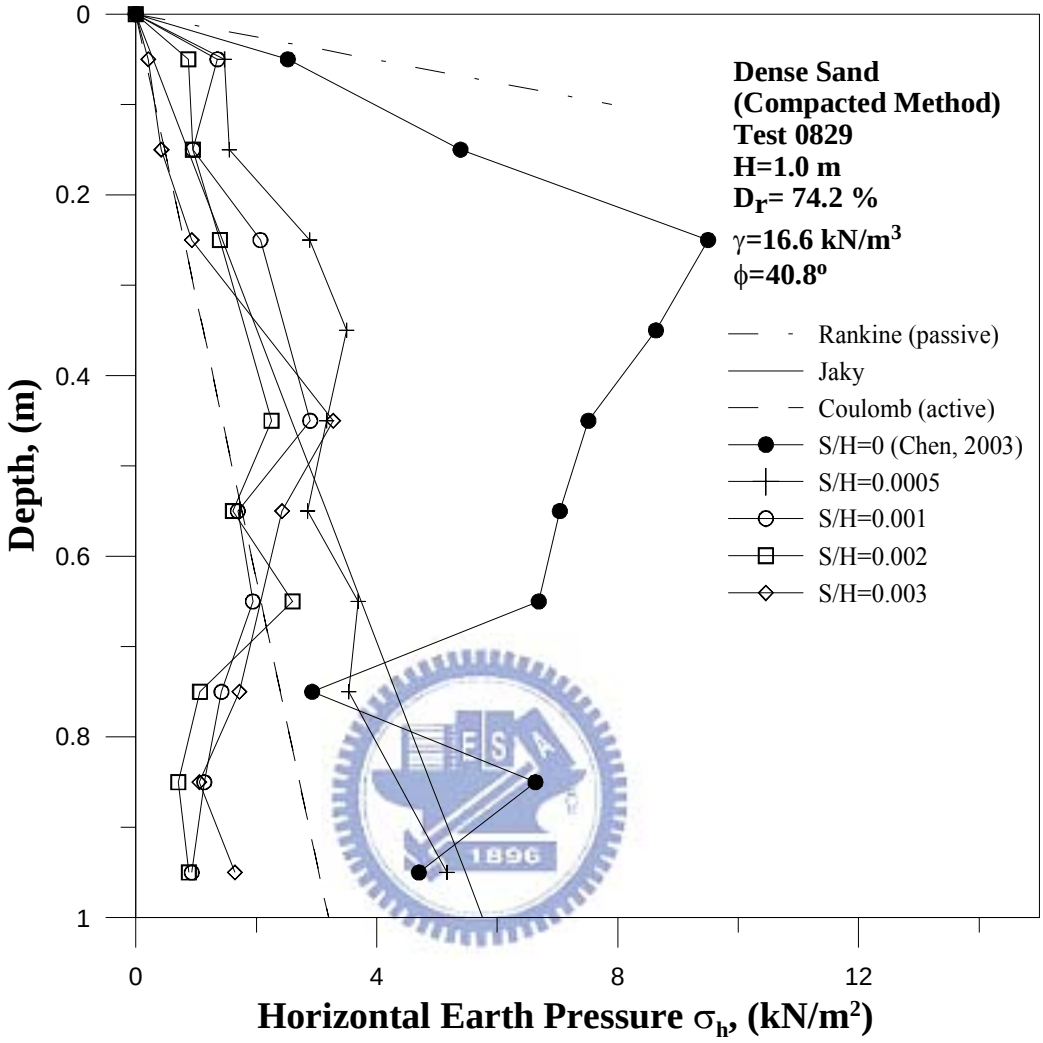

Fig. 5.6 Distribution of horizontal earth pressure (Test 0829)

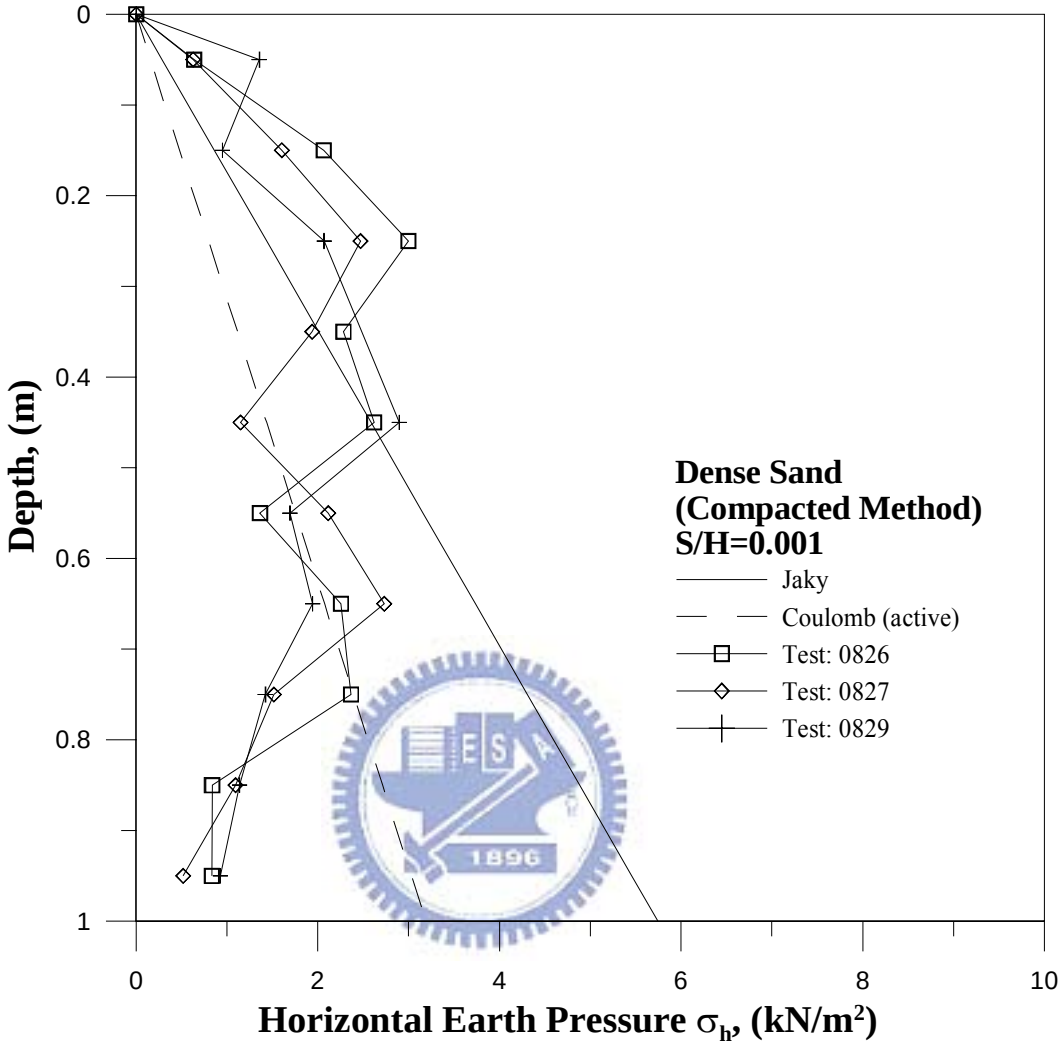

Fig. 5.7 Distribution of lateral earth pressure from different tests at S/H = 0.001

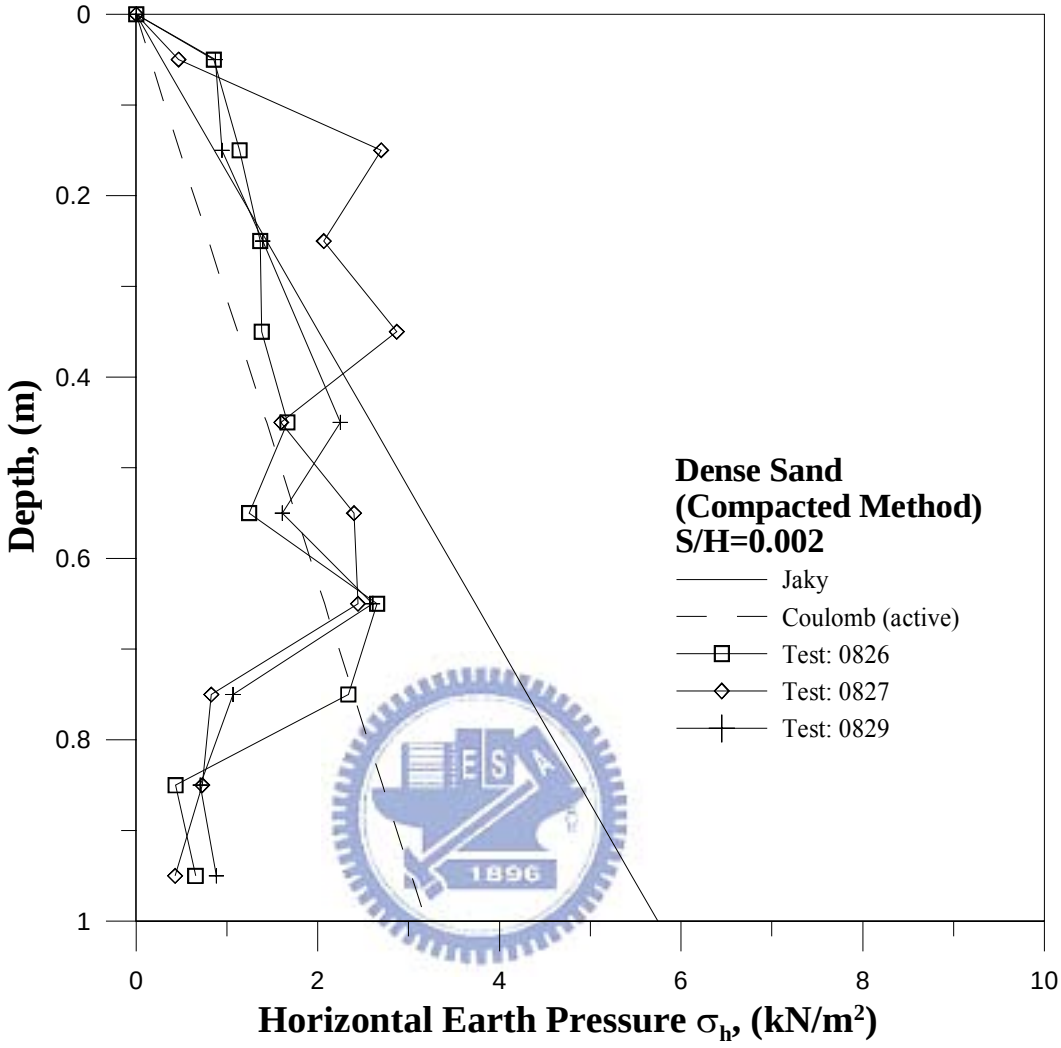

Fig. 5.8 Distribution of lateral earth pressure from different tests at S/H = 0.002

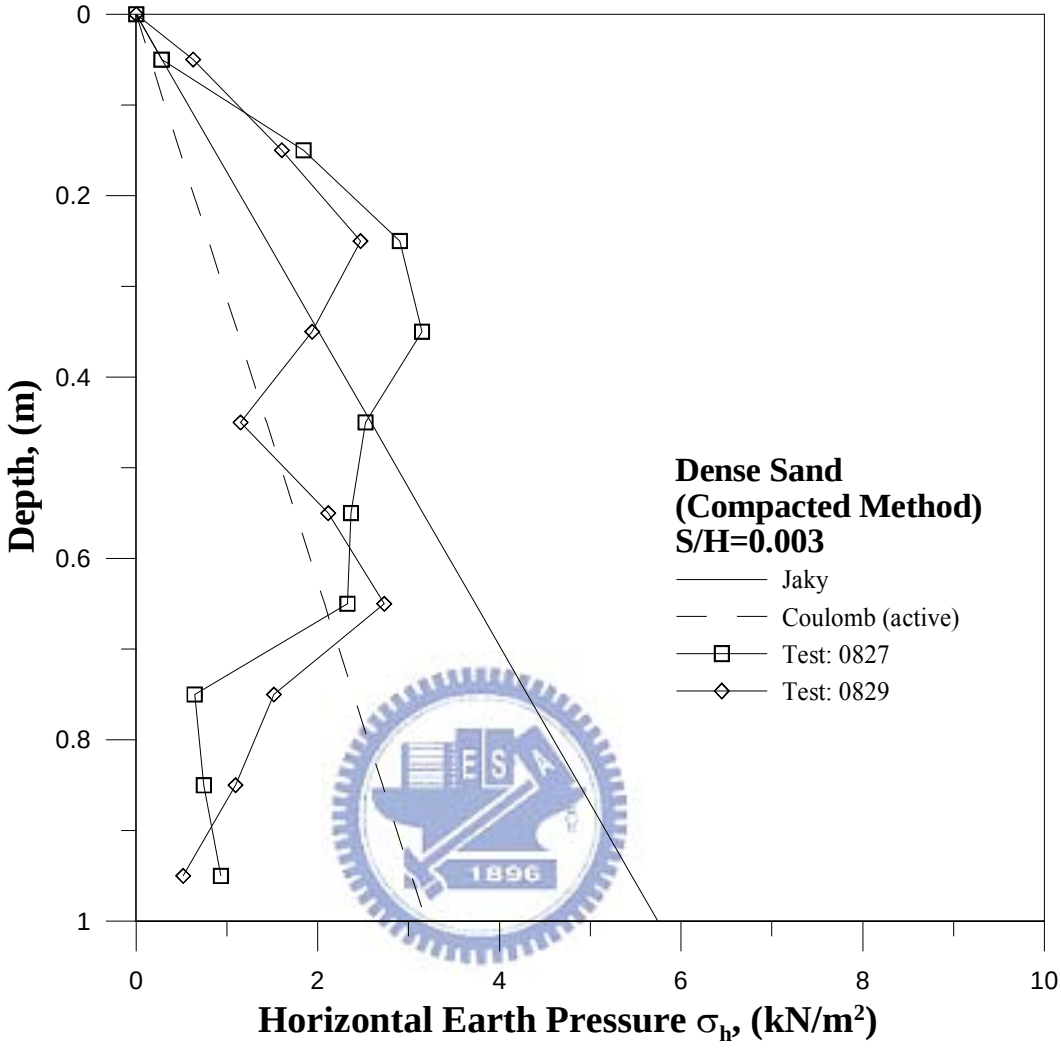

Fig. 5.9 Distribution of lateral earth pressure from different tests at S/H = 0.003

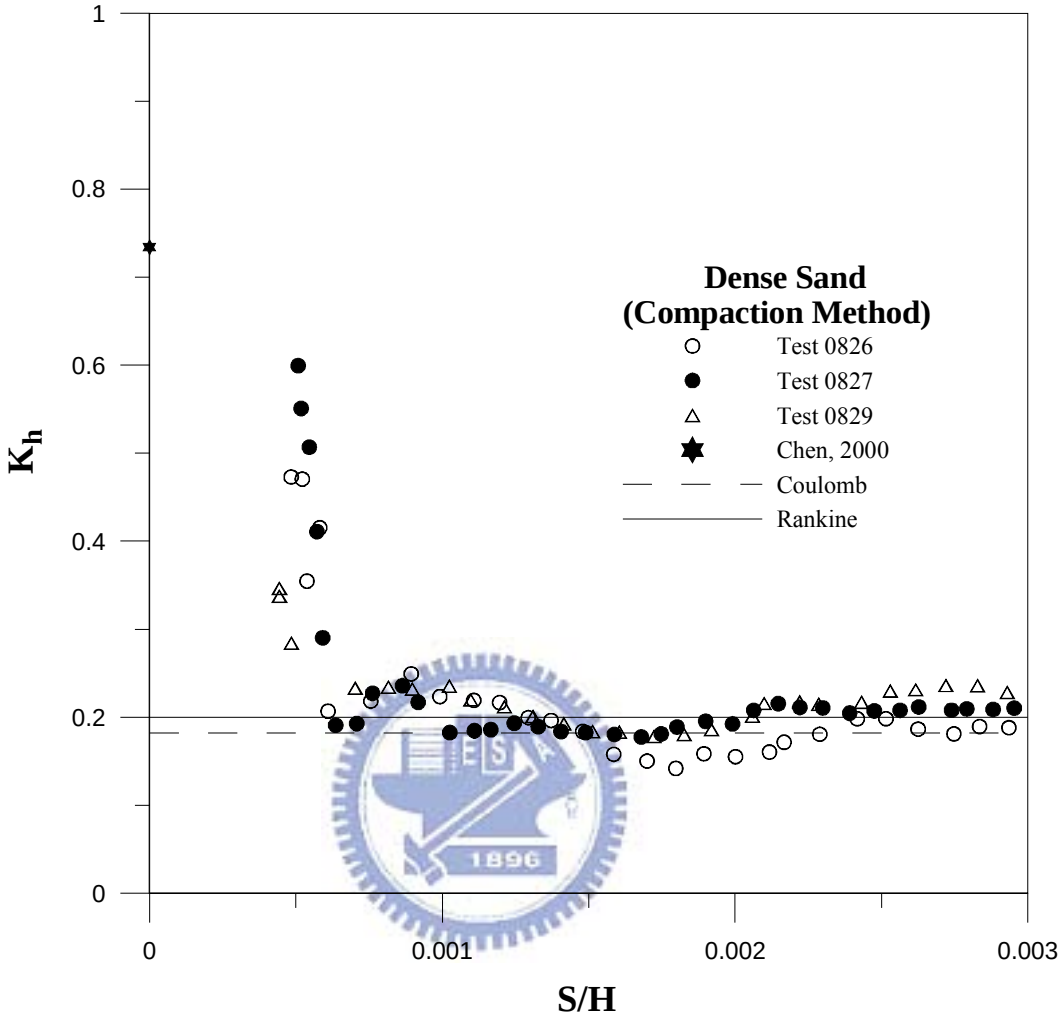

Fig. 5.10 Variation of K_h as a function of wall movement

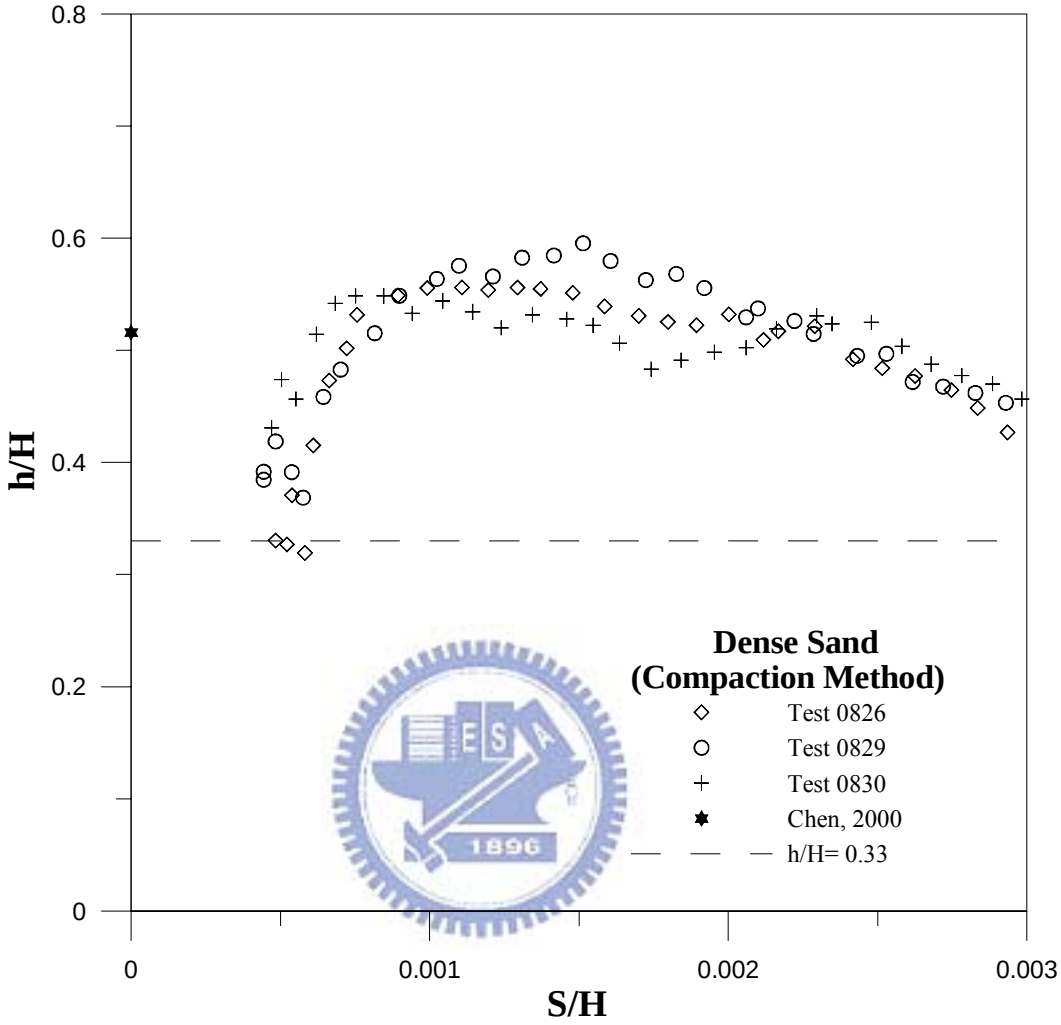

Fig. 5.11 Location of total soil thrust as a function of wall movement

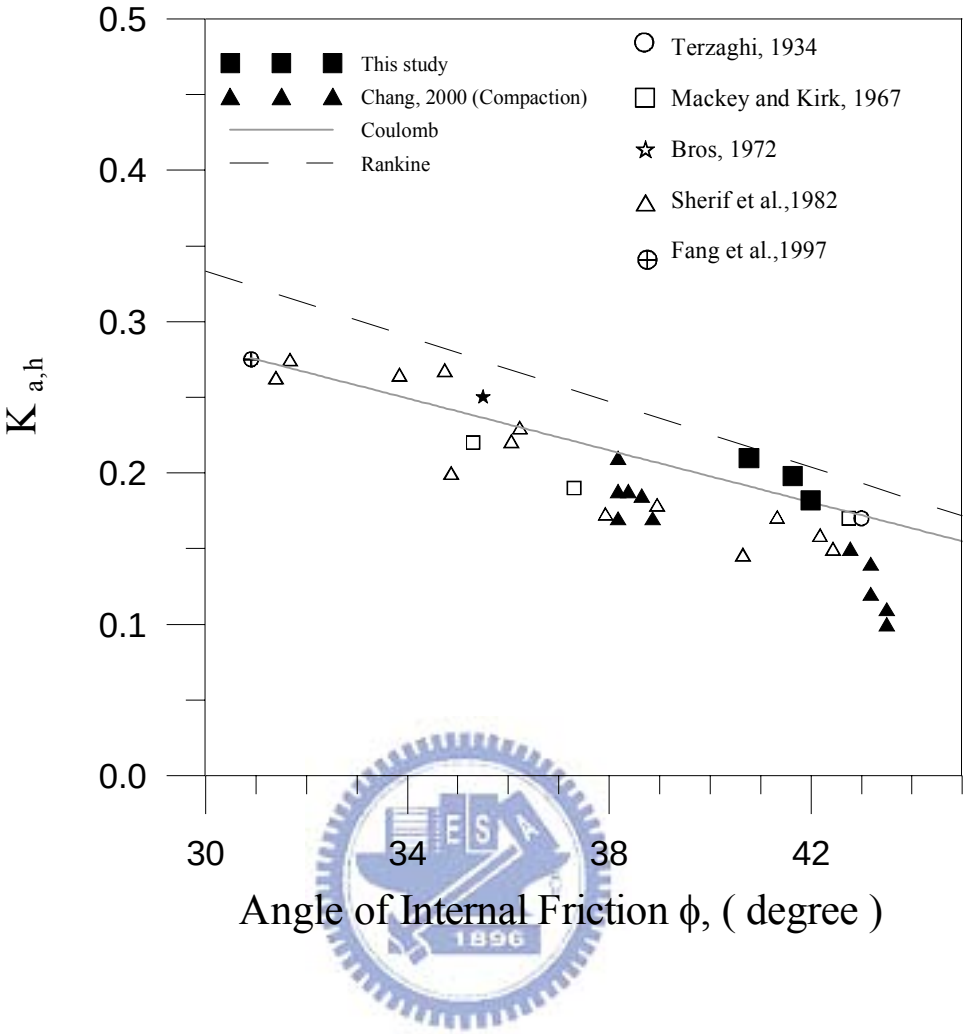

Fig. 5.12 Activeearth pressure coefficient $K_{a,h}$ for soils with different internal frction angles

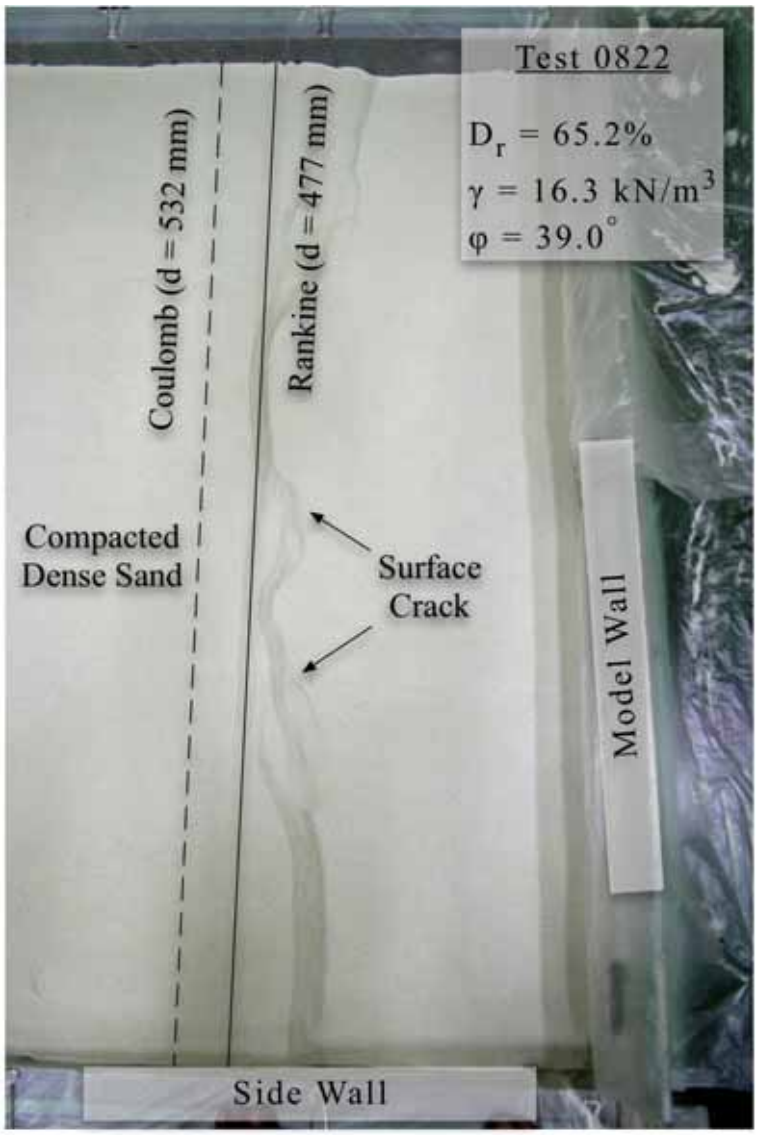

Fig. 5.13 Surface crack of active failure (S/H=0.016)

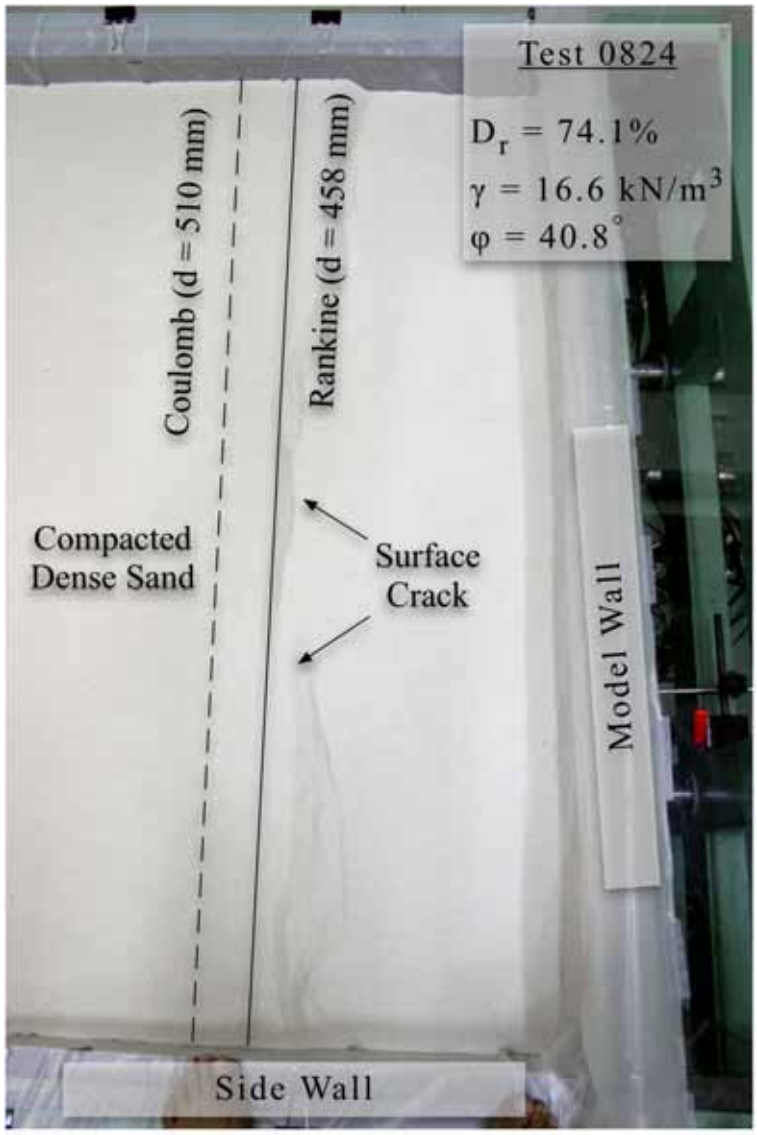

Fig. 5.14 Surface crack of active failure (S/H=0.016)

Appendix A:

Calibration of Soil Pressure Transducers

To investigate the lateral earth pressure acting on the model retaining wall, ten strain-gage type soil pressure transducers (SPT) were used. The transducers PGM-02KG manufactured by KYOWA are installed on the surface of model retaining wall to measure the lateral earth pressure against the retaining wall. The pressure acts between soil particles and the transducer is quite different from the pressure that acts between liquid and transducer. It is necessary to calibrate the soil pressure transducer in an environment similar to that of the actual testing condition. A special system was designed for the calibration of the strain-gage type soil-pressure transducers. The system consists of the calibration device, the controlled air-pressure system, signal conditioner, and the sensor data acquisition system, as indicated in Fig.A1and Fig. A2.

The calibration device is a shallow cylindrical chamber with an inner diameter of 400 mm and a height of 30 mm. The chamber is made of a solid steel plate, which is the same material as the model retaining wall. The soil-pressure transducer was inserted through the bottom of the chamber. It is important that the surface of the sensor was installed flush with the upper face of the chamber. To simulate the interface between the sand particle and soil pressure transducer, 10 mm-thick sand layer was poured into the calibration device over the transducer. Then a 0.2 mm-thick rubber membrane was placed over the sandy layer, as shown

in Fig.A.1. A uniformly distributed air-pressure was applied on the membrane, over the soil particles, and transmitted to the transducer. The output voltage of the transducer was found to increase linearly with the increase of applied pressure.

A rubber O-ring was arranged to prevent air leakage between the chamber and the cap. It should be noted that the air pressure applied for the calibration of transducer should be consistent with the operating pressure range for model wall experiments. For this study, the transducers were calibrated for the pressure range of 0 to 9.81 kPa. To reduce the effect of sidewall friction, the thickness of sand layer in the chamber should be limited, so that the side-friction between the sand the sidewall of the chamber could be minimized. Fig.A.3 to Fig.A.10 shows the test results of the soil pressure transducers calibrated without the compressible layer. Table A.1 is a summary of the calibration factors of each soil pressure transducer.

Table A1. Soil Pressure Transducer Calibration Factors

Transducer No.	Dynamic Strain Amplifier			Capacity(kN/m^2)	Calibration Factor[(kN/m^2)/volt]
	No.	Range Selector (*100 $\mu\xi$)	Calibration Setter($\mu\xi$)		
EX3270003	1	5	1981	19.62	3.621
EG6210026	2	5	1906	19.62	3.481
EZ0660029	3	5	2090	19.62	2.860
YT4030029	4	5	2465	19.62	4.417
YT4030042	5	5	2510	19.62	2.977
EE2450023	6	5	1984	19.62	2.643
EZ0660017	7	5	2014	19.62	3.179
EG6210005	8	5	2005	19.62	3.771
YT4030032	9	5	2220	19.62	3.539
EX3270002	10	5	2014	19.62	3.824

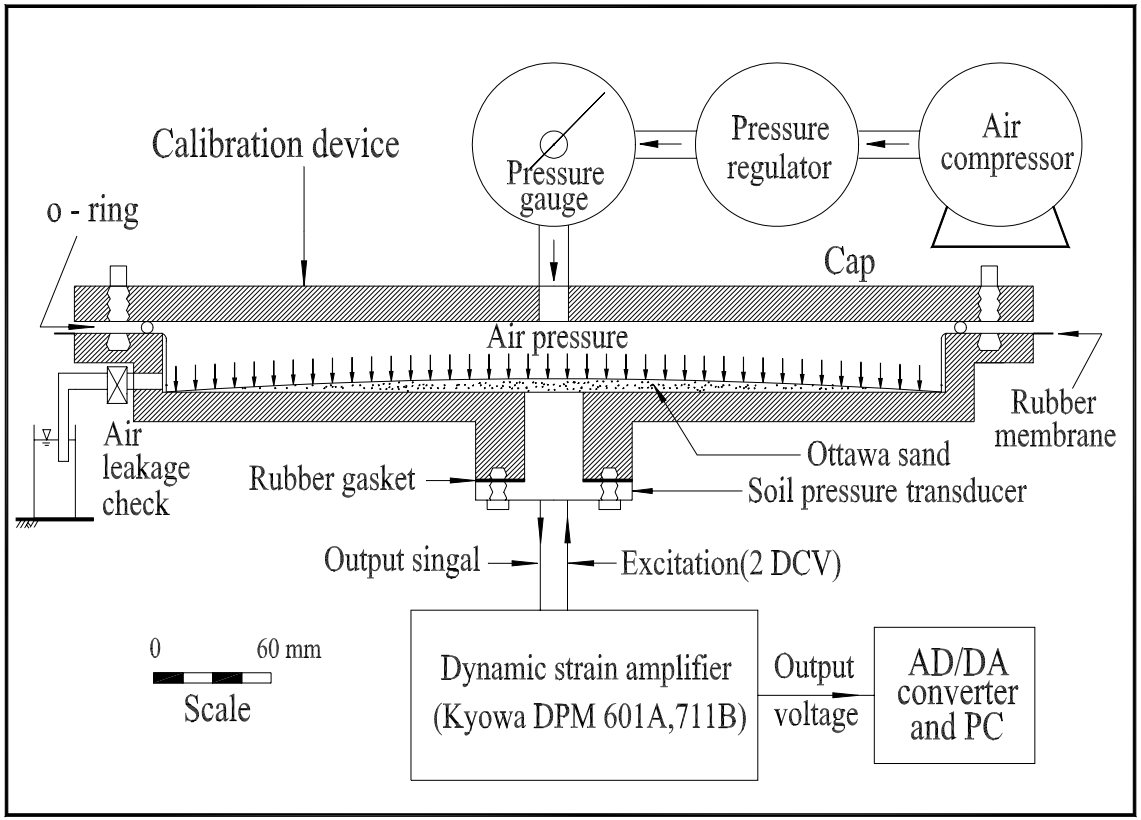

Fig. A1 Schematic diagram of the soil pressure transducer calibration system.

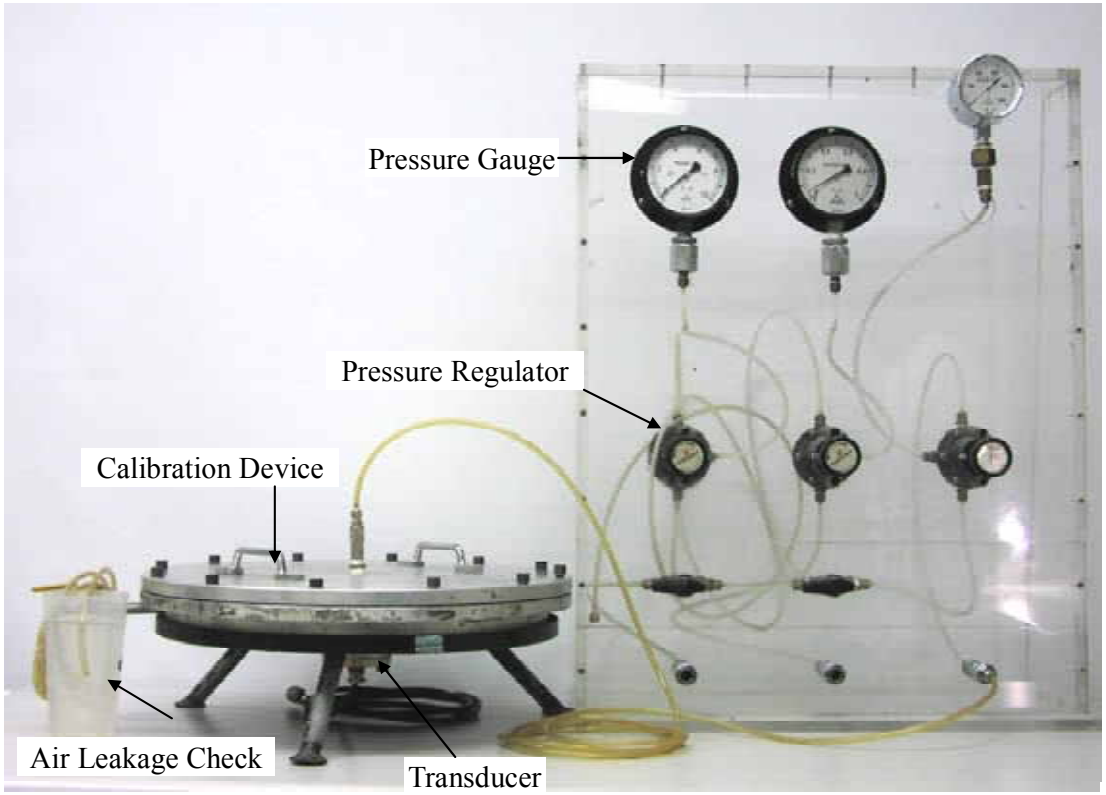

Fig. A2. Soil pressure transducer calibration system

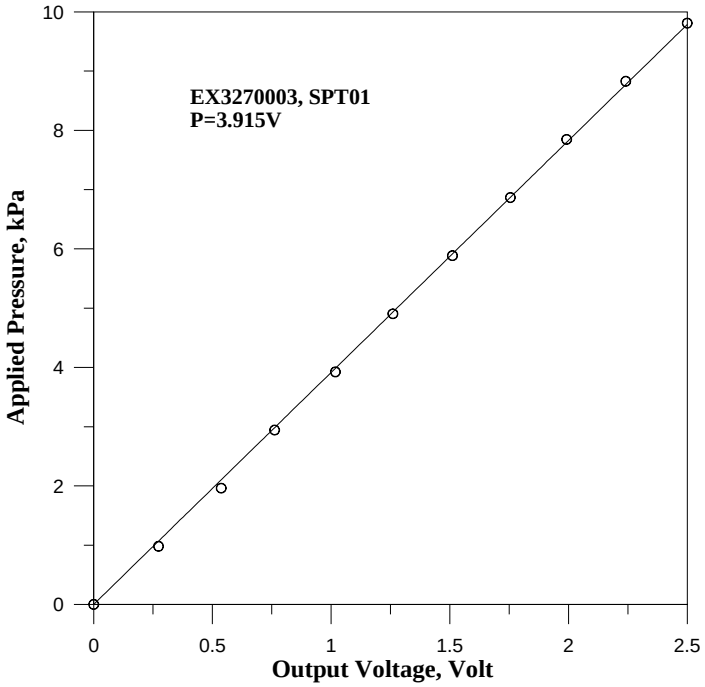

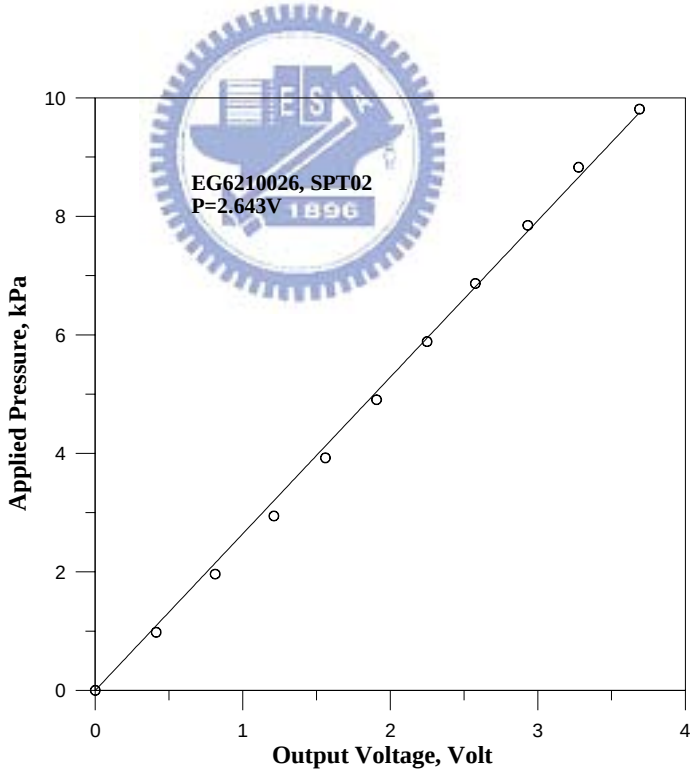

Fig. A3. Applied pressure versus voltage output for soil pressure transducer SPT01 and SPT02

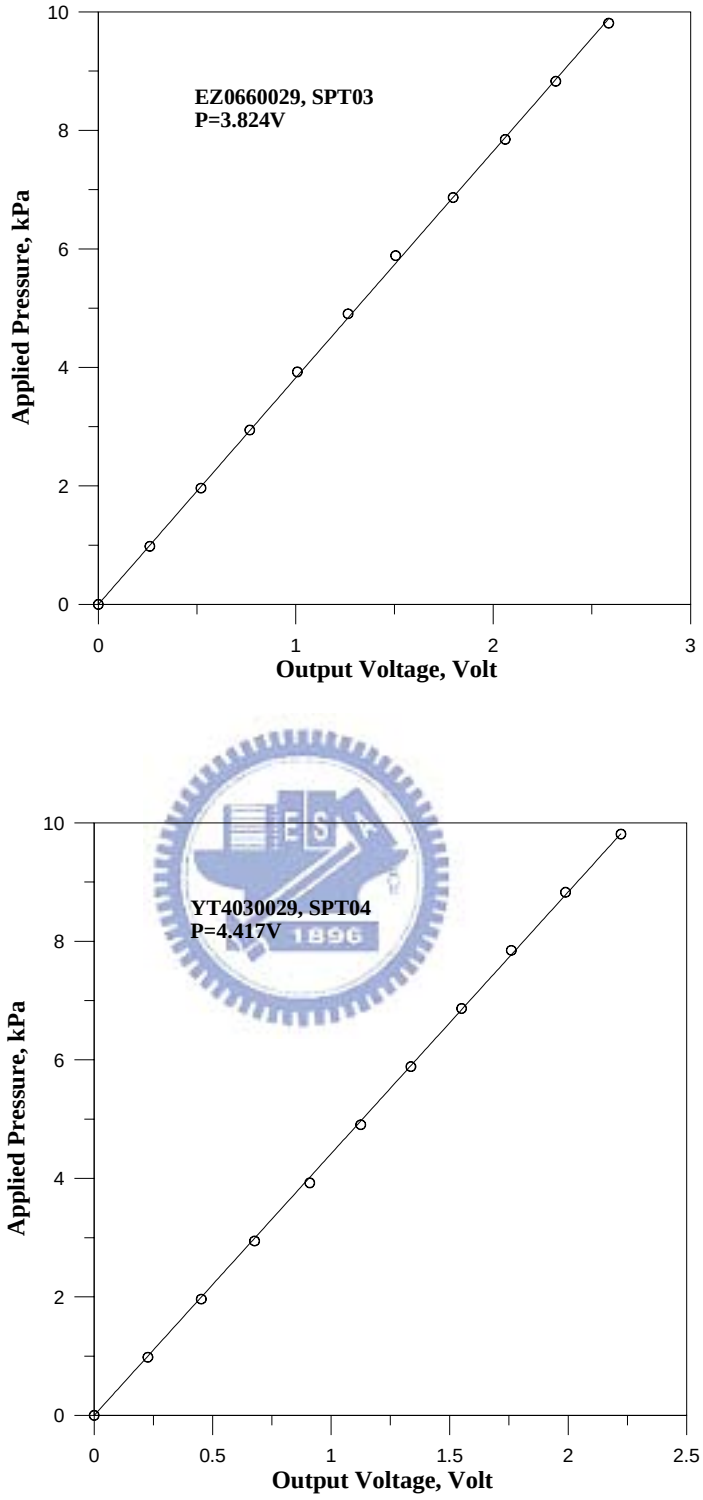

Fig. A4. Applied pressure versus voltage output for soil pressure transducer SPT03 and SPT04

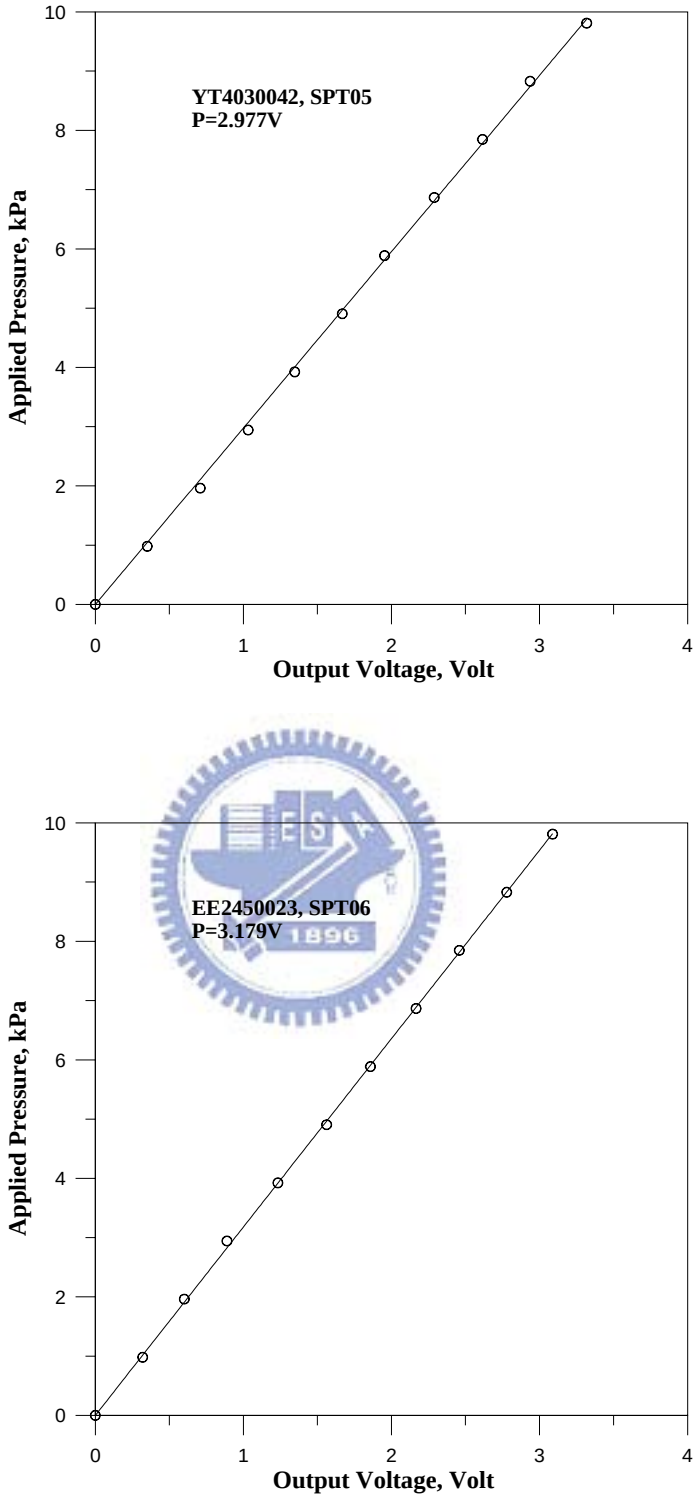

Fig. A5. Applied pressure versus voltage output for soil pressure transducer SPT05 and SPT06

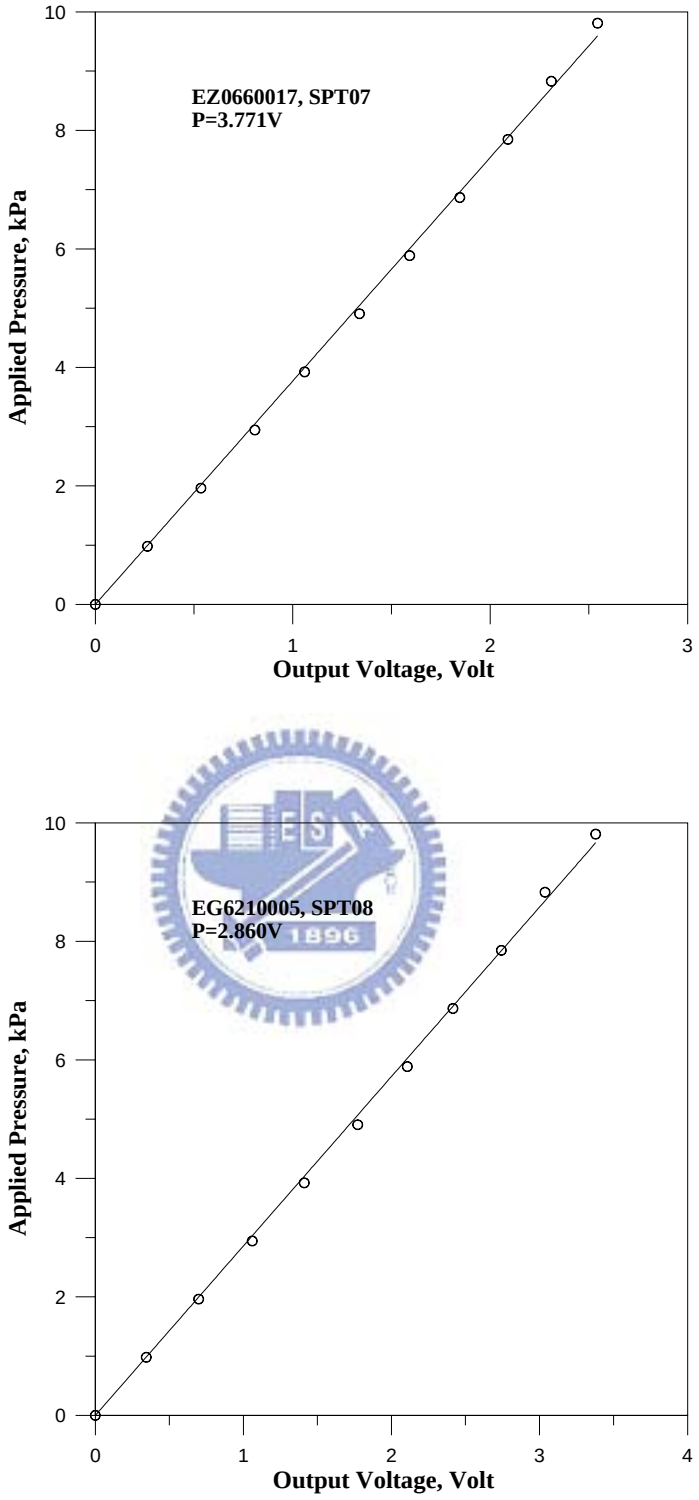

Fig. A6. Applied pressure versus voltage output for soil pressure transducer SPT07 and SPT08

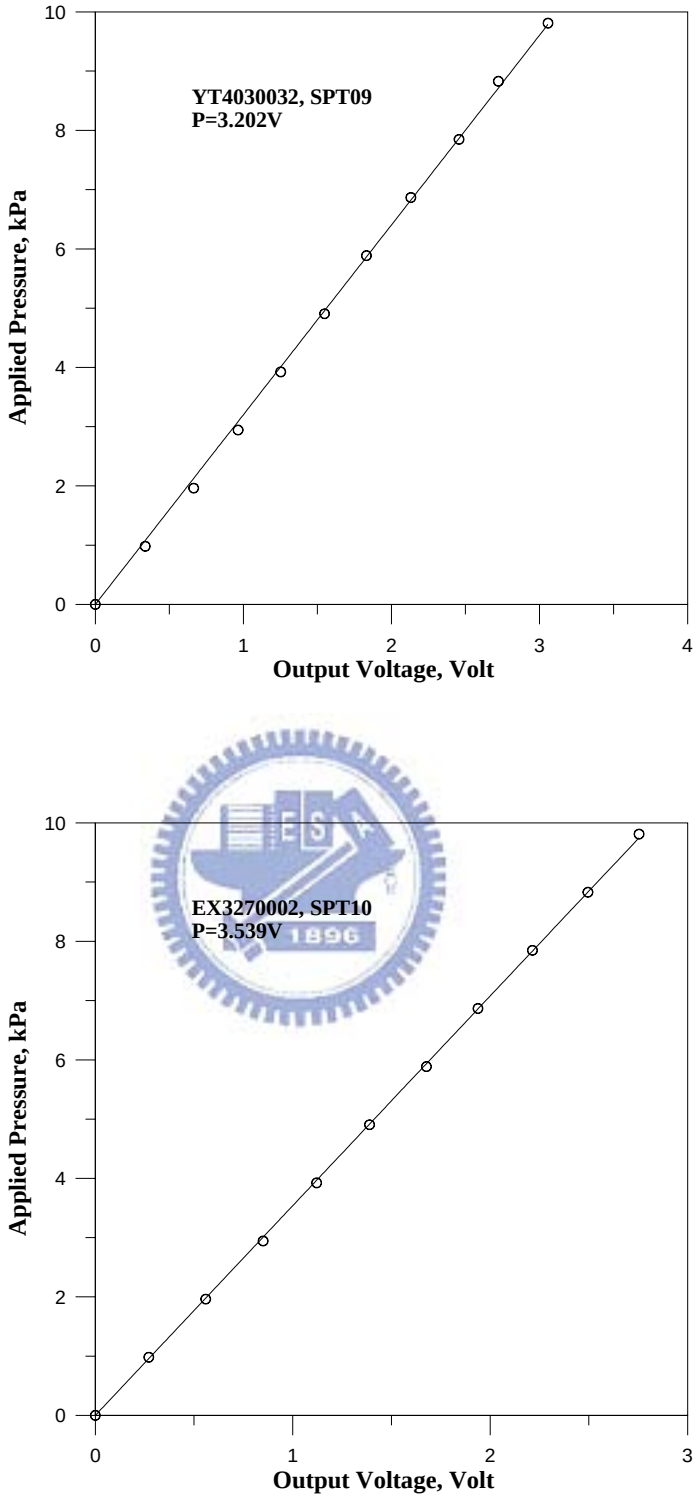

Fig. A7. Applied pressure versus voltage output for soil pressure transducer SPT09 and SPT10